ISSN 2812-9474

Engineering TODAY

VOL. 4 / NO. 4 / 2025

PUBLISHED BY

The Faculty of Mechanical and Civil Engineering
in Kraljevo of the University of Kragujevac

ISSN 2812-9474

VOL. 4 / NO. 4 / 2025

Engineering TODAY

PUBLISHED BY

The Faculty of Mechanical and Civil Engineering
in Kraljevo of the University of Kragujevac

Engineering TODAY

PUBLISHER

The Faculty of Mechanical and Civil Engineering in Kraljevo of the University of Kragujevac

ADDRESS

Faculty of Mechanical and Civil Engineering

Dositejeva 19, 36000 Kraljevo
Republic of Serbia

CONTACT

Tel: +381 36 383 269
+381 36 383 377
+381 36 383 378

Fax: +381 36 383 269

Email: editor@engineering-today.com

Web: www.engineering-today.com

FREQUENCY

4 issues per year

PRINTED BY

SaTCIP d.o.o., Vrnjačka Banja

CIRCULATION

50 copies/issue

INSTRUCTION FOR AUTHORS

A Engineering TODAY manuscript should by written clearly and concisely in correct English. The length of a reviewing paper is up to 12 pages. All papers are subject to a reviewing process. Final acceptance of a paper for publication in the Journal is based on the decision of the Editorial Board.

TEMPLATE FOR MANUSCRIPT

Template can be downloaded from the journal's website.

SUBMISSION OF PAPERS

All manuscripts for consideration by the Engineering TODAY should be submitted via the journal's website.

CIP - Каталогизација у публикацији
Народна библиотека Србије, Београд

621(497.11)

ENGINEERING Today / editor in chief Goran Marković. - [Štampano izd.]. - Vol. 1, no. 1 (2022)- . - Kraljevo : The Faculty of Mechanical and Civil Engineering of the University of Kragujevac, 2022- (Vrnjačka Banja : SaTCIP). - 30 cm

Tromesečno. - Je nastavak: IMK-14 = ISSN 0354-6829. -
Drugo izdanje na drugom medijumu:
Engineering Today (Kraljevo. Online) = ISSN 2812-9938
ISSN 2812-9474 = Engineering Today (Kraljevo. Štampano izd.)
COBISS.SR-ID 64530953

Mirko Blagojević
Faculty of Engineering Sciences
University of Kragujevac, Serbia

Lozica Ivanović
Faculty of Engineering Sciences
University of Kragujevac, Serbia

Dragan Pršić
Faculty of Mechanical and Civil Engineering in Kraljevo
University of Kragujevac, Serbia

Zoran Đinović
ACMIT Gmbh
Wiener Neustadt, Austria

Ivana Atanasovska
Mathematical Institute of the Serbian Academy
of Sciences and Arts
Belgrade, Serbia

Ivana Miličević
Josip Juraj Strossmayer University of Osijek
Croatia

Boris Jerman
Faculty of Mechanical Engineering
University of Ljubljana, Slovenia

Santosh Patil
Department of Mechanical Engineering
Manipal University Jaipur, Rajasthan, India

Naser Safaeian Hamzehkolaei
Department of Civil Engineering
Bozorgmehr University of Qaenat, Qaen, Iran

Nedeljko Dučić
Faculty of Technical Sciences Čačak
University of Kragujevac, Serbia

Victor Roda Casanova
Department of Mechanical Engineering and Construction-
Universitat Jaume I, Spain

Mile Savković
Faculty of Mechanical and Civil Engineering in Kraljevo
University of Kragujevac, Serbia

Danijela Milošević
Faculty of Technical Sciences Čačak
University of Kragujevac, Serbia

Francisco Peñuñuri
Universidad Autónoma de Yucatán
Merida, Mexico

Zuzana Palková
Institute of Electrical Engineering, Automation,
Informatics and Physics, Faculty of Engineering
Slovak University of Agriculture in Nitra, Slovakia

Siniša Bikić
Faculty of Technical Sciences
University of Novi Sad, Serbia

Iva Despotović
Faculty of Mechanical and Civil Engineering in Kraljevo
University of Kragujevac, Serbia

Nebojša Radić
University of East Sarajevo
East Sarajevo, Bosnia and Herzegovina

Dejan Ubavin
Faculty of Technical Sciences
University of Novi Sad, Serbia

Sorin Aurel RAȚIU
Universitatea Politehnica Timisoara
Timisoara, Romania

Vangelče Mitrevski
Faculty of Technical Sciences
University St. Kliment Ohridski, North Macedonia

Rade Karamarković
Faculty of Mechanical and Civil Engineering in Kraljevo
University of Kragujevac, Serbia

Danijela Nikolić
Faculty of Engineering Sciences
University of Kragujevac, Serbia

Marija Blagojević
Faculty of Technical Sciences Čačak
University of Kragujevac, Serbia

Gordana Bogdanović
Faculty of Engineering Sciences
University of Kragujevac, Serbia

Bojan Knežević
Faculty of Mechanical Engineering
University of Banja Luka, Bosnia and Herzegovina

Bojan Milošević
Faculty of Mechanical and Civil Engineering in Kraljevo
University of Kragujevac, Serbia

Dragan Petrović
Faculty of Mechanical and Civil Engineering in Kraljevo
University of Kragujevac, Serbia

Miloš Šešlija
Faculty of Technical Sciences
University of Novi Sad, Serbia

Elvis Žic
Faculty of Civil Engineering
University of Rijeka, Croatia

Marko Rosić
Faculty of Technical Sciences Čačak
University of Kragujevac, Serbia

Nicolae-Florin Cofaru
Faculty of Engineering
Lucian Blaga University of Sibiu, Romania

Mišo Bjelić
Faculty of Mechanical and Civil Engineering in Kraljevo
University of Kragujevac, Serbia

Milan Bižić
Faculty of Mechanical and Civil Engineering in Kraljevo
University of Kragujevac, Serbia

Mircea Viorel Dragoi
Department of Manufacturing Engineering
University of Brasov, Romania

Đorđe Damnjanović
Faculty of Technical Sciences Čačak
University of Kragujevac, Serbia

Branko Radičević
Faculty of Mechanical and Civil Engineering in Kraljevo
University of Kragujevac, Serbia

AIMS AND SCOPE

Engineering Today is an international peer-reviewed scientific journal that publishes original papers, both theoretical and experimental, covering the whole spectrum of engineering sciences, but focusing mostly on mechanical, electrical and civil engineering. The primary objective is to provide a high-level platform for researchers and practitioners to disseminate theoretical or engineering-oriented research output achievements within the context of engineering systems that fosters knowledge sharing in different branches of engineering discipline. Engineering Today also publishes novel theoretical methods, algorithms, simulations, experiments, and case studies as applications of state-of-the-art research in the field of engineering.

The topics of interest include, but are not limited to:

- Mechanical engineering
- Electrical/electronic engineering
- Civil engineering
- Manufacturing engineering
- Software engineering
- Thermal technique and environment protection
- Applied mathematics and physics
- Theoretical and applied mechanics
- Optimization algorithms
- Metaheuristic algorithms
- Railway engineering
- Earth-moving, construction and transportation machinery
- Automatic control and fluid technique
- Computer science
- Information systems
- Fault detection and diagnosis
- Learning systems
- Robust systems
- Neuro-fuzzy systems
- Internet of things
- Cybernetics
- System identification
- Stochastic systems
- Complex networks
- Computational complexity
- Mechatronics
- Production technologies
- Computer design and computer integrated processes design
- Design of machining processes
- Engineering management and entrepreneurship
- Mechanical construction and material technology
- Interdisciplinary applications

It provides an effective medium for researchers and a way to quickly publish high-quality original papers, so as to convey the latest important progress in their professional field to scientists in related disciplines. Engineering Today offers authors rigorous peer review, rapid publication, and maximum visibility. The journal expects to accept only the most relevant manuscripts and will provide very rapid evaluation to prevent publication delays. The Editors reserve the right to reject papers without sending them out for review.

From time to time, Engineering Today will publish review articles, short communications, discussions as well as special issues on a specific sub-field of engineering science. Authors are encouraged to contact the Editor-in-Chief if they would like to submit a review article or propose and edit a special issue of the journal.

Engineering
TODAY

VOL. 4 / NO. 4 / 2025

CONTENTS

REVIEW PAPER OPEN ACCESS

Acoustic analysis in gas metal arc welding: Physical mechanisms, signal processing, and applications

Mladen Rasinac[1*], Mišo Bjelić[1], Branko Radičević[1], Tanja Dulović[1], Stefan Pajović[1]

[1] University of Kragujevac, Faculty of Mechanical and Civil Engineering, Kraljevo, Serbia

ARTICLE INFO

* **Correspondence:** rasinac.m@mfkv.kg.ac.rs

DOI: 10.5937/engtoday2600005R

UDC: 621(497.11) **ISSN:** 2812 – 9474

Article history: Received 9 January 2026; Revised 23 February 2026; Accepted 28 February 2026

ABSTRACT

Acoustic analysis has emerged as a promising, non-intrusive approach for process monitoring and quality assessment in gas metal arc welding (GMAW). The sound generated during the GMAW process originates from complex physical phenomena, including arc plasma dynamics, metal transfer mechanisms, weld pool oscillations, and shielding gas flow. Therefore, acoustic signal contains significant information related to process stability and weld formation. During the previous decades, numerous researches have been focused on the application of audible sound and acoustic emission for real-time monitoring of the GMAW process. This paper provides an overview of the application of acoustic analysis in the GMAW process. The basic mechanisms of acoustic signal generation, as well as signal acquisition and processing techniques in the time, frequency, and time-frequency domains, are considered. Key application areas are reviewed, including process stability monitoring, weld quality assessment, metal transfer mode classification, and welding defects detection. Special attention is paid to contemporary trends, challenges and the integration of acoustic analysis with intelligent welding systems, highlighting its potential as a supplementary tool for advanced GMAW process monitoring.

KEYWORDS

Gas metal arc welding, Acoustic analysis, Acoustic emission, Signal processing, Metal transfer modes, Process stability, Weld quality, Machine learning.

1. INTRODUCTION

Gas metal arc welding (GMAW) is one of the most commonly applied arc welding processes in the modern manufacturing industry, thanks to its high productivity, convenience for automation, and the possibility of welding a wide range of materials and thicknesses. However, the quality and stability of the GMAW process largely depend on complex and extremely dynamic phenomena, such as the behavior of the electric arc, metal transfer mechanisms, dynamics of the molten pool, as well as the mutual interactions of electrical, thermal, and mechanical effects. Changes in these phenomena can lead to the occurrence of various welding defects, including lack of fusion, porosity, excessive spatter, burn-through, and inconsistent penetration, which directly affect the mechanical properties and reliability of welded joints [1-5].

Traditionally, the monitoring and control of the GMAW process have been based primarily on the analysis of electrical signals, such as welding current and voltage, as well as optical measurement methods and non-destructive testing (NDT) techniques applied after the process is completed. Although these methods provide valuable information about welding flow and joint quality, they often have significant limitations, including sensitivity to intense arc radiation and fumes, high complexity of measurement systems, and delayed error detection. These limitations have been documented in numerous studies dealing with welding process monitoring and multi-sensor approaches [6,7]. For this reason, in recent years, there has been a growing interest in alternative sensor approaches that enable the monitoring of processes in real time, in a non-intrusive and economically profitable manner.

Among these approaches, acoustic analysis stood out as a promising tool for monitoring and diagnosing the welding process. Sound generated during the GMAW process originates from multiple physical sources, primarily associated with arc plasma fluctuations, metal transfer events, and fluid-electromagnetic interactions. As a consequence, the acoustic signal inherently contains information about the stability of the process, the mode of metal transfer, and the quality of the welded joint [8-12]. In addition to physically measurable acoustic characteristics, psychoacoustic research has shown that experienced operators can subjectively assess welding stability based solely on sound perception, which further confirms the information richness of acoustic emissions in the GMAW process [13,14].

The application of acoustic emission in welding can be traced back to the pioneering work of Jolly [15,16], who showed that acoustic emission signals can be used to detect crack initiation, porosity, and inclusions in real time, during the welding process itself and subsequent cooling of the weld metal. One of the first systematic studies of acoustic emission signals in welded joints further demonstrated that acoustic emission signals activity is strongly related to the occurrence of defects and structural changes occurring during welding [17]. Early experimental research also confirmed that acoustic emission signals during welding is closely related to transient metallurgical processes and defect formation mechanisms, thus confirming the feasibility of applying acoustic emission signals methods for process monitoring directly during welding [18].

This early research pointed to one of the key advantages of acoustic monitoring compared to conventional NDT methods, which is the ability to obtain real-time process information. This enables earlier identification of defect mechanisms and reduces the need for subsequent inspection of welded joints and corrective actions after welding [15], [19-21]. Subsequent studies further confirmed the applicability of acoustic emission signals diagnostics for identifying the lack of fusion and other irregularities in welded joints in industrial conditions [3].

After these initial investigations, numerous works have dealt with the application of audible sound and acoustic emission signals for online monitoring of the GMAW process. Research has shown that acoustic characteristics extracted in the time, frequency, and time-frequency domains can be effectively related to welding stability, short circuit behavior, and metal transfer dynamics [22-25]. In particular, different metal transfer modes, such as short-circuit, globular, spray, and pulsed GMAW, have been shown to possess characteristic acoustic signatures, enabling reliable classification of transfer modes based on sound analysis [11,12], [26-28].

In addition to process stability assessment and metal transfer mode identification, acoustic measurement was also applied to weld quality assessment and defect detection. Successful examples of burn-through detection, lack of fusion, porosity, and penetration variations using acoustic characteristics in combination with statistical analysis, regression models, and machine learning methods (ML) have been recorded in the literature [1-5]. Recent works have further improved these approaches by introducing advanced methods of signal processing, sensor fusion, and artificial intelligence, including neural networks and deep learning, thus increasing the robustness and accuracy of prediction in industrial settings [29-32]. A comprehensive review of acoustic emission signals techniques for the evaluation of welded structures and their structural reliability is provided by Nedoseka [20].

In parallel with experimental research, efforts were made to improve the physical understanding of sound generation mechanisms in the GMAW process. Analytical and numerical models describing the dynamics of metal transfer and arc behavior have provided a deeper insight into the relationship between droplet motion, electromagnetic forces and acoustic emission signals [27,28],[33-35]. Recently, models with lumped parameters have been proposed, as well as numerical models that explicitly consider the generation of sound in the GMAW process, which further strengthens the theoretical basis of acoustic monitoring [35]. However, despite extensive experimental research, the physical modeling of sound generation in the GMAW process is still fragmentary and incomplete, which limits the predictive capabilities of acoustic analysis.

Despite significant progress made over the last few decades, the application of acoustic analysis in the GMAW process still faces challenges related to ambient noise, sensor positioning, process variability, and the lack of standardized measurement and analysis procedures. At the same time, the growing need for intelligent welding systems and solutions within the Industry 4.0 concept has refocused attention on acoustic measurement as a complementary or alternative monitoring method, thanks to its simplicity, non-intrusive nature, and rich informational content (Figure 1). Despite extensive experimental research, a large number of existing studies remain limited to specific applications and do not possess a unique physical framework that would relate acoustic characteristics to basic welding phenomena. In this context, this paper provides a comprehensive overview of acoustic analysis in the GMAW process. The physical sources of welding sound, acoustic measurement approaches, signal processing techniques, and the main areas of application, including process stability monitoring, weld quality assessment, metal transfer mode classification, and defect detection, are presented. Current challenges and future directions of research were also discussed to highlight the potential of acoustic measurement for the development of intelligent and reliable GMAW process monitoring systems. In addition to works focused on specific processes, several review and survey papers have provided a broader methodological and technological context of the application of acoustic and audible sound for real-time monitoring of welding transient phenomena and processes [36-38].

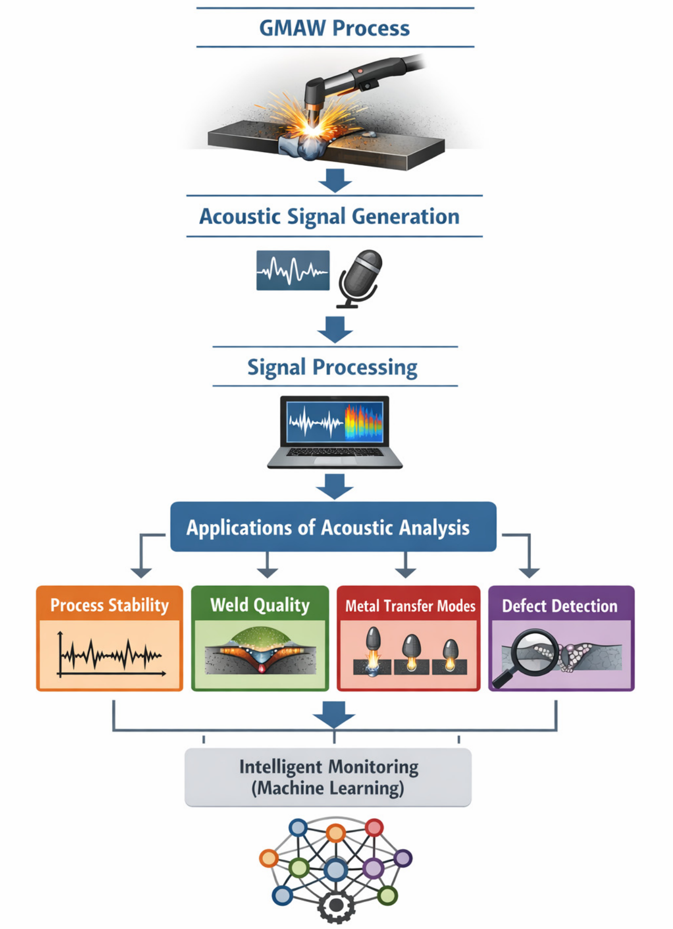

Figure 1: Conceptual workflow of acoustic analysis in GMAW

1.1. Scope and methodology of the review

This review paper focuses on acoustic signal analysis applied exclusively to GMAW. The scope of the paper is deliberately limited to the GMAW process in order to allow a detailed and physically based elaboration of sound generation mechanisms, signal processing approaches, and practical applications relevant to this welding process. The literature reviewed was selected based on its relevance to acoustic measurement, sound emission, or acoustic emission signals techniques in the GMAW process, with particular emphasis on studies dealing with process stability, metal transfer modes, weld quality assessment, and defect detection. Both classic and contemporary works are included in the consideration to cover the historical development of the field, as well as current research trends.

The review gives priority to papers published in peer-reviewed scientific journals and doctoral dissertations, while conference papers are included in cases where they provide a significant methodological or conceptual contribution. Selected studies were analyzed and synthesized in relation to the applied type of sensor, signal features, used models, and processing techniques, as well as basic conclusions and reported results.

1.2. Acoustic sensing modalities in GMAW

Acoustic monitoring of the GMAW process is most commonly performed using microphone-based airborne sound measurements or acoustic emission (AE) sensors that register waves propagating through the material structure. Microphones measure sound pressure fluctuations emitted into the surrounding air and are particularly sensitive to arc plasma dynamics and metal transfer events. Due to their non-contact nature and simple installation, microphone-based systems represent an attractive solution for industrial applications, although they are more susceptible to ambient noise and reflections. In contrast, AE sensors are typically mounted directly on the workpiece and detect elastic waves propagating through the material. Acoustic emission measurements performed using AE sensors are less sensitive to airborne noise and are particularly suitable for the detection of high-frequency transient events, such as crack initiation or burn-through. However, their application requires physical contact and proper mechanical coupling between the sensor and the surface, which may limit their practical applicability in certain industrial environments.

Numerous studies have shown that both approaches provide complementary information about the welding process, and hybrid systems combining microphones and AE sensors have been proposed in order to increase the robustness and reliability of process monitoring. In this review, measurements of airborne sound and measurements of acoustic emission signals through a structure are discussed within the common concept of acoustic sensing, since both types of signals originate from the same basic phenomena in the welding process, but differ in the propagation medium and characteristic frequency range.

1.3. Positioning of acoustic analysis among welding monitoring techniques

Compared to traditional monitoring methods based on electrical and optical measurements, acoustic analysis offers a unique combination of non-intrusiveness, sensitivity to dynamic phenomena, and relatively low implementation costs. Electrical signals, such as welding current and voltage, provide direct information about energy delivery, but are often not sensitive enough to detect subtle disturbances associated with metal transfer or molten pool dynamics. Optical monitoring systems, although extremely informative, as a rule require complex measuring equipment and can be sensitive to harsh conditions in the welding zone, such as intense arc radiation, fume, metal spatter, and lighting changes. Acoustic sensing complements these approaches by providing indirect but physically meaningful information on arc dynamics, metal droplet detachment, and process instabilities. As a result, acoustic analysis is increasingly considered an important component of multi-sensor and intelligent welding process monitoring systems.

2. ACOUSTIC SIGNAL GENERATION IN GMAW

The acoustic signal produced during the GMAW process originates from the interaction of several physical phenomena that take place within the electric arc, the molten metal, and the surrounding shielding gas. Unlike purely electrical or optical signals, welding sound is a macroscopic manifestation of the rapid energy exchanges and dynamic instabilities inherent in the GMAW process. Understanding the origin of acoustic signals is therefore crucial to correctly interpret their relationship to process stability, metal transfer mechanisms, and weld quality.

2.1. Arc plasma dynamics as a sound source

One of the primary sources of acoustic emission in the GMAW process is the electric arc plasma. Temporal fluctuations of current and arc voltage lead to rapid changes in pressure, temperature, and electrical conductivity of the plasma, resulting in periodic expansion and contraction of the plasma column. These pressure oscillations spread into the surrounding environment in the form of acoustic waves and represent a significant part of the measured sound signal [8-10]. In the short-circuit and globular metal transfer modes, abrupt changes in arc length during droplet formation and detachment introduce pronounced transient disturbances in the arc plasma. These events generate pulsed acoustic emissions with broadband frequency content, which are clearly visible in both time domain and spectral representations of the sound signal [22],[23-25]. In contrast, in stable metal spray transfer, the electric arc remains relatively constant, resulting in more continuous acoustic signatures with narrower spectral distributions [26],[39].

2.2. Metal transfer phenomena and droplet dynamics

Metal transfer is widely recognized as one of the dominant sources of acoustic activity in the GMAW process. The formation, growth, detachment, and impact of molten metal droplets are determined by the balance of electromagnetic forces, surface tension, gravity, and drag of the plasma. Each of these mechanisms contributes to the force fluctuations that excite acoustic radiation during the welding process [27,28], [33,34], [40].

The short-circuit transfer mode in particular generates pronounced acoustic pulses associated with repeated arc extinguishing and reignition events. These impulses strongly correlate with the frequency and duration of short circuits, which explains the close connection between statistical acoustic features and process stability, as confirmed in numerous studies [1-5],[29,30]. In contrast, globular and spray modes of metal transfer are characterized by a more uniform behavior during droplet separation, which leads to acoustic emissions dominated by periodic components associated with droplet oscillations and their detachment frequency [28],[33,34].

Newer research has additionally shown that the resonant phenomena of droplets and their oscillatory movement can significantly affect the acoustic spectrum, especially in the pulsed and controlled GMAW process. Changes in droplet size, droplet detachment time, and impact dynamics result in characteristic acoustic patterns that can be used to classify metal transfer modes and monitor the welding process [11,12], [26], [39].

2.3. Gas flow, arc–droplet interaction, and molten pool dynamics

In addition to arc plasma dynamics and metal transfer, shielding gas flow and interaction between the arc and metal droplets contribute significantly to the overall acoustic emission during the GMAW process. Turbulent gas flow in the arc zone generates broadband noise, while interactions between the plasma jet and the molten metal surface cause pressure fluctuations that further modulate the sound signal [9-12].

The dynamics of the molten metal pool also play a secondary but significant role in the generation of acoustic signals.

Oscillations of the pool surface, especially in conditions of thermal or electromagnetic instability, can be coupled with arc pressure variations and droplet impacts, which lead to the amplification of low-frequency acoustic components, as observed in several experimental studies dedicated to penetration instability and burn-through phenomena [1,2]. These effects become more pronounced in cases of burn-through, excessive penetration, or unstable heat input, which explains the high sensitivity of acoustic signals to the occurrence of weld defects and variations in penetration depth, noted in numerous experimental studies [1-4],[31].

2.4. Statistical and physical interpretation of GMAW sound

From the aspect of signal processing, the acoustic emission during the GMAW process exhibits a stochastic and impulsive character, which reflects the inherently unstable and non-linear behavior of the welding process. Statistical analyses have shown that sound pressure distributions often deviate from the Gaussian distribution and are characterized by "heavy tails", especially in unstable welding modes [11,12],[41]. These properties provide the physical basis for the effectiveness of time-domain statistical features, such as root mean square (RMS), kurtosis, and variance, in characterizing process stability and weld defect formation. In addition to empirical observations, newer models seek to explicitly link the physical parameters of the process with the mechanisms of acoustic signal generation. Lumped-parameter and numerical models, including arc dynamics, metal transfer forces, and energy balance, have provided significant insight into the coupling between the physics of the welding process and sound generation [35]. Such models strengthen the theoretical basis of acoustically based monitoring methods and enable the interpretation of measured signals in the context of basic physical phenomena.

From a practical point of view, the acoustic emission during the GMAW process is characterized by relatively high sound pressure levels and a wide frequency range, where both the amplitude and the spectral distribution are strongly dependent on the welding parameters and the metal transfer mode [8],[42]. Short-circuit metal transfer is usually associated with impulsive, broadband acoustic emissions originating from arc extinction and reignition, while globular and spray modes of transfer produce more continuous acoustic signatures with dominant frequency components associated with periodic droplet detachment and arc plasma oscillations [9-12]. In the pulsed GMAW process, additional spectral components synchronized with the pulse frequency additionally shape characteristic time-frequency patterns, which differ from those present in conventional metal transfer modes [26],[39],[43,44]. These systematic differences in sound pressure level and spectral content provide the physical basis for the statistical acoustic features and analysis approaches discussed in the following chapters. The overall connection between physical phenomena in the GMAW process, acoustic signal generation, signal processing, feature extraction, and their application in process monitoring tasks is shown schematically in Figure 2.

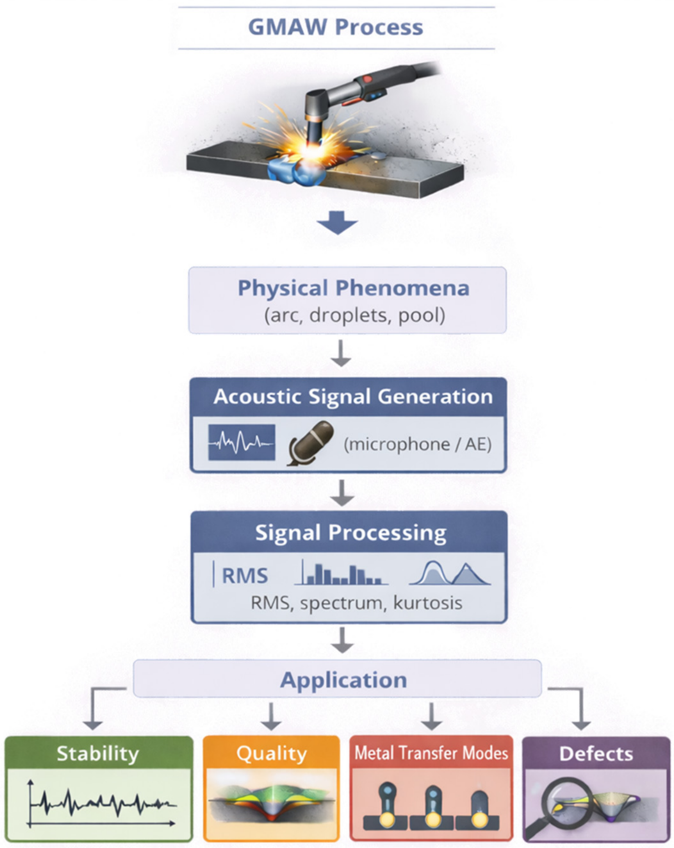

Figure 2: Overview of main application domains of acoustic analysis in GMAW

3. ACOUSTIC MEASUREMENT AND SIGNAL PROCESSING IN GMAW

The effectiveness of the acoustic analysis in the GMAW process is highly dependent on the applied measurement strategy and subsequent signal processing techniques. Given the complex and noisy industrial environment in which GMAW is most often performed, careful selection of acoustic sensors, measurement configurations, and signal processing methods is necessary to ensure reliable extraction of information relevant to the welding process. Over the past decades, various approaches to acoustic monitoring and analysis have been proposed, ranging from simple audible sound measurements to advanced acoustic emission systems combined with machine learning algorithms.

3.1. Acoustic sensing techniques and sensor configurations

Acoustic monitoring of the GMAW process is most often carried out using measurements of airborne sound, based on the use of microphones or using structural AE sensors. Airborne sound measurement relies on microphones placed near the welding arc, which register the audible sound generated during the process. This approach is non-intrusive, simple to implement, and economically viable, which makes it particularly suitable for industrial applications [8],[45,46]. Microphone-based measurements have been successfully applied for online monitoring of welding process stability, metal transfer behavior, and weld quality. Several studies have shown that even a single microphone can provide enough acoustic information for the detection of process instabilities and welding defects, if appropriate signal processing techniques are applied [1,2], [22], [25].

In recent research, systems with microphone arrays have been introduced to improve spatial resolution and resistance to the influence of ambient noise, which enables dynamic localization and monitoring of acoustic sources in the welding zone [47]. Using spatial filtering and beamforming techniques, microphone arrays enable the separation of the sound associated with the welding arc from ambient noise and reflections, which is of particular importance in industrial environments with complex acoustic conditions. Early methodological frameworks for the systematic characterization of the acoustics of the GMAW process, including the selection of sensor positions and frequency ranges, were discussed in [48], which laid the foundation for the later development of spatial and array acoustic monitoring. In addition to process stability monitoring, arc sound measurement has also been applied in spatial process monitoring tasks, such as seam monitoring in GMAW welding in narrow grooves, which further confirms the versatility of microphone-based acoustic measurements [49].

Unlike airborne sound measurement, acoustic emission measurements using AE sensors involve piezoelectric transducers mounted directly on the workpiece or welding fixture to detect high-frequency elastic waves propagating through the material. AE sensors are particularly sensitive to transient microstructural events, such as crack initiation, plastic deformation, and molten metal droplet impact, which is why measurements obtained using AE sensors have been widely applied in welding research and in NDT methods [3],[15],[19]. Compared to microphones, acoustic emission measurements performed using AE sensors are less susceptible to the influence of ambient acoustic noise; however, their practical application requires careful positioning of the sensors and high-quality mechanical coupling with the material. These requirements may limit the applicability of AE sensor-based measurement systems in certain manufacturing environments, despite their high sensitivity to defect-related phenomena.

3.2. Signal acquisition and preprocessing

Acoustic signals collected during the GMAW process are typically characterized by non-stationary behavior, a wide dynamic range, and a pronounced influence of ambient noise. Therefore, signal preprocessing plays a key role in extracting meaningful information from raw measurements. Common preprocessing steps include signal amplification, analog and digital filtering, segmentation, and normalization.

Band-pass filtering is widely used to suppress low-frequency mechanical noise and high-frequency electronic interference, which separates the frequency bands that are most relevant for phenomena in the welding process [9,10],[50]. Signal segmentation, which is usually based on windows of fixed length or synchronized with welding current and voltage signals, allows time-resolved analysis of transient events, such as short circuits and the separation of molten metal droplets [23-25]. In industrial settings, additional noise reduction techniques, including spectral subtraction, adaptive filtering, and robust statistical thresholding, are applied to improve signal-to-noise ratio and increase detection reliability [23],[25]. These procedures are particularly important for microphone-based measurements, which are carried out in acoustically harsh environments typical of welding processes.

3.3. Time-domain and frequency-domain analysis

Time domain analysis is the simplest and historically the earliest approach to the characterization of acoustic signals in the GMAW process. Due to its simplicity and low computational cost, time-domain analysis has been widely applied in both early and modern GMAW process research. The most commonly used statistical acoustic features in the time domain include RMS, peak amplitude, variance, skewness, kurtosis, and zero-crossing rate. These descriptors provide concise statistical representations of the amplitude fluctuations and impulse character of an acoustic signal.

Numerous studies have shown that statistical acoustic features in the time domain are strongly correlated with the stability of the welding process, especially in the short-circuit GMAW mode. Improper metal transfer, arc extinction and enhanced spatter lead to increased signal variability and impulse amplitude distributions, which are effectively detected by means of RMS value, variance, and kurtosis [22], [24,25]. As a result, time domain statistical acoustic features have been successfully used to detect unstable welding conditions and to monitor the regularity of short circuits in real time.

Frequency domain analysis, which is most often based on the fast Fourier transform (FFT), provides complementary information by revealing the dominant frequency components and spectral energy distribution of the welding sound. Spectral analysis enables the identification of periodic phenomena associated with arc dynamics and metal transfer mechanisms, which are not always clearly visible in the time domain. Several studies have shown that different welding regimes and modes of metal transfer have characteristic spectral features, expressed through dominant frequency peaks, changes in spectrum width, and spectral energy concentration [9-12], [51].

Frequency features, such as dominant frequency, spectral centroid, spectral width, and spectral energy ratios, have been effectively applied to classify process stability and metal transfer modes. In stable spray transfer, the acoustic spectrum is typically characterized by more concentrated and narrowband frequency content, while short-circuit transfer produces broadband spectra with pronounced low-frequency components [9,10], [26], [39]. These spectral differences represent the physical basis for the classification of welding modes based on acoustic signals.

Despite their effectiveness, time and frequency domain analyses have inherent limitations when applied to non-stationary welding signals. Conventional FFT methods assume the stationarity of the signal within the analyzed time window, which can lead to the masking of transient events, such as short-circuit transitions and sudden arc disturbances. Therefore, although time and frequency features remain valuable for the global characterization of welding process behavior, they are often supplemented with time-frequency analysis techniques to capture the dynamic evolution of acoustic phenomena during the GMAW process [24].

3.4. Time-frequency analysis and advanced signal processing

Considering the non-stationary character of the acoustic signals generated during the GMAW process, time-frequency analysis methods have attracted considerable attention in modern research. Short-time Fourier transform (STFT) and spectrogram-based analyses allow the simultaneous observation of temporal and spectral signal changes, which makes them particularly suitable for the detection of transient events and the identification of welding process instabilities [24], [25].

More advanced techniques, including wavelet-based methods and other adaptive time-frequency approaches, have been applied to improve time-frequency resolution and increase sensitivity to localized phenomena, such as short-circuit transitions and defect initiation [29,30],[50]. In addition, advanced signal decomposition techniques, such as empirical mode decomposition (EMD), have been used to analyze airborne acoustic signals in welding processes, enabling more accurate characterization of non-stationary acoustic behavior [52].

These approaches enable the adaptive decomposition of acoustic signals into components that can be directly related to the underlying dynamics of the welding process. In this way, time-frequency and adaptive methods significantly contribute to a more precise extraction of statistical acoustic features and a more reliable classification of welding modes and process conditions.

3.5. Statistical acoustic feature extraction and data-driven analysis

The extracted statistical acoustic features represent input quantities for statistical and data-driven models used in monitoring the welding process and evaluating the quality of the welded joint. Classical approaches include correlation analysis, regression modeling, and statistical decision-making methods, where the feasibility of predicting weld quality indicators based on acoustic data has been demonstrated [4,5]. However, most existing data-driven approaches rely on empirical correlations between features and process states, while physically based sound source models are still rarely integrated into such analyses.

In addition to conventional physical and statistical acoustic features, psycho-acoustic descriptors were investigated in a limited number of studies in order to characterize subjectively perceived sound quality during the GMAW process. These works indicate a potential connection between human auditory perception and the stability of the welding process, further confirming the informational value of the acoustic signal [13].

In recent years, ML techniques, such as support vector machines (SVM), artificial neural networks (ANN), and convolutional neural networks (CNN), have been increasingly applied in the analysis of acoustic signals in GMAW. These approaches enable automated classification of metal transfer modes, detection of process anomalies, and prediction of weld quality with increased model robustness and adaptability [29-32], [53]. Despite the encouraging results, the success of such models still largely depends on the quality of signal acquisition, preprocessing procedures, and the selection of relevant features.

It should be emphasized that the goal of this review paper is not an exhaustive consideration of the theory of signal processing and ML, but to highlight representative approaches that have shown practical relevance for the acoustic analysis of the GMAW process.

4. APPLICATIONS OF ACOUSTIC ANALYSIS IN GMAW

Acoustic analysis has been intensively researched over the past decades as a non-intrusive and information-rich method for monitoring and diagnostics of the GMAW process. Due to its sensitivity to arc behavior, metal transfer dynamics, and molten pool instability, acoustic measurement has found application in several key areas of GMAW process analysis, including process stability monitoring, weld quality assessment, metal transfer mode classification, and weld defect detection (Figure 2). This chapter provides a structured overview of the main application areas of acoustic analysis identified in the relevant literature.

4.1. Process monitoring and stability assessment

One of the earliest and most frequently researched applications of acoustic analysis in the GMAW process is process stability monitoring. Welding stability is closely related to metal transfer regularity, arc length consistency, and controlled heat input, all of which directly affect the acoustic emission generated during welding. Numerous studies have shown that stable and unstable welding modes exhibit clearly different acoustic characteristics in the time and frequency domains, thus confirming the sensitivity of sound signals to changes in process stability [22-25].

In the short-circuit GMAW process, instability is most often associated with irregular short circuit durations, increased metal spatter, and arc extinction. These phenomena lead to the appearance of impulsive acoustic emissions characterized by increased amplitude variability and broadband spectral content. It has been shown that temporal acoustic parameters, such as RMS, variance, and kurtosis, strongly correlate with the regularity of short circuits and the overall stability of the welding process [1-5], [25].

Analyzes in the frequency and time-frequency domains further increase the sensitivity to transient disturbances, enabling the early detection of unstable operating conditions that may not be clearly observed solely based on electrical current and voltage signals [23,24]. Several authors pointed out that acoustic monitoring of process stability can complement, and in certain cases replace, conventional analysis of electrical signals, especially when current and voltage measurements are not sensitive enough to subtle disturbances in arc behavior.

An additional advantage of acoustic process monitoring is reflected in the non-contact character of microphone-based measurements, which makes this method particularly suitable for industrially oriented research and experimental applications where sensor integration and maintenance requirements are of key importance [45,46]. In addition to single-sensor approaches, spatially distributed measurements using microphone arrays have been proposed to increase robustness and spatial resolution in dynamic monitoring of welding processes, especially in industrial environments with complex acoustic conditions [47]. In addition to stability assessment, arc sound analysis has also been successfully applied in spatial process monitoring tasks, such as seam monitoring in GMAW procedures with a narrow gap, which further confirmed the versatility of acoustic signals in monitoring welding processes [49].

4.2. Weld quality evaluation and penetration assessment

In addition to process stability monitoring, acoustic analysis has been intensively researched in the context of weld quality assessment, including penetration depth, weld geometry, and overall weld integrity. Changes in heat input, arc behavior, and weld pool dynamics directly affect the acoustic emission generated during the GMAW process, making sound signals sensitive indicators of weld formation and weld quality. In this way, acoustic measurement enables a non-contact and indirect approach to the assessment of weld quality in real time during the welding process itself.

Numerous studies have indicated a strong correlation between statistical acoustic parameters and penetration conditions during GMAW. Temporal and spectral descriptors of arc sound have been shown to reflect changes in weld pool behavior associated with insufficient or excessive penetration [14], [31], [50],[54]. Unstable penetration conditions often lead to increased variability of the acoustic signal and the appearance of characteristic spectral patterns, which makes it possible to separate acceptable welds from those with defects.

Regression and statistical models are widely applied to quantify the relationship between statistical acoustic parameters and weld quality indicators. Shahabi and Kolahan [5] showed that acoustic signals contain complementary information compared to conventional electrical parameters, whereby combining these two types of signals leads to an increase in the accuracy of quality prediction. These results confirm the potential of acoustic measurement as a soft-sensor approach for online assessment of weld quality parameters.

More recent research is focused on the application of ML methods to improve the assessment of weld quality based on acoustic data. ANN, SVM, and deep learning models have been successfully used to classify penetration states and predict quality metrics under controlled experimental conditions [5], [31,32]. These approaches enable the automated interpretation of complex acoustic patterns that are often difficult to capture with classical methods based solely on manually defined features.

Given that welding technique and process stability directly affect local stresses, deformations, and microstructural evolution in welded joints, acoustic signals that reflect these dynamic phenomena can also be seen as indirect indicators of the structural integrity of the weld [55]. Nevertheless, despite the encouraging results, the robustness and general applicability of acoustic models for quality assessment are still limited by process variability, the influence of ambient noise, and differences in experimental and industrial settings. These limitations point to the need for further validation and integration of acoustic measurement with complementary sensing approaches in industrial applications.

4.3. Acoustic-based classification of metal transfer modes

The classification of metal transfer modes represents one of the most important areas of application of acoustic analysis in GMAW. Different transfer modes - short-circuit, globular, spray, and pulse are based on different droplet formation and separation mechanisms, which largely determine arc stability, heat input, spatter occurrence, and weld quality. As these physical processes directly affect pressure fluctuations in the arc and molten metal, they are naturally reflected in the emitted acoustic signal. Figure 3 shows schematically the characteristic physical behavior and corresponding acoustic signatures associated with different modes of metal transfer in the GMAW process.

Experimental research has consistently shown that each metal transfer mode possesses characteristic acoustic signatures. Short-circuit metal transmission is associated with pulsed acoustic patterns synchronized with arc extinguishing and reignition events, resulting in broadband spectral content and high temporal variability of the signal. In contrast, spray metal transfer generates more continuous and stable acoustic emissions, dominated by periodic components associated with droplet separation frequency [9,10],[27,28]. In the pulse GMAW procedure, additional modulation effects appear, which lead to the appearance of characteristic time-frequency structures in the acoustic signal [33], [34].

Time-frequency representations, such as spectrograms and STFTs, have proven particularly effective for analyzing transitions between different metal transfer modes and identifying unstable operating regions. These methods enable the visualization of transient events and periodic structures that are difficult to observe using only temporal or frequency analysis [24],[29,30]. Therefore, time-frequency features are widely used as discriminative descriptors in the classification of metal transfer modes.

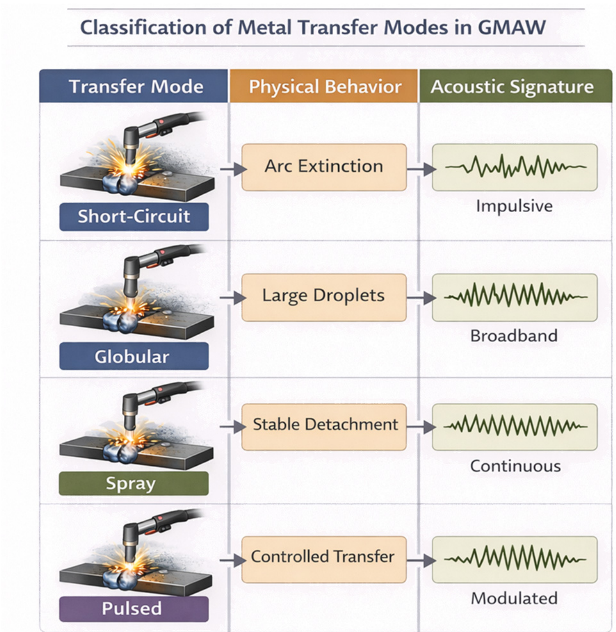

Figure 3: Classification of metal transfer modes in GMAW
and their corresponding physical behavior and acoustic signatures

In recent research, increasing attention has been paid to the automated classification of metal transfer modes using acoustic features in combination with ML methods. Supervised approaches, including ANNs and other classifiers, have demonstrated reliable transmission mode discrimination based solely on sound measurements [11,12], [26], [39], [56]. These results indicate the feasibility of identifying metal transfer modes without direct access to electrical signals, which is particularly relevant for non-contact process monitoring and adaptive control applications.

Despite the encouraging results, the robustness of the acoustic classification of the metal transfer mode is still affected by process variability, sensor position, and ambient noise. In transient or unstable welding modes, overlapping acoustic characteristics may occur, making it difficult to clearly separate the modes. Therefore, acoustic classification is often most effective when combined with complementary sensory approaches or physically based constraints. Nevertheless, the strong connection between metal transfer physics and acoustic emission validates sound analysis as a powerful tool for identifying metal transfer modes and represents a natural link between process stability assessment and weld quality evaluation.

4.4. Detection and identification of welding defects

The detection and identification of welding defects is one of the earliest and most established areas of application of acoustic measurement in welding processes. Acoustic emission techniques have a long tradition in the field of NDT and are among the first methods to demonstrate the possibility of detecting phenomena associated with errors in real time, during the welding process itself. Pioneering research by Jolly [15,16] showed that acoustic emission signals can detect crack initiation, porosity occurrence, and the presence of inclusions during welding and subsequent cooling of the weld metal, thus highlighting the potential of acoustic monitoring for in-process defect detection.

In the GMAW process, various types of defects, including burn-through, lack of fusion, porosity, and crack formation, are associated with characteristic disturbances in arc behavior and molten pool dynamics, which are reflected in the acoustic signal. Experimental research has shown that sudden changes in acoustic emission energy, impulse activity, and frequency content of the signal are closely related to mechanisms of error initiation and growth [3], [18,19], [57,58]. These results established a direct link between physical events associated with defects and measurable statistical acoustic features.

Burn-through detection represents one of the most successful and extensively researched applications of acoustic monitoring in the field of defect identification. Rapid changes in molten pool stability and excessive heat input generate characteristic acoustic signatures that can be detected earlier than by visual inspection or post-process NDT methods [1-3], [19]. The sensitivity of acoustic signals to these transient events enables the timely identification of critical defects and supports the implementation of corrective interventions during the process.

In addition to the detection itself, several studies investigated the possibility of classifying the types of defects based on the characteristics of the acoustic emission. Parameters such as signal energy, amplitude distribution, and frequency content have been linked to specific defect mechanisms, allowing the distinction of lack of fusion, porosity-related phenomena, and other imperfections [3,4],[59]. These approaches confirm that acoustic features contain defect type-specific information, although reliable classification often requires careful feature selection and appropriate calibration.

In recent research, increasing attention has been paid to the application of data-based methods to improve the detection and identification of defects using acoustic signals. ML techniques have been applied to acoustic data to automatically recognize defect-related patterns and process anomalies with greater robustness compared to rule-based methods [4], [29,30], [32]. These approaches are particularly promising for complex industrial environments, but their success still depends on data quality, labeling accuracy, and process variability.

Despite its proven effectiveness, acoustic defect detection in the GMAW process faces limitations related to ambient noise, overlapping acoustic signatures, and sensitivity to sensor position. Statistical acoustic features associated with defects can overlap with signals generated by transient but non-destructive process instabilities, making reliable identification difficult under certain conditions. Therefore, defect detection is most effective when acoustic measurement is combined with complementary monitoring methods or integrated into multi-sensor systems. Nevertheless, the proven ability of acoustic analysis to detect and characterize welding defects in real time highlights its importance as a non-contact diagnostic method within intelligent GMAW process monitoring systems.

5. CHALLENGES AND FUTURE RESEARCH DIRECTIONS

Despite the significant progress achieved in the application of acoustic analysis in the GMAW process, numerous technical and methodological challenges still limit its wider industrial application. At the same time, the development of new technologies and modern research directions opens up new opportunities for the improvement of acoustically based monitoring and management of GMAW processes.

5.1. Challenges in acoustic-based monitoring of GMAW

One of the main challenges associated with the application of acoustic measurement in the GMAW process is the pronounced sensitivity to ambient noise. Industrial environments where welding is most commonly performed are characterized by high levels of ambient noise, originating from auxiliary equipment, ventilation systems, and adjacent manufacturing operations. This problem is particularly pronounced when measuring sound in the air using a microphone, where reflections and ambient disturbances can significantly degrade the quality of the signal [25], [45].

Although some noise effects can be mitigated by applying appropriate signal preprocessing and filtering techniques, reliable noise suppression still represents one of the key challenges.

Sensor position and measurement configuration represent additional sources of acoustic signal variability. The measured acoustic signal strongly depends on the relative position of the microphone or AE sensor in relation to the arc, the geometry of the workpiece, and the fixture conditions. As a result, repeatability and comparability of acoustic measurements between different experimental and industrial settings are difficult to achieve without clearly defined and standardized guidelines [9,10],[46]. The absence of standardization further limits the transferability of acoustically based models between laboratory research and real industrial applications.

An additional challenge is the complex and non-linear relationship between statistical acoustic features and physical phenomena in the welding process. The acoustic signal is simultaneously influenced by arc dynamics, metal transfer behavior, shielding gas flow, and molten metal pool oscillations, which significantly complicates the physical interpretation of isolated features [11,12],[35]. Although data-driven models have shown encouraging performance, their dependence on large and reliably annotated data sets raises issues of overlearning and generalization, especially when changing welding parameters, material type, or joint configuration [29,30],[32].

5.2. Integration with multi-sensor and intelligent welding systems

Future research in the field of acoustically based monitoring of GMAW processes is expected to increasingly focus on the integration of acoustic measurement with other monitoring modalities, such as electrical signals, optical sensors, and thermal measurements. Each of these measurement techniques covers different aspects of the welding process, while their combination allows a more complete and robust representation of the process behavior. In this context, acoustic signals represent a valuable complementary source of information, thanks to their sensitivity to dynamic phenomena and their non-intrusive nature.

It has been shown that data fusion from multiple sensors significantly improves the reliability and robustness of welding process monitoring, compensating for the limitations of individual measurement methods. Electrical signals provide direct information on energy delivery, while optical and thermal measurements provide spatially resolved insight into the behavior of the arc and molten metal pool. Acoustic measurement complements these techniques by recording indirect but physically meaningful manifestations of arc dynamics, metal transfer, and process instabilities [6,7]. As a result, hybrid monitoring systems can realize increased sensitivity to subtle process disturbances and early stages of defect formation.

Growing interest in intelligent welding systems and Industry 4.0 concepts has further stimulated research aimed at integrating acoustic measurement into data-driven frameworks for process monitoring and control. ML methods enable automatic feature extraction, anomaly detection, and classification based on heterogeneous sensor data sets, including acoustic signals. Recent research has shown that acoustic information can significantly improve the performance of intelligent monitoring systems when combined with other sensory inputs, especially in quality prediction and anomaly detection tasks [31,32], [38].

In addition to monitoring, acoustic measurement has also been investigated as an input for adaptive control and robotic welding systems. Early cognitive and learning welding concepts demonstrated the feasibility of using acoustic data to guide process corrections and support automated decision-making in robotic environments. These early approaches represent important precursors to modern intelligent welding systems, in which real-time feedback is used to optimize process parameters and ensure consistent weld quality.

Despite the encouraging results, the integration of acoustic measurement into multi-sensor and intelligent welding systems still faces significant challenges. Differences in sampling rates, data synchronization, sensor placement, and signal interpretation make efficient data fusion difficult. In addition, many data-driven models still suffer from a lack of physical interpretability, which may limit their acceptance and confidence in industrial applications. Therefore, future research should be directed towards the development of physically informed and explainable models, standardized data fusion strategies and robust validation under different welding conditions and for different materials, to fully exploit the potential of acoustic measurement within intelligent GMAW process monitoring systems.

5.3. Toward physically grounded modeling and standardization

One of the key directions of future research in the field of acoustic analysis of the GMAW process is the development of physically based models capable of explaining and predicting the mechanisms of sound generation during welding. Although numerous experimental studies have shown strong correlations between statistical acoustic features and welding process behavior, most existing approaches rely on empirical relationships. Such an approach limits their general applicability and predictive power, especially when changing process parameters, materials or geometry of the welded joint.

Recent research efforts have begun to overcome this gap by developing analytical and numerical models that explicitly link arc plasma dynamics, metal transfer behavior, and energy release mechanisms to acoustic emission. Lumped-parameter models and simplified physical representations provided valuable insight into the coupling between welding physics and sound generation, further strengthening the theoretical basis of acoustically based process monitoring [35]. However, these models often include simplifying assumptions and remain limited in their ability to fully capture the complex, nonlinear, and multi-physics nature of the GMAW process.

Further progress in this area is expected to benefit significantly from a closer integration of physical modeling and data-driven approaches. Physically informed ML models represent a promising direction towards improved interpretability and robustness, as they enable the incorporation of domain knowledge into data-driven frameworks. Such hybrid approaches could reduce the dependence on large, precisely labeled data sets, while improving the ability to extrapolate to previously unexplored welding conditions, thereby addressing one of the key limitations of purely empirical acoustic analysis.

In parallel with the improvement of physical modeling, the establishment of standardized measurement procedures and analysis methodologies is a necessary step towards the maturation of acoustically based welding monitoring. Currently, there is considerable variability in the literature regarding sensor types, their positioning strategies, analyzed frequency ranges, feature definitions, and evaluation criteria. The absence of standardization makes it difficult to compare results and slows down the transfer of research achievements to industrial practice. The development of consensus guidelines for acoustic measurements in the GMAW process would contribute to greater reproducibility, comparability and wider acceptance of this technology.

Efforts toward standardization, combined with improved physical modeling, would significantly increase the credibility and industrial relevance of acoustic measurement. Clearly defined measurement protocols and physically interpretable models would enable reliable verification, validation, and integration of acoustic monitoring systems into production environments. Ultimately, the convergence of physically based understanding, data-driven intelligence, and standardized practices is expected to play a key role in transitioning acoustic analysis from a promising research tool to a reliable component of intelligent systems for monitoring and managing GMAW processes.

6. CONCLUSIONS

This paper provides a comprehensive overview of the application of acoustic analysis in GMAW, with special emphasis on its role as a valuable supplementary method for monitoring the welding process, especially in applications that require real-time insight into dynamic phenomena during welding. The reviewed literature shows that the acoustic signals generated during the GMAW process originate from fundamental physical phenomena, including arc plasma dynamics, metal transfer behavior, shielding gas flow, and molten pool oscillations. As a consequence, welding sound inherently reflects key aspects of process stability and weld formation.

During decades of research, acoustic measurement has been successfully applied to a wide range of tasks associated with the GMAW process. These applications include real-time process stability monitoring, metal transfer mode classification, weld quality and penetration depth assessment, as well as welding defect detection, such as penetration, lack of fusion, and porosity. Techniques based on audible sound and acoustic emission have been shown to provide valuable and complementary information compared to conventional electrical and optical measurement methods, especially in applications requiring non-contact monitoring and real-time process monitoring.

6.1. Scope and contribution of the review

Unlike earlier review papers that consider acoustic measurement in welding at a broader or predominantly technological level, this review paper provides a focused and physically grounded synthesis of acoustic analysis, specifically applied to the GMAW process. By explicitly relating sound generation mechanisms to arc plasma dynamics, metal transfer behavior, and molten pool phenomena, the work contributes to bridging the gap between welding physics and signal analysis-based approaches for process monitoring. Compared to previous reviews, this paper uniquely emphasizes the physical interpretation of acoustic signals in the context of arc dynamics and metal transfer mechanisms in the GMAW process. Additionally, the paper systematically categorizes the primary application areas of acoustic analysis in the GMAW process, including process stability assessment, weld quality evaluation, metal transfer mode classification, and welding defect detection. Contemporary trends towards intelligent, data-driven, and multi-sensor welding systems are also highlighted, providing a coherent frame of reference for both researchers and practicing engineers. The analyzed literature as a whole shows the diversity of sensor approaches, analysis methods, and application areas of acoustic analysis in the GMAW process, ranging from early rule-based systems to modern systems based on ML and data analysis.

6.2. Current limitations and future perspectives

Advances in the field of signal processing and data-driven analysis have significantly expanded the possibilities of acoustic monitoring of the welding process. The characteristics in the time, frequency, and time-frequency domains, in combination with statistical methods and ML algorithms, enabled an increasingly precise classification and prediction of the state of the welding process. The latest developments in the field of artificial intelligence and intelligent welding systems, conceptually illustrated in Figure 4, indicate the growing potential of integrating acoustic measurement into adaptive control frameworks and production environments based on Industry 4.0 concepts.

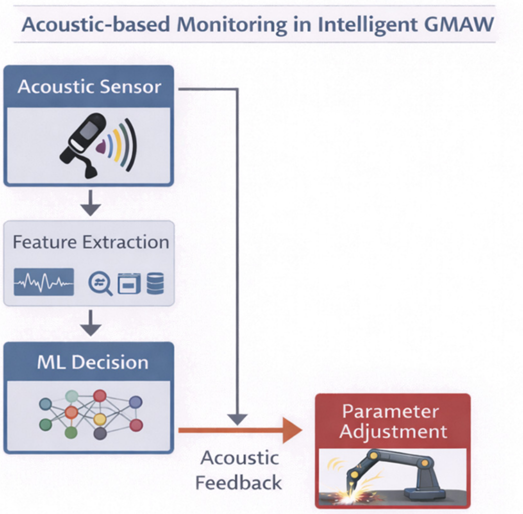

Figure 4: Conceptual framework of acoustic-based monitoring and intelligent control in GMAW

Despite these achievements, significant challenges remain, including sensitivity to ambient noise, dependence on sensor position, limited standardization, and the complexity of interpreting statistical acoustic features in highly dynamic welding conditions. Overcoming these limitations will require continuous development of robust signal processing methods, efficient data fusion from multiple sensors, physically based modeling of sound generation mechanisms, as well as establishment of standardized measurement and evaluation procedures.

Taken as a whole, acoustic analysis represents a mature but still evolving research area with significant potential for improving the monitoring and management of GMAW processes. Further integration of physical process understanding, advanced signal processing methods, and intelligent data-driven approaches is expected to further strengthen the role of acoustic measurement as a practical and reliable tool for ensuring weld quality and process stability in modern welding applications.

ACKNOWLEDGEMENTS

The authors express their gratitude to the Ministry of Science, Technological Development and Innovation of the Republic of Serbia for supporting this research (Contract No. 451-03-34/2026-03/200108). This research contributes to the United Nations 2030 Agenda for Sustainable Development, specifically to Sustainable Development Goal 9: Build resilient infrastructure, promote inclusive and sustainable industrialization and foster innovation.

REFERENCES

[1] E. H. Cayo and S. C. A. Alfaro, "GMAW process stability evaluation through acoustic emission by time and frequency domain analysis", Journal of Achievements in Materials and Manufacturing Engineering, Vol. 34, pp. 157-164, (2009)

[2] E. H. Cayo and S. C. A. Alfaro, "A non-intrusive GMA welding process quality monitoring system using acoustic sensing", Sensors, Vol. 9, pp. 7150-7166, https://doi.org/10.3390/s90907150, (2009)

[3] A. M. Apasov and A. A. Apasov, "Acoustic emission diagnostics of faulty fusion in welding", Proceedings of the 7th International Forum on Strategic Technology - IFOST 2012, September 2012, https://doi.org/10.1109/IFOST.2012.6357718, (2012)

[4] W. Wang, Y. Dou, H. Wei, H. Heng, and Y. Zhen, "Study on acoustic emission source character of various welding defect types", Advanced Materials Research, Vol. 383-390, pp. 1926-1932, https://doi.org/10.4028/www.scientific.net/AMR.383-390.1926, (2012)

[5] H. Shahabi and F. Kolahan, "Regression modeling of welded joint quality in gas metal arc welding process using acoustic and electrical signals", Proceedings of the Institution of Mechanical Engineers, Part B: Journal of Engineering Manufacture, Vol. 229, pp. 1711-1721, https://doi.org/10.1177/0954405414539933, (2015)

[6] S. C. A. Alfaro and E. H. Cayo, "Sensoring fusion data from the optic and acoustic emissions of electric arcs in the GMAW-S process for welding quality assessment", Sensors, Vol. 12, pp. 6953-6966, https://doi.org/10.3390/s120606953, (2012)

[7] J. Grum, Z. Bergant, and I. Polajnar, "Monitoring the GMAW process by detection of welding current, light intensity and sound", Proceedings of the NDE for Safety/Defektoskopie 2012, Seč u Chrudimi (Czech Republic), 30 October 1 November 2012, pp. 291-300, (2012)

[8] E. Schiebeck, "Audible range acoustic diagnosis of the MAG welding arc", Welding International, Vol. 5, pp. 572-576, https://doi.org/10.1080/09507119109447842, (1991)

[9] M. Čudina and J. Prezelj, "Evaluation of the sound signal based on the welding current in the gas-metal arc welding process", Proceedings of the Institution of Mechanical Engineers, Part C: Journal of Mechanical Engineering Science, Vol. 217, pp. 483-494, https://doi.org/10.1243/095440603765226777, (2003)

[10] J. Prezelj and M. Čudina, "Noise as a signal for on-line estimation and monitoring of welding process - The initial research", Acta Acustica United with Acustica, Vol. 89, pp. 280-286, (2003)

[11] S. Zhao, X. Qiu, I. Burnett, M. Rigby, and A. Lele, "GMAW metal transfer mode identification from welding sound", Proceedings of the Australian Acoustical Society Annual Conference – Acoustics 2018, Adelaide (Australia), 7-9 November 2018, pp. 482-491, https://doi.org/10.13140/RG.2.2.29265.97123, (2018)

[12] S. Zhao, X. Qiu, I. Burnett, M. Rigby, and A. Lele, "Statistical characteristics of gas metal arc welding (GMAW) sound", Proceedings of the 23th International Congress on Acoustics - ICA 2019, Aachen (Germany), 9-13 September 2019, pp. 7594-7601, https://doi.org/10.18154/RWTH-CONV-238970, (2019)

[13] J. Tam and J. Huissoon, "Developing psycho-acoustic experiments in gas metal arc welding", Proceedings of the IEEE International Conference on Mechatronics & Automation 2005, Niagara Falls (Canada), July 2005, pp. 1112-1117, https://doi.org/10.1109/ICMA.2005.1626707, (2005)

[14] Y. Gao, J. Zhao, Q. Wang, J. Xiao, and H. Zhang, "Weld Bead penetration identification based on human-welder subjective assessment on welding arc sound", Measurement: Journal of the International Measurement Confederation, Vol. 154, https://doi.org/10.1016/j.measurement.2020.107475, (2020)

[15] W. D. Jolly, "The use of acoustic emission as a weld quality monitor", Battelle Memorial Institute, Research Report BNWL-SA-2727, Richland Washington (USA), (1969)

[16] W. D. Jolly, "The application of acoustic emission to in-process weld inspection", Battelle Memorial Institute, Research Report BNWL-SA-2212, Richland Washington (USA), (1973)

[17] T. Hopwood and J. H. Havens, "Acoustic emission monitoring of weldments", Journal of Testing and Evaluation, Vol. 7, pp. 216-222, https://doi.org/10.1520/JTE11383J, (1979)

[18] A. Sala, F. Tonolini, G. Villa and G. Nardoni, "Monitoring of acoustic emission during the welding process", Welding International, Vol. 1, pp. 655-658, https://oi.org/10.1080/09507118709453014, (1987)

[19] P. G. Bentley, D. G. Dawson, and D. W. Prine, "An evaluation of acoustic emission for the detection of defects produced during fusion welding of mild and stainless steels", NDT International, Vol. 15, pp. 243-249, https://doi.org/10.1016/0308-9126(82)90033-5, (1982)

[20] A. Nedoseka, "Fundamentals of evaluation and diagnostics of welded structures", Woodhead Publishing, Cambridge (United Kingdom), (2012)

[21] A. M. Apasov and A. A. Apasov, "Examination of acoustic emission in welding of austenitic steels", Welding International, Vol. 15, pp. 466-472, https://doi.org/10.1080/09507110109549388, (2001)

[22] D. Saini and S. Floyd, "An investigation of gas metal arc welding sound signature for on-line quality control", Welding Journal, Vol. 77, pp. 172-179, (1998)

[23] L. Grad, J. Grum, I. Polajnar, and J. M. Slabe, "Feasibility study of acoustic signals for on-line monitoring in short circuit gas metal arc welding", International Journal of Machine Tools and Manufacture, Vol. 44, pp. 555-561, https://doi.org/10.1016/j.ijmachtools.2003.10.016, (2004)

[24] E. J. Macías, A. S. Roca, H. C. Fals, J. B. Fernández, and M. P. de La Parte, "Time-frequency diagram applied to stability analysis in gas metal arc welding based on acoustic emission", Science and Technology of Welding and Joining, Vol. 15, pp. 226-232, https://doi.org/10.1179/136217110X12665778348588, (2010)

[25] J. Horvat, J. Prezelj, I. Polajnar, and M. Čudina, "Monitoring gas metal arc welding process by using audible sound signal", Strojniški Vestnik - Journal of Mechanical Engineering, Vol. 57, pp. 267-278, https://doi.org/10.5545/sv-jme.2010.181, (2011)

[26] M. Cullen, S. Zhao, and J. C. Ji, "Acoustic based classification of transfer modes in gas metal arc welding", Proceedings of the Annual Conference of the Australian Acoustical Society 2021: Making Waves, Wollongong (Australia), 21-23 February 2021, pp. 51-57, (2021)

[27] K. Pal, S. Bhattacharya, and S. K. Pal, "Prediction of metal deposition from arc sound and weld temperature signatures in pulsed MIG welding", The International Journal of Advanced Manufacturing Technology, Vol. 45, pp. 1113-1130, https://doi.org/10.1007/s00170-009-2052-5, (2009)

[28] K. Pal, S. Bhattacharya, and S. K. Pal, "Investigation on arc sound and metal transfer modes for on-line monitoring in pulsed gas metal arc welding", Journal of Materials Processing Technology, Vol. 210, pp. 1397-1410, https://doi.org/10.1016/j.jmatprotec.2010.03.029, (2010)

[29] A. S. Roca, H. C. Fals, J. B. Fernández, E. J. Macías, and M. P. de la Parte, "Artificial neural networks and acoustic emission applied to stability analysis in gas metal arc welding", Science and Technology of Welding and Joining, Vol. 14, pp. 117-124, https://doi.org/10.1179/136217108X382981, (2009)

[30] A. S. Roca, H. C. Fals, J. B. Fernández, F. S. Adán, and E. J. Macías, "Stability analysis of the gas metal arc welding process based on acoustic emission technique", Welding International, Vol. 23, pp. 173-180, https://doi.org/10.1080/09507110802543385, (2009)

[31] L. Na, X. Yanling, L. Sichen, Y. Xinwen, and C. Shanben, "Automated control of welding penetration based on audio sensing technology", Journal of Materials Processing Technology, Vol. 250, pp. 81-98, https://doi.org/10.1016/j.jmatprotec.2017.07.005, (2017)

[32] M. Rohe, B. N. Stoll, J. Hildebrand, J. Reimann, and J. P. Bergmann, "Detecting process anomalies in the GMAW process by acoustic sensing with a convolutional neural network (CNN) for classification", Journal of Manufacturing and Materials Processing, Vol. 5, https://doi.org/10.3390/jmmp5040135, (2021)

[33] L. Yi, D. Yunfei, Z. Liang, H. Jingtao, W. Rui, and X. Xiaojian, "Study on the thermo-effect of P-GMAW characterized by structure-borne acoustic emission signals detected in welding on aluminum alloy", Measurement: Journal of the International Measurement Confederation, Vol. 92, pp. 200-207, https://doi.org/10.1016/j.measurement.2016.06.027, (2016)

[34] L. Yi, Z. Yang, X. Xiaojian, and W. Rui, "Study on the transient impact energy of metal droplet transfer in P-MIG welding based on acoustic emission signals analysis", Materials & Design, Vol. 90, pp. 22-28, https://doi.org/10.1016/j.matdes.2015.10.112, (2016)

[35] S. Zhao, X. Qiu, I. Burnett, M. Rigby, and A. Lele, "A lumped-parameter model for sound generation in gas metal arc welding", Mechanical Systems and Signal Processing, Vol. 147, https://doi.org/10.1016/j.ymssp.2020.107085, (2021)

[36] M. Čudina, J. Prezelj, and P. Lipar, "Use of audible sound for monitoring of transient phenomena in mechanical engineering - An overview", (2016)

[37] M. F. M. Yusof, M. Ishak, and M. F. Ghazali, "Acoustic methods in real-time welding process monitoring: Application and future potential advancement", Journal of Mechanical Engineering and Sciences, Vol. 15, pp. 8490-8507, https://doi.org/10.15282/jmes.15.4.2021.03.0669, (2021)

[38] L. Na and C. Shanben, "Key Technologies of intelligentized welding manufacturing - Welding arc acoustic sensing and monitoring technology", Springer Nature, Singapore (Singapore), https://doi.org/10.1007/978-981-15-2002-0, (2020)

[39] M. Cullen, S. Zhao, J. Ji, and X. Qiu, "Classification of transfer modes in gas metal arc welding using acoustic signal analysis", International Journal of Advanced Manufacturing Technology, Vol. 115, pp. 3089-3104, https://doi.org/10.1007/s00170-021-07305-x, (2021)

[40] L. Yi, Z. Yan, X. Xiaojian, Z. Yang, and W. Rui, "Effect of welding heat input to metal droplet transfer characterized by structure-borne acoustic emission signals detected in GMAW", Measurement: Journal of the International Measurement Confederation, Vol. 70, pp. 75-82, 2015, https://doi.org/10.1016/j.measurement.2015.03.046, (2015)

[41] X. Liu and E. Kannatey-Asibu, "Classification of AE signals for monitoring martensite formation from welding", Welding Journal, Vol. 69, pp. 389-394, (1990)

[42] P. Szłapa and W. Marczak, "Arc welding noise assessment from the measured ultrasound pressure levels - Part I: The metal active gas welding", Ultrasonics, Vol. 90, pp. 71-79, https://doi.org/10.1016/j.ultras.2018.06.011, (2018)

[43] P. Szłapa and W. Marczak, "Arc welding noise assessment from the measured ultrasound pressure levels. Part III: Modern welding techniques", Ultrasonics, Vol. 108, https://doi.org/10.1016/j.ultras.2020.106220, (2020)

[44] P. Szłapa and W. Marczak, "Arc welding noise assessment from the measured ultrasound pressure levels. Part II: Pulsed and double pulsed metal active gas welding", Ultrasonics, Vol. 100, https://doi.org/10.1016/j.ultras.2019.105976, (2020)

[45] M. Čudina, J. Prezelj and I. Polajnar, "Use of audible sound for on-line monitoring of gas metal arc welding process", Metalurgija, Vol. 47, pp. 81-85, (2008)

[46] I. Polajnar, Z. Bergant, and J. Grum, "Arc welding process monitoring by audible sound", Proceedings of the 12th International Conference of the Slovenian Society for Non-Destructive Testing: Application of Contemporary Non-Destructive Testing in Engineering 2013, Portorož (Slovenia), 4-6 September 2013, pp. 613-620, (2013)

[47] L. Na, C. Shao-jie, C. Qi-heng, T. Wei, Z. Hui, and C. Shan-ben, "Dynamic welding process monitoring based on microphone array technology", Journal of Manufacturing Processes, Vol. 64, pp. 481-492, https://doi.org/10.1016/j.jmapro.2020.12.023, (2021)

[48] J. Tam, "Methods of characterizing gas metal arc welding acoustics for process automation", MSc Thesis, University of Waterloo (Canada), (2005)

[49] L. Wenji, G. Zhenyu, J. Xiao, L. Li, and Y. Jianfeng, "Research on the seam tracking of narrow gap P-GMAW based on arc sound sensing", Sensors and Actuators, A: Physical, Vol. 292, pp. 205-216, https://doi.org/10.1016/j.sna.2019.04.015, (2019)

[50] L. Liu, H. Lan, H. Zheng, and X. Jian, "Feature extraction and dimensionality reduction of arc sound under typical penetration status in metal inert gas welding", Chinese Journal of Mechanical Engineering, Vol. 25, pp. 293-298, https://doi.org/10.3901/CJME.2012.02.293, (2012)

[51] Y. Ping, Z. Kang, and Z. Qiang, "Quantitative Evaluation method of arc sound spectrum based on sample entropy", Mechanical Systems and Signal Processing, Vol. 92, pp. 379-390, https://doi.org/10.1016/j.ymssp.2017.01.016, (2017)

[52] M. F. M. Yusof, M. Ishak, M. F. Ghazali, and M. R. Islam, "Analysis of an air borne acoustic signatures from welding process using empirical mode decomposition", Advanced Materials Research, Vol. 889-890, pp. 770-775, https://doi.org/10.4028/www.scientific.net/AMR.889-890.770, (2014)

[53] S. Gourishetti, J. Chauhan, S. Grollmisch, M. Rohe, M. Sennewald, J. Hildebrand, and J. P. Bergmann, "Arc welding process monitoring using neural networks and audio signal analysis", Proceedings of the Conference Sensor and Measurement Science International - SMSI 2023, Nuremberg (Germany), 8-11 May 2023, pp. 249-250, https://doi.org/10.5162/SMSI2023/D7.2, (2023)

[54] E. H. Cayo and S. C. A. Alfaro, "Welding quality measurement based on acoustic sensing", Proceedings of the 19th International Congress of Mechanical Engineering 2007, Brasilia DF (Brazil), 5-8 November 2007, pp. 571-579, (2007)

[55] A. N. Smirnov, V. I. Danilov, E. A. Ozhiganov, V. V. Gorbatenko, and V. V. Murav'ev, "The dependence of local deformations and internal stress fields on welding technique for grade VSt3sp structural steel: I. The influence of welding technique on the mechanical characteristics and acoustic emission parameters of grade VSt3sp steel", Russian Journal of Nondestructive Testing, Vol. 51, pp. 705-712, https://doi.org/10.1134/S1061830915110066, (2015)

[56] M. Cullen, "Development of a smart gas metal arc welding system using acoustic sensing", PhD Thesis, University of Technology Sydney (Australia), (2023)

[57] Y. Tao, W. Wang, and B. Sun, "Nondestructive online detection of welding defects in track crane boom using acoustic emission technique", Advances in Mechanical Engineering, Vol. 6, https://doi.org/10.1155/2014/505464, (2014)

[58] J. M. Griffin, S. Jones, B. Perumal, and C. Perrin, "Investigating the detection capability of acoustic emission monitoring to identify imperfections produced by the metal active gas (MAG) welding process", Acoustics, Vol. 5, pp. 714-745, https://doi.org/10.3390/acoustics.5030043, (2023)

[59] A. Aboali, M. El-Shaib, A. Sharara, and M. Shehadeh, "Screening for welding defects using acoustic emission technique", Advanced Materials Research, Vol. 1025-1026, pp. 7-12, https://doi.org/10.4028/www.scientific.net/AMR.1025-1026.7, (2014)

ORIGINAL SCIENTIFIC PAPER OPEN ACCESS

Settlement analysis of isolated footings using two soil models

Stefan Mihajlović[1*], Iva Despotović[1], Jovana Bojković[1],
Marijana Janićijević Milačak[1], Vladimir Mandić[1]

[1] University of Kragujevac, Faculty of Mechanical and Civil engineering in Kraljevo, Serbia

ARTICLE INFO

[*] **Correspondence:** mihajlovic.s@fmgkv.kg.ac.rs

DOI: 10.5937/engtoday2600006M

UDC: 621(497.11) **ISSN:** 2812 – 9474

Article history: Received 28 January 2026; Revised 27 February 2026; Accepted 28 February 2026

ABSTRACT

This paper investigates the influence of soil idealization on stress distribution and settlement beneath isolated footings of building structures. Two basic soil models commonly used in geotechnical engineering practice are analyzed: the elastic half-space model and the finite-thickness soil layer model resting on a rigid base. Stress and settlement analyses were performed for square isolated footings of different dimensions subjected to a constant uniformly distributed surface load, while varying the mechanical properties of the soil. Particular attention is devoted to comparing the soil deformation response at characteristic points along the footing–soil interface. The obtained results indicate a significant influence of the selected soil model, soil deformability (soil stiffness, E), and footing geometry on settlement values, confirming the necessity of a careful choice of the calculation model in geotechnical design.

KEYWORDS

Geotechnical modeling, Elastic half-space soil model, Finite soil layer model, Shallow foundations, Isolated footing.

1. INTRODUCTION

Soil modeling beneath building structures represents one of the key aspects of geotechnical and structural design, as it directly affects stress distribution at the footing–soil interface as well as the magnitude and character of soil settlements. The stresses transferred from the structure to the soil depend on the stiffness of the footing, the mechanical properties of the soil, and the geometry of the contact surface; inaccurate assessment may lead to exceeding allowable soil stresses [1]. The consequences of such conditions include uneven settlements, cracking of structural elements, and a reduction in structural bearing capacity. Therefore, a realistic numerical or analytical model of soil–foundation interaction is essential for a reliable assessment of structural behavior during service life [2]. This issue is particularly significant for isolated footings, which—unlike strip footings and raft foundations—behave as independent structural systems. Due to the relatively small area through which the load is transferred to the soil, isolated footings induce higher stress concentrations and more pronounced local settlements [3]. These settlements may be differential relative to adjacent foundations, leading to additional internal forces in the superstructure. Consequently, accurate soil modeling beneath isolated footings is crucial to ensure the safety, serviceability, and durability of the entire structure [4]. In the early stages of geotechnical engineering development, soil models were based on simplified assumptions in which the soil beneath structures was treated as a homogeneous and isotropic medium. Such models assumed exclusively elastic deformations that were linearly related to applied stress. One of the most well-known examples of this approach is the Winkler soil model, in which the soil is idealized as a system of independent springs [2]. This model is directly based on Hooke's law and enables a simplified analysis of soil–

foundation interaction. However, practical experience and experimental investigations have shown that soil behavior cannot be fully described using purely elastic laws. Under structural loading, both elastic and plastic deformations occur in the soil, with plastic deformations potentially being permanent and significantly affecting foundation settlement [5]. As a result, more advanced constitutive soil models have been developed to realistically describe nonlinear behavior and stress-history dependency [6]. These models allow for more accurate determination of stresses at the footing–soil interface as well as total and differential settlements. Modern soil modeling approaches based on the finite element method include various constitutive soil models, such as the linear elastic model [7], the elasto-plastic Mohr–Coulomb model [8], the Hardening Soil model [9], the Modified Cam-Clay model [10], and advanced hypoplastic models [11]. Their primary advantage lies in the ability to represent layered soil profiles, nonlinear behavior, plastic deformation, and soil–structure interaction under complex loading conditions. This enables detailed stress distribution analysis and reliable prediction of total and differential settlements. However, the main disadvantages include strong dependence of results on the selected constitutive model and input parameters, increased data requirements, and higher computational complexity compared to simpler analytical approaches[12].

In soil–foundation interaction analyses, two basic idealized soil models are most commonly considered [3]. The first is the elastic half-space model, in which the soil is treated as a continuum extending infinitely in depth [13]. It is referred to as a half-space because it is bounded at the top by the plane representing the contact surface between the foundation and the soil. This idealization is particularly suitable for stress and settlement analyses when deep soil layers are significantly thicker than the foundation dimensions [14]. The second approach considers soil as a finite-thickness layer, accounting for the presence of a rigid or significantly stiffer layer at a certain depth [15]. In this case, stress distribution and settlement magnitude depend not only on soil properties but also on the depth and characteristics of the lower boundary. This model is more realistic for sites where bedrock or very dense soil exists beneath the bearing layer and enables a more accurate assessment of settlements under conditions of limited soil deformability. The present study analyzes stress and settlement results beneath an isolated footing using both soil modeling approaches: the elastic half-space model and the finite-thickness soil layer model. The main objective of the paper is to highlight differences in results obtained using these models and to provide practical recommendations for their application in engineering practice.

2. METHODS

In the numerical analyses, the soil beneath the foundation is modeled as a continuum using three-dimensional finite elements with appropriate material properties. Theoretically, the elastic half-space is bounded at the top by the ground surface and extends infinitely in depth and width. The soil is characterized by its deformation modulus, also referred to as soil stiffness (E), Poisson's ratio, and unit weight. Due to the complexity of this modeling approach, it is necessary to reasonably estimate the dimensions of the analyzed domain, thereby simplifying the numerical model while maintaining acceptable accuracy.

2.1. Soil Modeled as an Elastic Half-Space of Infinite Thickness

In this study, the soil beneath the isolated footing is modeled as an elastic half-space of infinite thickness, bounded at the top by the footing–soil contact plane [16]. The soil is assumed to be homogeneous, isotropic, and continuous, behaving according to the laws of linear elasticity. The load is transferred from the footing to the soil through a finite contact area, and the distribution of normal stresses and the soil deformation response are analyzed. This approach allows analytical or semi-analytical determination of the stress state and settlement beneath the isolated footing. Figure 1 shows a rigid footing resting on a single-layer soil represented as an elastic continuum. Soil properties are described by Poisson's ratio μ and the soil deformation modulus (soil stiffness) E.

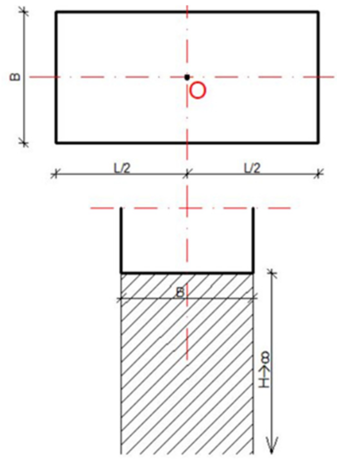

Figure 1: Soil model as an elastic half-space of infinite thickness beneath an isolated footing

The problem of determining stresses and displacements induced by a uniformly distributed vertical load over a rectangular area was studied by Newmark, Steinbrenner, and Florin. Vertical stresses along the axis passing through the center point (O) are expressed using established analytical solutions. Corresponding expressions allow calculation of vertical displacements, i.e., settlements, as functions of load intensity, footing geometry, soil stiffness (E), and Poisson's ratio:

$$\sigma_z = \frac{2p}{\pi}\left(arctg\frac{ab}{z\sqrt{a^2+b^2+z^2}} + \frac{abz(a^2+b^2+2z^2)}{\left(a^2+z^2\right)\left(b^2+z^2\right)\sqrt{a^2+b^2+z^2}} \right) \tag{1}$$

where:

p – intensity of the applied uniformly distributed vertical load, z – coordinate along the z-axis, i.e., the depth within the elastic half-space, and a and b – coordinates in the horizontal plane defining the position of the axis along which the vertical stresses are evaluated.

By substituting the known geometric parameters and the physical–mechanical properties of the materials involved in the soil–foundation interaction into the above expression, the calculation of vertical stresses is reduced to the following form:

$$\sigma_z = p\, I_{43} \tag{2}$$

where:

p – intensity of the applied uniformly distributed vertical load, I_{43} – tabulated coefficient depending on the soil type (defined by Poisson's ratio μ) and the geometric characteristics of the footing (expressed by the length-to-width ratio L/B) [3]. The displacement components in the direction of the z-axis can be determined using the following expression:

$$w = \frac{P(1+\mu)}{2\pi E}\frac{1}{R}\left(\frac{z^2}{R^2} + 2(1-\mu)\right) \tag{3}$$

The values of the elastic constants of the medium, m and G, are given by expressions that depend on the soil deformation modulus (soil stiffness) E and Poisson's ratio μ:

$$m = \frac{1}{\mu};\quad G = \frac{E}{2(1+\mu)} \tag{4}$$

By substituting the known geometric parameters and the physical–mechanical properties of the materials involved into the preceding settlement expression, the calculation of deformations (settlements) is reduced to the following form:

$$w = \frac{pB}{E} I_{53} \tag{5}$$

where:

p – intensity of the applied uniformly distributed vertical load, B – width of the considered footing, E – soil deformation modulus (soil stiffness), and I_{53} – tabulated coefficient depending on the soil type (defined by Poisson's ratio μ) and the geometric characteristics of the footing (expressed by the length-to-width ratio L/B).

The main advantage of the infinite half-space model lies in its mathematical simplicity and clearly defined assumptions, enabling relatively fast and stable estimation of stresses and settlements. The model is particularly suitable for isolated footings, where loads are transferred through a relatively small area and the influence of deep soil layers is dominant. However, its main limitation is the neglect of soil layering and the presence of a rigid base at finite depth, which may lead to deviations from real soil behavior. Additionally, the assumption of purely elastic behavior does not account for plastic deformations, potentially leading to underestimated settlement values under higher loads.

2.2. Soil Modeled as a Finite-Thickness Layer

Soil–foundation interaction can also be analyzed for cases in which the soil layer beneath the footing–soil interface has a finite thickness. In this approach, the stress and deformation calculation procedure is similar to that of the half-space model, but boundary conditions differ. Soil properties are again defined by Poisson's ratio μ and soil stiffness E. In comparison with the infinite half-space model, stress and deformation distributions additionally depend on the thickness of the compressible soil layer. This modeling approach is commonly applied when soil layer thicknesses and their mechanical properties are known to a certain depth, below which a rigid or incompressible layer exists. Figure 2 illustrates the geometry and boundary conditions of this soil model.

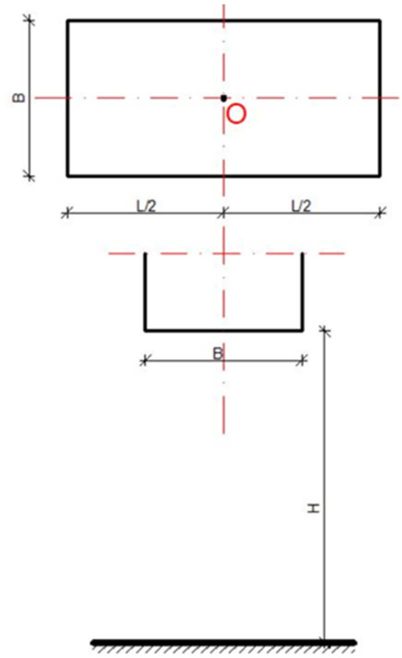

Figure 2: Soil model as a finite-thickness layer beneath an isolated footing

The problem of determining stresses and deformations (settlements, w) induced by a uniformly distributed load acting through a flexible rectangular footing has been investigated by several researchers. For the purpose of determining stress components and displacements in the soil caused by a uniformly distributed vertical load, the following assumptions are adopted: the footing is flexible and rectangular in shape; the compressible soil layer is elastic and isotropic; its thickness is limited by an incompressible base; and the contact between the footing and the soil is assumed to be smooth in one case and fully rough in the other. The vertical stresses, σ_z, are given by the following expression:

$$\sigma_z = \sum_m \sum_n \left(\alpha A_{12} U + \beta A_{12} V + A_{11} \frac{dW}{dz} \right) cos\alpha x \, cos\beta y \tag{6}$$

The integration constants in the above expression are determined from the boundary conditions. The displacements w for the case of smooth contact is given by the following expression:

$$w_{m,n} = \frac{1}{2G} \left\{ \left[(3-4\mu) C_4 - C_2 \gamma \right] sh\, \gamma z - C_4 \; \gamma z \; ch\, \gamma z \right\} \tag{7}$$

The displacements w for the case of rough contact is given by the following expression:

$$w_{m,n} = \frac{1}{2G} \left\{ \left[(3-4\mu) C_4 - \gamma z \, C_3 \right] sh\, \gamma z - \; \gamma z \, C_4 \; ch\, \gamma z \right\} \tag{8}$$

where:

C_2, C_3, and C_4 – integration constants given in [18], and G – value of the elastic constant of the medium. By substituting the known geometric parameters and the physical–mechanical properties of the materials into the above expression, the calculation of vertical stresses is reduced to the following form:

$$\sigma_z = p \; I_{109} \tag{9}$$

where:

p – intensity of the applied uniformly distributed vertical load, I_{109} – tabulated coefficient depending on the soil type (defined by Poisson's ratio μ), the geometric characteristics of the footing (expressed by the length-to-width ratio L/B and the ratio of footing width to the depth of the compressible soil layer H/B), and the position of the z-axis along which the vertical stresses are evaluated.

As in the previous model, displacement components can also be calculated for the soil modeled as a finite-thickness layer, for given geometric characteristics and material properties involved in the soil–foundation interaction, using the following expression:

$$w = \frac{p\,B}{E} I_{112} \qquad (10)$$

where:

p – intensity of the applied uniformly distributed vertical load, B – width of the considered footing, E – soil deformation modulus (soil stiffness), and I_{112} – tabulated coefficient depending on the soil type (defined by Poisson's ratio μ), the geometric characteristics of the footing (expressed by the length-to-width ratio L/B and the ratio of footing width to the depth of the compressible soil layer H/B), and the position of the z-axis depending on the location of the point on the footing–soil contact surface at which the deformations (settlements) are evaluated.

The main advantage of this model lies in its more realistic representation of actual geotechnical conditions, especially when bedrock or very dense soil exists beneath the foundation. This approach generally results in smaller settlement values compared to the infinite half-space model due to constrained soil deformation. However, its disadvantages include increased computational complexity and the requirement for reliable data on soil layer thickness and lower boundary properties.

3. RESULTS AND DISCUSSION

This section presents the results of stress and settlement analyses at the footing–soil interface for the previously described soil models. The analyses were conducted for an isolated footing with a thickness of 0.40 m and square plan dimensions of 2.50 m, 3.25 m, and 4.00 m. A constant uniformly distributed surface load of 200 kPa was applied over the entire contact area.

Soil parameters were defined assuming a Poisson's ratio of v = 0.30, while soil deformability (soil stiffness) E was varied between 10 and 50 MPa to cover a wide range of realistic geotechnical conditions. For the finite-thickness soil layer model, a compressible layer thickness of H = 10 m was assumed, underlain by a rigid base.

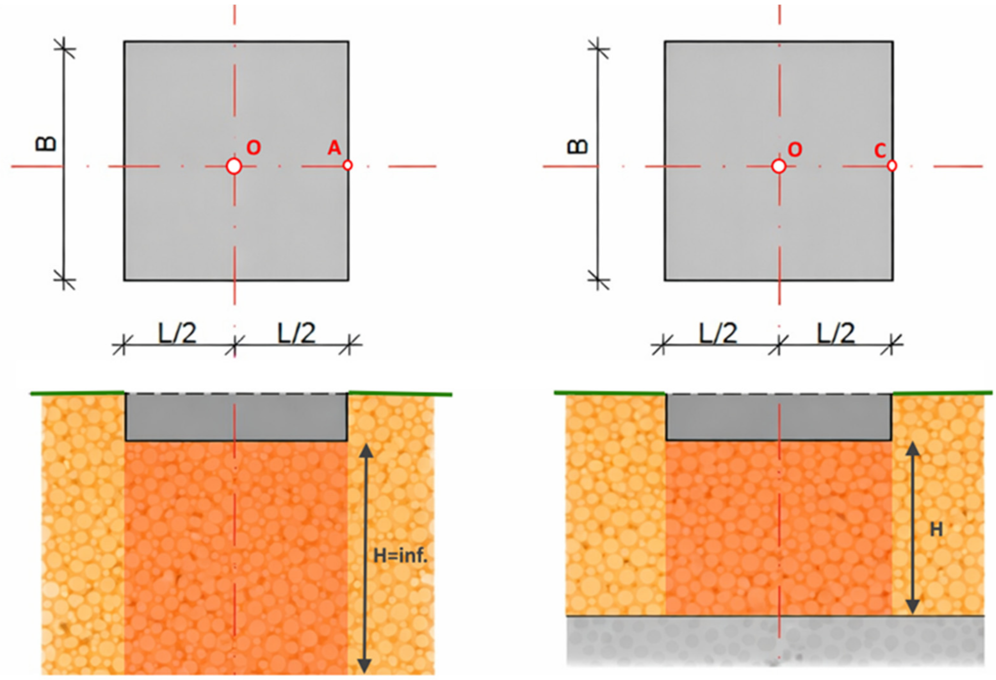

Figure 3: Geometric characteristics of the isolated footing for the two analyzed soil models with control points

The obtained results enable an analysis of the influence of soil stiffness and finite bearing layer thickness on stresses at the footing–soil contact interface and on settlements beneath the isolated footing. The settlement calculation results for the isolated footing obtained using the elastic half-space model and the finite-thickness soil layer model are presented in the following tables.

Table 1: Settlement results for soil modeled as an elastic half-space

E [MPa]	L/B=2.50/2.50m		L/B=3.25/3.25m		L/B=4.0/4.0m	
	w_o [cm]	w_a [cm]	w_o [cm]	w_a [cm]	w_o [cm]	w_a [cm]
10	4.858	3.237	6.316	4.209	7.773	5.180

E [MPa]	L/B=2.50/2.50m		L/B=3.25/3.25m		L/B=4.0/4.0m	
	w_o [cm]	w_a [cm]	w_o [cm]	w_a [cm]	w_o [cm]	w_a [cm]
15	3.239	2.158	4.211	2.806	5.182	3.453
20	2.429	1.619	3.158	2.105	3.860	2.590
25	1.944	1.295	2.527	1.684	3.109	2.072
30	1.620	1.079	2.106	1.403	2.591	1.727
35	1.388	0.925	1.805	1.203	2.221	1.480
40	1.215	0.810	1.579	1.053	1.943	1.295
45	1.080	0.720	1.404	0.936	1.727	1.151
50	0.972	0.648	1.264	0.842	1.555	1.036

Table 2: Settlement results for soil modeled as a finite-thickness layer (H = 10 m)

E [MPa]	L/B=2.50/2.50m		L/B=3.25/3.25m		L/B=4.0/4.0m	
	w_o [cm]	w_c [cm]	w_o [cm]	w_c [cm]	w_o [cm]	w_c [cm]
10	4.498	2.040	5.694	2.502	6.744	2.820
15	2.998	1.360	3.796	1.668	4.496	1.880
20	2.249	1.020	2.847	1.251	3.372	1.410
25	1.799	0.816	2.278	1.001	2.698	1.128
30	1.499	0.680	1.898	0.834	2.248	0.940
35	1.285	0.583	1.627	0.715	1.927	0.806
40	1.124	0.510	1.423	0.626	1.686	0.705
45	0.999	0.453	1.265	0.556	1.499	0.627
50	0.900	0.408	1.139	0.500	1.349	0.564

In the following section, a comparative presentation of the deformation, i.e., soil settlement calculation results obtained using the two analyzed soil models is provided. The subsequent figures illustrate a comparison of soil behavior modeled as an elastic half-space of infinite thickness and as a finite-thickness soil layer. This comparative analysis enables evaluation of the influence of soil idealization on the magnitude and distribution of settlements beneath the isolated footing.

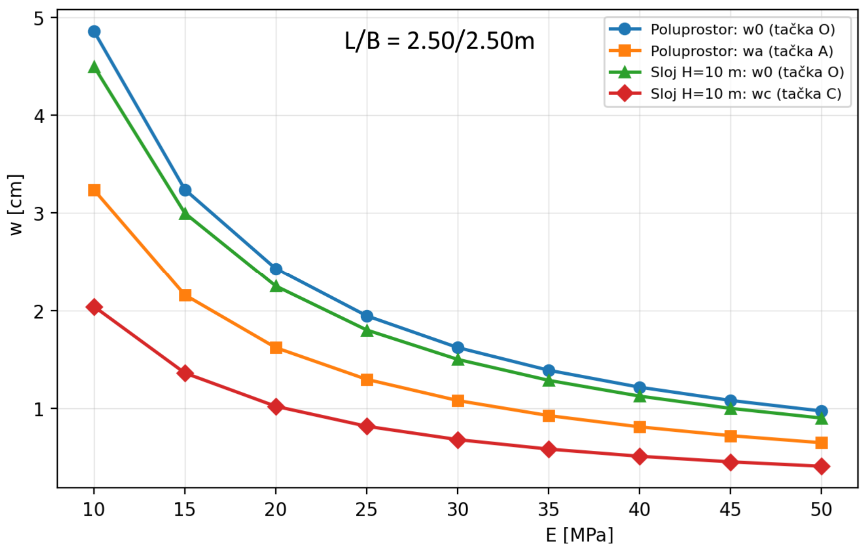

Figure 4: Comparative settlement values for an isolated footing with L/B = 2.50/2.50 m for the two analyzed soil models

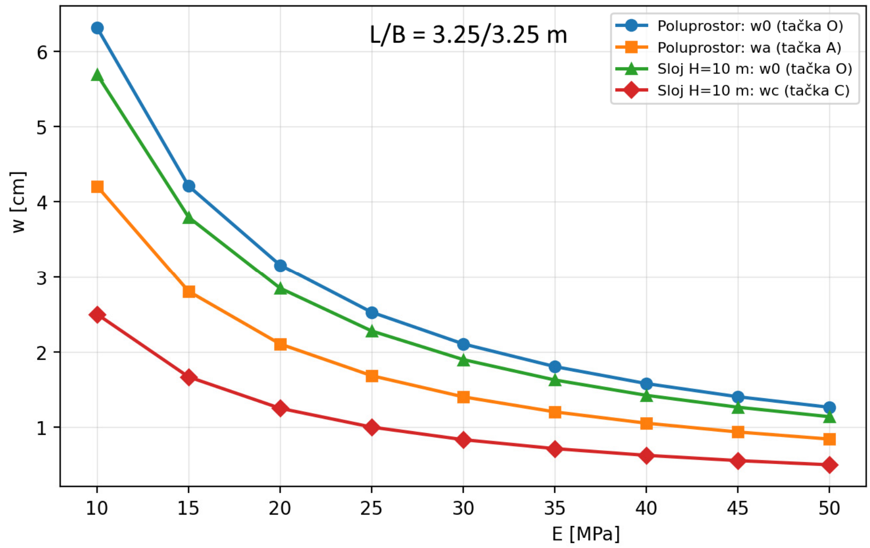

Figure 5: Comparative settlement values for an isolated footing with L/B = 3.25/3.25 m for the two analyzed soil models

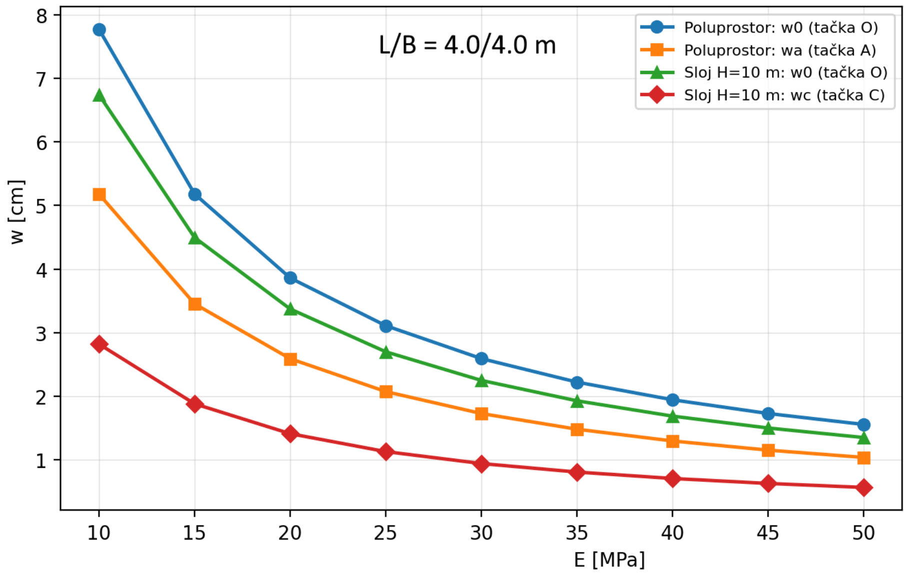

Figure 6: Comparative settlement values for an isolated footing with L/B = 4.00/4.00 m for the two analyzed soil models

The diagrams indicate that soil settlement decreases in all analyzed cases with increasing soil deformability (soil stiffness) E, which is consistent with theoretical expectations and the physical behavior of soil. For both soil models, the maximum settlement values occur at the lowest values of E, while with increasing soil stiffness the differences between individual curves gradually decrease. It is also observed that settlements at the characteristic center point (O) are greater than those at points A and C, indicating a more pronounced deformation response of the soil beneath the central part of the footing. The diagrams further show that settlement values at the center point (O) are similar for both soil models, whereas settlement values at the footing edge points, A and C, exhibit significantly larger differences depending on the selected soil model. These observations apply consistently to all three analyzed isolated footing dimensions.

A comparative analysis of the two soil models shows that the elastic half-space model yields higher settlement values than the finite-thickness soil layer model, particularly for lower values of soil stiffness E. This behavior is attributed to the unlimited deformability of the soil with depth in the half-space model, whereas the presence of a rigid base in the finite-thickness model restricts the development of deformations. The differences between the models become more pronounced with increasing footing dimensions, indicating a significant influence of footing geometry on the soil deformation response. These results confirm the importance of selecting an appropriate soil model when analyzing settlements of isolated footings.

4. CONCLUSION

This study analyzed soil stresses and settlements beneath isolated footings for two soil modeling approaches: an elastic half-space of infinite thickness and a finite-thickness soil layer with H = 10 m. Settlements were evaluated at characteristic footing points while varying soil deformability (soil stiffness) E in the range of 10–50 MPa at a constant Poisson's ratio of 0.30. The analyses were performed for square isolated footings with plan dimensions of 2.50 m, 3.25 m, and 4.00 m.

It can be concluded that, for both soil models, settlement decreases with increasing soil deformability (soil stiffness). The calculation results indicate that settlements at the footing center point (O) are greater than those at the edge points (A or C). For both soil models and for all analyzed square isolated footing dimensions, settlement values at the center point are approximately the same, whereas this is not the case for the footing edge points. Differences in settlement values at the center point range between 10% and 15%, while differences in settlement at the edge points may reach values of up to 50%, depending on soil deformability.

Finally, it is recommended that, in practical applications of the presented soil models for settlement analysis of isolated footings in building structures, results obtained using both soil models should always be compared. This approach provides increased reliability in structural design and enables verification that settlement values determined by the two soil models remain within acceptable limits.

ACKNOWLEDGEMENTS

This paper is a result of the research conducted within the project grant number 451-03-34/2026-03/200108 supported by the Ministry of Science, Technology and Innovation of the Republic of Serbia, and the CEEPUS project grant "Building Knowledge and Experience Exchange in CFD - RS-1012-10-2425" supported by the Central European Exchange Program for University Studies.

REFERENCES

[1] M. Djogo, M. Vasić, I. Despotović, and S. Mihajlović, "Geological and Geotechnical Aspects of the Most Significant Deep Landslides in the Danube Area on the Territory of Vojvodina," Applied Sciences, Vol. 14(9), p. 3622, https://doi.org/10.3390/app14093622, (2024)

[2] S. Mihajlović, "Projekat fundiranja višespratne zgrade i analiza interakcije temeljne ploče i tla," Zbornik radova Fakulteta tehničkih nauka u Novom Sadu, Vol. 35(02), pp. 222–225, https://doi.org/10.24867/06CG06Mihajlovic , (2020)

[3] D. Milović and M. Đogo, "Greške u fundiranju", Fakultet Tehničkih nauka, Novi Sad (Serbia), (2005)

[4] M. Mohyla, "Experimentally measurement and analysis of stress under foundation slab", International Journal of GEOMATE, Vol. 13(35), pp. 128–135, https://doi.org/10.21660/2017.35.6694, (2017)

[5] R. Cajka, J. Labudkova, and P. Mynarcik, "Numerical solution of soil-foundation interaction and comparison of results with experimetal measurements", International Journal of GEOMATE, Vol. 11(23), pp. 2116–2122 https://doi.org/10.21660/2016.23.1208, (2016)

[6] W. Pakos and A. Helowicz, "Theoretical and numerical modeling of a shallow foundation stiffness based on the theory of elastic half-space", Studia Geotechnica et Mechanica, Vol. 46(4), pp. 302–314, https://doi.org/10.2478/sgem-2024-0022, (2024)

[7] I. F. Collins, "Elastic/plastic models for soils and sands", International Journal of Mechanical Sciences, Vol. 47(4–5), pp. 493–508, https://doi.org/10.1016/j.ijmecsci.2004.12.016, (2005)

[8] R. G. Mikola, K. Hatami, and D. Doolin, "Elastic–plastic discontinuous deformation analysis using Mohr–Coulomb model", Mining Technology, Vol. 120(3), pp. 148–157, https://doi.org/10.1179/1743286311Y.0000000006, (2011)

[9] J. T. H. Wu and S. C.-Y. Tung, "Determination of Model Parameters for the Hardening Soil Model", Transportation Infrastructure Geotechnology, Vol. 7(1), pp. 55–68, https://doi.org/10.1007/s40515-019-00085-8, (2020)

[10] K. Liu, S. L. Chen, and G. Z. Voyiadjis, "Integration of anisotropic modified Cam Clay model in finite element analysis: Formulation, validation, and application", Computers and Geotechnics, Vol. 116, p. 103198, https://doi.org/10.1016/j.compgeo.2019.103198, (2019)

[11] J. Jerman and D. Mašín, "Evaluation of hypoplastic model for soft clays by modelling of Nicoll highway case history", Computers and Geotechnics, Vol. 134, p. 104053, https://doi.org/10.1016/j.compgeo.2021.104053, (2021)

[12] J. Labudková and R. Čajka, "Comparison of Measured Displacement of the Plate in Interaction with the Subsoil and the Results of 3D Numerical Model", Advanced Materials Research, Vol. 1020, pp. 204–209, https://doi.org/10.4028/www.scientific.net/AMR.1020.204, (2014)

[13] Z. Ba, J. Liang, V. W. Lee, and Z. Kang, "Dynamic impedance functions for a rigid strip footing resting on a multi-layered transversely isotropic saturated half-space", Engineering Analysis with Boundary Elements, Vol. 86, pp. 31–44, https://doi.org/10.1016/j.enganabound.2017.10.009 , (2018)

[14] H. Lemmen, S. Jacobsz, and E. Kearsley, "The influence of foundation stiffness on the behaviour of surface strip foundations on sand", Journal of the South African Institution of Civil Engineering, Vol. 59(2), pp. 19–27, https://doi.org/10.17159/2309-8775/2017/v59n2a3, (2017)

[15] Z. Bonić, E. Zlatanović, N. Romić, D. Č. Lukić, and D. Cvetković, "Punching shear capacity of reinforced concrete column footings accounting for the soil–structure interaction effect", Journal of Building Engineering, Vol. 46, p. 103706, https://doi.org/10.1016/j.jobe.2021.103706, (2022)

[16] A. Helowicz, "Analysis of numerical models of an integral bridge resting on an elastic half-space", Studia Geotechnica et Mechanica, Vol. 46(4), pp. 337–348, https://doi.org/10.2478/sgem-2024-0026, (2024)

ORIGINAL SCIENTIFIC PAPER OPEN ACCESS

CFD simulation of heat transfer in a combustion chamber

Đorđe Novčić[1*], Rade Karamarković[1] , Miloš Nikolić[1]

[1] University of Kragujevac, Faculty of Mechanical and Civil Engineering, Kraljevo, Serbia

ARTICLE INFO

[*] **Correspondence:** novcic.d@mfkv.kg.ac.rs

DOI: 10.5937/engtoday2600007N

UDC: 621(497.11) **ISSN:** 2812 – 9474

Article history: Received 15 January 2026; Revised 20 February 2026; Accepted 28 February 2026

ABSTRACT

Solid biomass represents the most important renewable energy source in the Republic of Serbia; however, its combustion in small-scale boilers is often associated with increased pollutant emissions. This study examines the influence of refractory elements on heat transfer in the combustion chamber of wood-log gasification boiler. These elements play a crucial role in multistage combustion systems, especially for moist biomass, by enhancing radiative and convective heat transfer, promoting more complete combustion, and reducing gaseous and particulate emissions while minimizing material usage. Special attention is given to the CFD optimization of the refractory ceramic length and the position of the producer gas inlet within the combustion chamber. Non-premixed combustion was modeled by solving the energy equation, applying the standard k–ε turbulence model and the DO radiation model. The results demonstrate that the most effective configuration employs a refractory element that creates a U-shaped flow path, which extends the residence time of flue gases in the chamber. Achieving this flow path requires the element to be at least one half to two thirds the length of the chamber, thereby positioning the combustion zone of the producer gas above the flue gas outlet.

KEYWORDS

Biomass, Wood, Flue gas, CFD, Combustion chamber.

1. INTRODUCTION

The Energy Strategy of the Republic of Serbia, along with the ongoing energy crisis, provides a strong impetus for intensified utilization and research of renewable energy sources [1]. Among these, solid biomass represent the most significant renewable energy resource in the Republic of Serbia [2]. Although wood has been used as a fuel since the earliest stages of human civilization, considerable potential for technical improvements in its combustion processes still exists [3]. Despite being a renewable energy source, wood combustion results in the emission of substantial quantities of pollutants into the atmosphere [4,5]. The scale and importance of these emissions are particularly evident in the elevated concentrations of various pollutants recorded in urban areas with a high density of individual heating systems across many cities in the Republic of Serbia [6]. This paper investigates how additional design measures can simultaneously improve heat transfer, achieve more complete combustion, suppress pollutant formation, and reduce emissions from solid biomass boilers. In order to decrease material consumption and emissions from these boilers, both primary [7] and secondary [8,9] measures are employed. Primary measures encompass technical solutions aimed at achieving complete combustion and preventing particulate matter emissions through the implementation of structural elements within the boiler itself. The paper places emphasis on the most efficient utilization of refractory elements in the combustion chambers of solid biomass boilers. These elements are applied in systems with multistage combustion, particularly in the combustion of moist biomass, and serve multiple functions: they reduce the dimensions of the zone in which heat is primarily transferred by radiation (thereby reducing material usage and, consequently, the final cost of the boiler), enable more complete combustion, enhance heat transfer, and contribute to the reduction of gaseous pollutant emissions as well as particulate matter. The aim of this paper was to determine the optimal size of the refractory ceramic and the optimal position of the producer gas inlet into the combustion chamber. In the literature, there are several classifications of refractory elements; hence, no single unifed classification exists. Based on their form, refractory materials are divided into shaped refractory bricks and unshaped (monolithic) materials, such as refractory concretes [10]. The most commonly used refractory brick shapes are shown in Fig. 1. Among various shapes, a standard rectangular refractory brick was selected for this study due to its simplicity and common use [10].

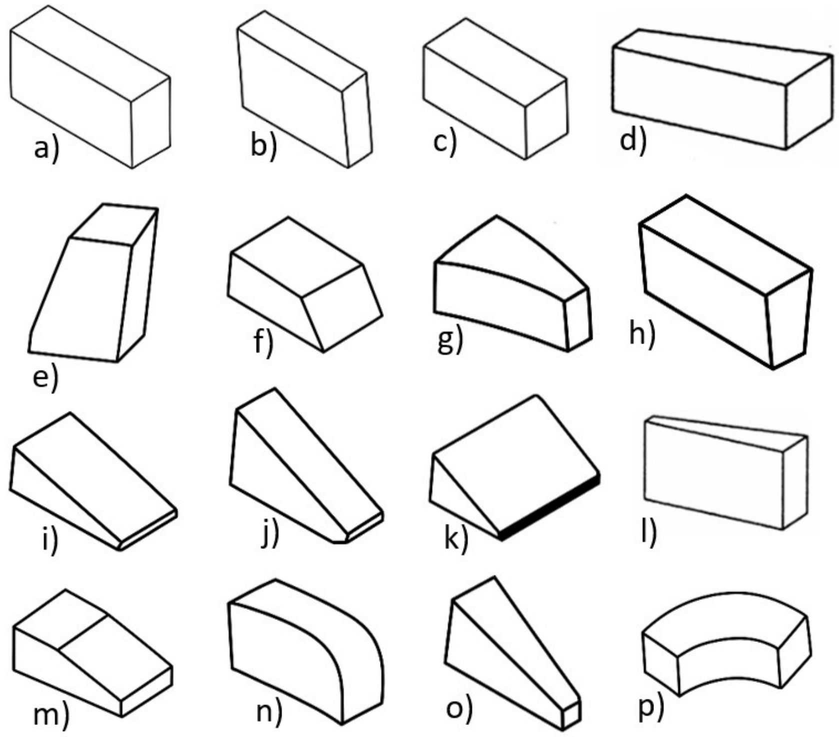

Figure 1: The most commonly used refractory brick shapes. a – straight, b - split, c – soap or closer, d – key brick, e – skew back, f – end skew on flat, g – end arch, h – side arch, i – feather end, j - feather end on edge, k – feather side, l – wedge, m – bevel brick, n – bullnose or jamb brick, o – dome brick, p – circle brick. [10,11]

2. THE CFD MODEL

A commercially available software ANSYS, together with its FLUENT 18.1 module, was employed to perform numerical simulations of producer gas combustion within the combustion chamber. The simulations were performed based on the defined geometry, generated computational mesh, and boundary conditions. In the development of the Non-premixed combustion model, the energy equation was solved, the standard k–ε turbulence model was adopted, and the Discrete Ordinates radiation model was applied. For radiation modeling, the wsggm-domain-based approach was used to determine the absorption coefficient. Figure 2a shows the 3D model of the proposed combustion chamber design of wood-log gasification boiler.

2.1. Mesh details

Figure 2b shows the computational mesh, represented by a cross-section of the combustion chamber. The mesh consists of 33064 nodes and 168327 elements. The minimum and maximum element side lengths are 0.545 mm and 20 mm, respectively. The mesh quality is considered satisfactory, as the average values of element quality, aspect ratio, orthogonal quality, and skewness fall within acceptable limits, amounting to 0.773, 2.21, 0.691, and 0.307, respectively [12].

2.2. Boundary conditions

The producer gas inlet (0.00373 kg/s, 497°C) to the combustion chamber was defined as a mass flow inlet with a uniform distribution over the cross-section (1 in Fig. 2). Combustion air (0.00713 kg/s, 300°C) was supplied through two inlet locations, both modeled as mass flow inlets with uniformly distributed flow (2 in Fig. 2). The flue gas outlet, corresponding to the inlet of the tubular heat exchanger (6 in Fig. 2), was specified as a pressure outlet with a relative static pressure of 0 Pa. Similarly, the boiler water inlet (0.2 kg/s, 55°C) was defined as a mass flow inlet with uniform distribution (8 in Fig. 2), while the water outlet was modeled as a pressure outlet with a relative pressure of 0 Pa (9 in Fig. 2). All remaining surfaces were defined as wall boundary conditions. The parameters used in the numerical simulations for the refractory ceramics (corundum 90) were taken from [13] and are as follows: λ=2.33 W/mK, C_p=1.118 kJ/kgK, and ρ=2.83 g/cm3. Table 1 presents the composition of producer gas used in the numerical simulations.

Table 1: Producer gas composition used in the numerical simulations.

CO %	CO_2 %	CH_4 %	H_2 %	H_2O %	N_2 %	O_2 %	C_7H_{16} %
2.344	19.043	0.293	0.195	21.484	53.906	0.293	2.442

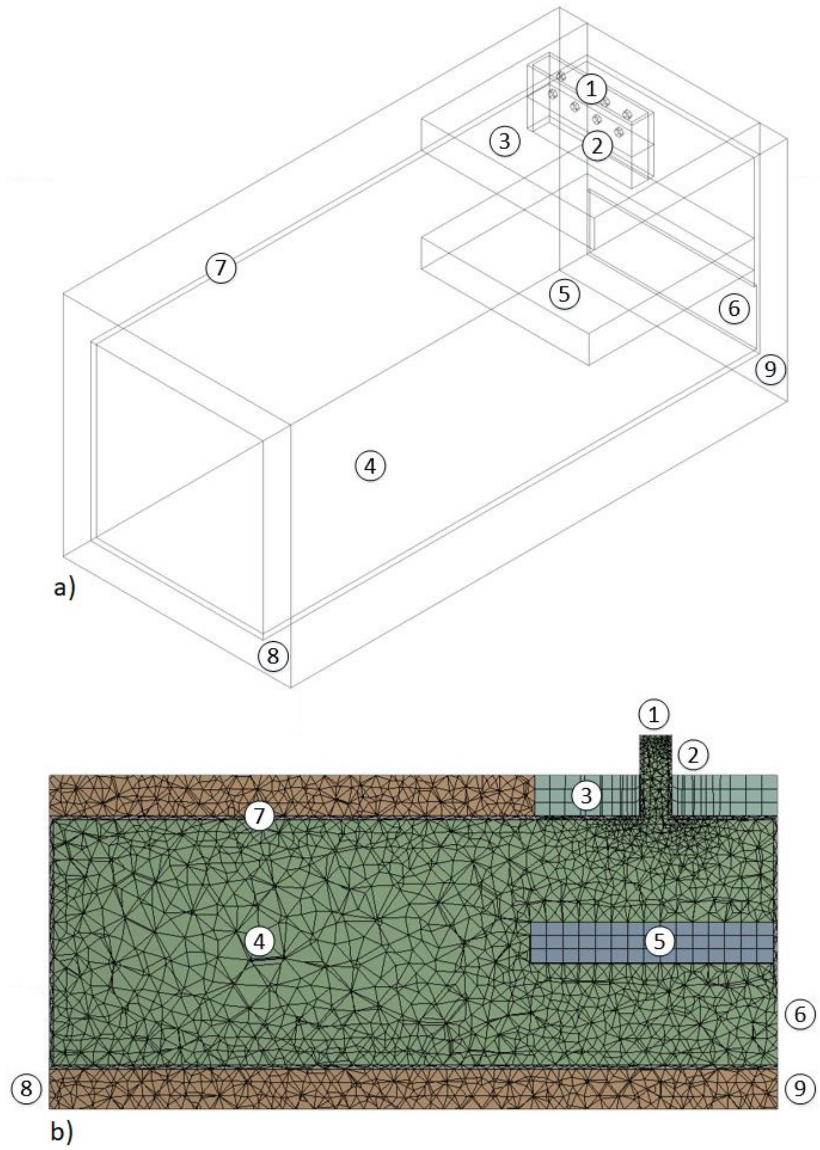

Figure 2: a - 3D model of the combustion chamber design of wood log gasification boiler, b – the computational mesh represented by a cross-section of the combustion chamber. 1 – producer gas inlet, 2 – combustion air inlet, 3 – refractory ceramics separating the gasification from the combustion chamber, 4 – combustion chamber, 5 – refractory ceramics inside the combustion chamber, 6 – flue gas outlet, 7 – boiler steel plate, 8 - boiler water inlet, 9 - boiler water outlet.

2.3. Effect of refractory length and gas inlet position on heat transfer

A total of 25 configurations were analyzed, combining five different lengths of the refractory ceramic with five positions of the producer gas inlet, as listed in Tab. 2. The producer gas inlet position is denoted by *x*, and the refractory ceramic length by *y*. Each configuration is labeled as x_iy_i, with the index *i* ranging from 1 to 5, starting from x_1y_1 up to x_5y_5.

Table 2: Configurations x_iy_i used in the numerical simulations.

Producer gas inlet position (x_i)	Refractory ceramic length (y_i)
x_1=150 mm	y_1=300 mm

Producer gas inlet position (x_i)	Refractory ceramic length (y_i)
x_2=250 mm	y_2=375 mm
x_3=350 mm	y_3=450 mm
x_4=450 mm	y_4=525 mm
x_5=550 mm	y_5=600 mm

Figure 3 shows the CFD model of the combustion chamber.

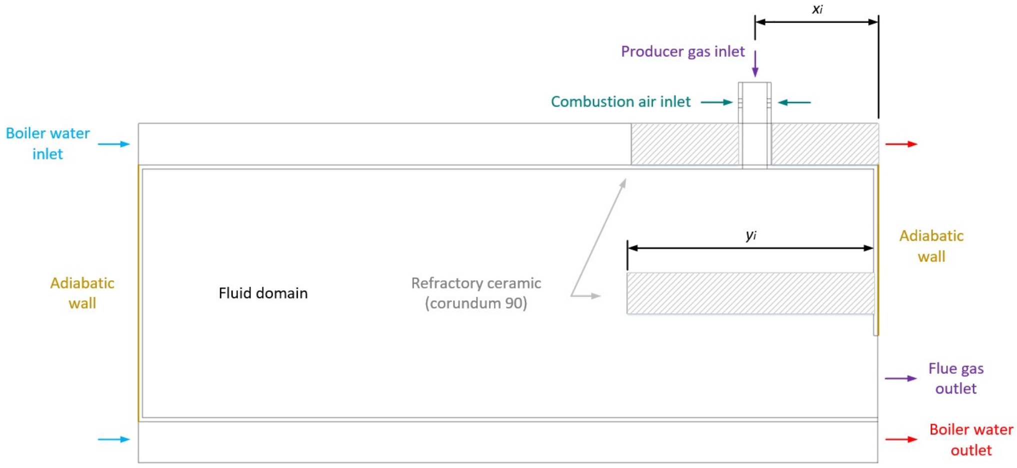

Figure 3: CFD model of the combustion chamber.

3. RESULTS

The results of the numerical simulations are presented in Fig. 4. The convergence criterion ($< 1\times10^{-4}$) was achieved just before the 13000th iteration, corresponding to a total computational time of approximately 35 minutes. In Fig. 4, the total heat transfer from the flue gas to the boiler water obtained from the CFD simulations is depicted by the black line, while the total energy brought in the combustion chamber is shown by the red dashed-dotted line. The analysis reveals that the most favorable heat transfer performance is achieved when the producer gas inlet is positioned closest to the flue gas outlet and the refractory ceramic length is at least half the combustion chamber length. Specifically, configurations x_1y_3, x_1y_4, and x_1y_5 (highlighted in gold) demonstrate this optimal geometry. In these cases, the extended refractory element creates a longer flow path, thereby increasing the residence time of the flue gases and enhancing heat transfer. The total heat transfer for these optimal configurations shows minimal variation, ranging from 13.33 to 13.5 kW. Conversely, the least favorable performance is observed when the producer gas inlet is positioned near the boiler water inlet, as seen in configurations x_3y_1, x_3y_2, and x_4y_3 (highlighted in green). In these arrangements, heat transfer is significantly reduced, with values varying only slightly between 10.91 and 10.99 kW. Overall, the difference between the most and least favorable configurations is approximately 2.5 kW.

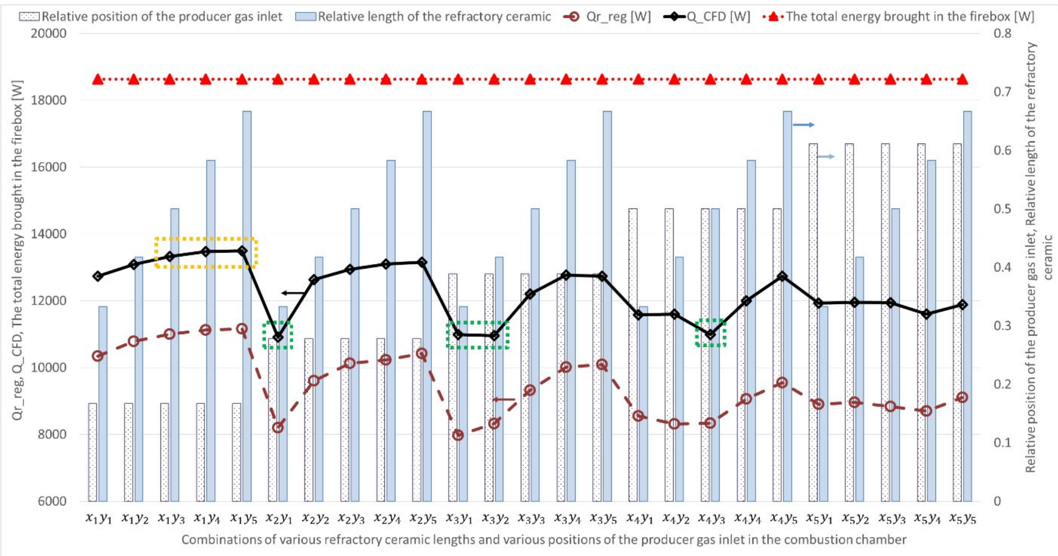

Figure 4: Results of CFD simulations.

In Fig. 4, radiative heat transfer from the flue gas to the boiler water is shown by the dark red dashed line. Regression analysis was used to derive the following mathematical equation (in watts) describing this process:

$$Q_{r\_reg} = c_0 + c_1 p_r + c_2 l_r + c_3 (p_r / l_r)^2 + c_4 (\Delta T_{gas} / \Delta T_{water})^2 + c_5 (\Delta T_{gas} - \Delta T_{water})^2 + c_6 (T_{gas_{mean}} / T_{water_{mean}})^2 + c_7 (p_r / l_r)^3 + c_8 (\Delta T_{gas} / \Delta T_{water})^3 + c_9 (T_{gas_{mean}} / T_{water_{mean}})^3 + c_{10} (p_r / l_r)^4 + c_{11} (\Delta T_{gas} / \Delta T_{water})^4 + c_{12} (T_{gas_{mean}} / T_{water_{mean}})^4 \quad (1)$$

Where c_i are constants (Tab. 3), $p_r = p_i/L$ and $l_r = l_i/L$ denote the relative inlet position and refractory length, respectively, with L=900 mm. ΔT_{gas} and ΔT_{water} are the gas and water inlet–outlet temperature differences, and T_{gas_mean} and T_{water_mean} are the corresponding mean temperatures.

Table 3: Constants used in (1)

c_0	c_1	c_2	c_3	c_4	c_5	c_6	c_7	c_8	c_9	c_{10}	c_{11}	c_{12}
322835	3644.1	-399.7	-8198.9	15.6	0.22	-267997.9	8131.5	-26.1	133772.7	-2197.2	3.5	-18662.9

Configuration p_1l_3 was selected as optimal, as it achieves near-maximal heat transfer performance while employing a shorter refractory length, thereby offering a favorable balance between efficiency and material economy. The numerical results for this configuration are shown in Fig. 5a. The flue gas temperature field indicates outlet temperatures between 425 and 549°C, confirming that the extended flow path, and correspondingly increased flue gas residence time, significantly enhances heat transfer. Although the primary role of the refractory ceramic is to separate the gas inlet from the outlet, positioning it closer to the outlet enhances convective heat transfer and promotes radiative heat exchange from hotter to cooler regions. The simulations also indicate an average water temperature rise of 9-20°C during heat exchange. Conversely, Fig. 5b presents configuration p_4l_3, which exhibits unfavorable heat transfer characteristics, with clearly visible colder zones caused by the more distant producer gas inlet position.

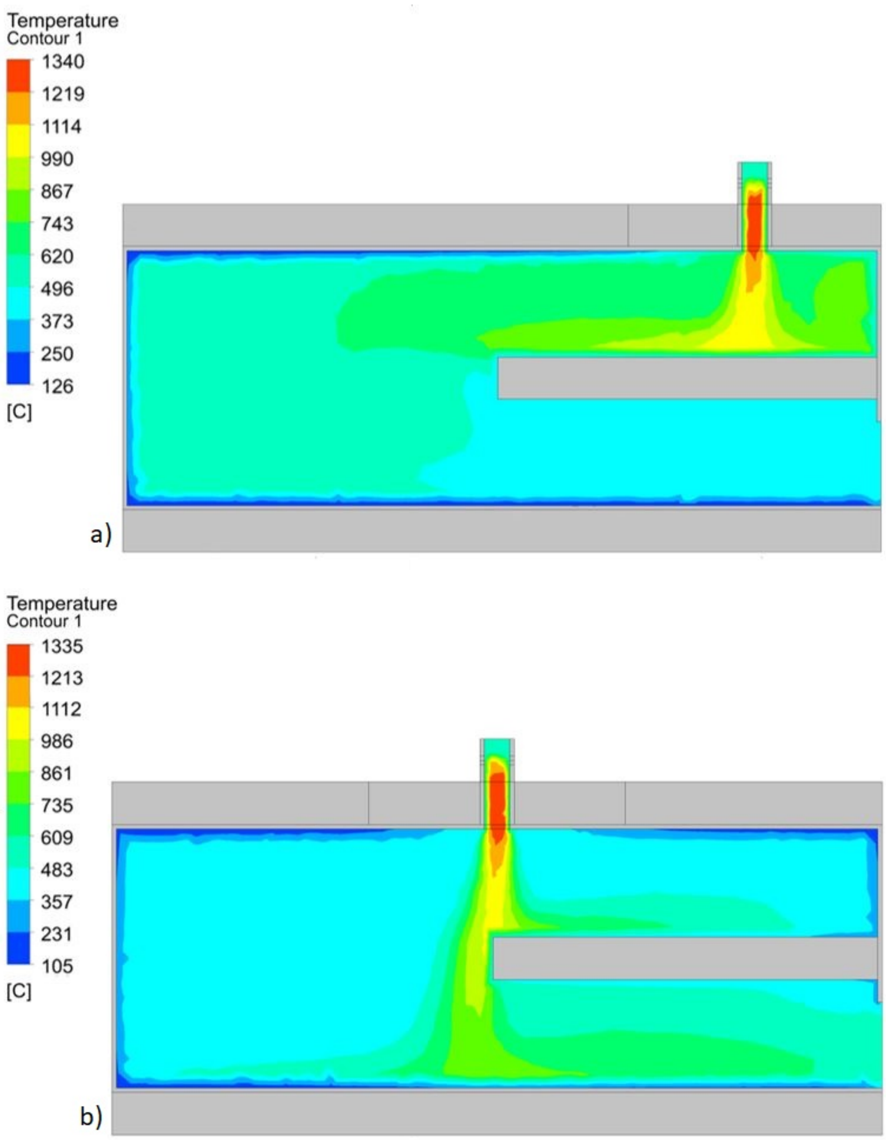

Figure 5: Results of CFD simulations. a - the optimal configuration p_1l_3, b - the least favorable configuration p_4l_3.

4. CONCLUSIONS

This paper investigates how the geometry and placement of refractory ceramics influence heat transfer and combustion performance in wood-log gasification boilers. The results shows that refractory ceramics in wood-log gasification boilers should be treated as flow-shaping and radiative elements rather than merely as thermal protection. By controlling the residence time, flow topology, and exposure of hot gas to radiative surfaces, the refractory layout governs the dominant heat-transfer mechanisms inside the combustion chamber.

The CFD simulations shows that the most effective configurations create a U-shaped flow path that separates the gas inlet from the outlet and extends the flue-gas residence time. A refractory length of approximately one half to two thirds of the chamber length is sufficient to achieve this effect. Positioning the ceramic closer to the gas outlet promotes heat transfer by directing radiative and convective fluxes from hotter to cooler regions.

ACKNOWLEDGEMENTS

This research was supported by the Science Fund of the Republic of Serbia, #GRANT No 5959, Active condensation hybrid systems in biomass combustion, AC-BC.

REFERENCES

[1] J. Kisin, J. Ignjatović, and A. Mashovic, "Energy crisis in Serbia: causes, effects, government response and potential for sustainable development", Proceedings of the 10th International Scientific Conference on Climate Change, Economic Development, Environment and People (CCEDEP), Travnik (Bosnia and Herzegovina), pp. 86-102, (2023)

[2] Ministarstvo rudarstva i energetike Republike Srbije, "Strategija razvoja energetike Republike Srbije do 2025. godine sa projekcijama do 2030. godine", https://arhiva.mre.gov.rs/latinica/dokumenta-efikasnost-izvori.php

[3] R. Karamarković, "Metode transformacije energije", Fakultet za mašinstvo i građevinarstvo u Kraljevu, Kraljevo (Srbija), (2022)

[4] H. A. C. Denier Van Der Gon, R. Bergström, C. Fountoukis, C. Johansson, S. N. Pandis, D. Simpson, and A. J. H. Visschedijk, "Particulate emissions from residential wood combustion in Europe - revised estimates and an evaluation", Atmospheric Chemistry and Physics, Vol. 15(11), p. 6503–6519, https://doi.org/10.5194/acp-15-6503-2015, (2015)

[5] A. Cincinelli, C. Guerranti, T. Martellini, and R. Scodellini, "Residential wood combustion and its impact on urban air quality in Europe", Curr. Opin. Environ. Sci. Heal., Vol. 8, p. 10–14, https://doi.org/10.1016/j.coesh.2018.12.007, (2019)

[6] Agencija za zaštitu životne sredine (SEPA), "Godišnji izveštaj o stanju kvaliteta vazduha u Republici Srbiji 2023. Godine", https://sepa.gov.rs/wp-content/uploads/2024/10/Vazduh2023.pdf

[7] T. Nussbaumer, "Combustion and Co-combustion of Biomass: Fundamentals, Technologies, and Primary Measures for Emission Reduction", Energy & Fuels, Vol. 17(6), p. 1510–1521, https://doi.org/10.1021/ef030031q, (2003)

[8] R. Singh and A. Shukla, "A review on methods of flue gas cleaning from combustion of biomass," Renewable and Sustainable Energy Reviews, Vol. 29, p. 854–864, https://doi.org/10.1016/j.rser.2013.09.005, (2014)

[9] O. Sippula, J. Hokkinen, H. Puustinen, P. Yli-Pirilä, and J. Jokiniemi, "Particle emissions from small wood-fired district heating units," Energy & Fuels, Vol. 23(6), p. 2974–2982, https://doi.org/10.1021/ef900098v, (2009)

[10] P. Sengupta, "Refractories for the Chemical Industries", Springer International Publishing, Cham (Switzerland), (2020)

[11] Harbison-Walker, "Harbison-Walker Handbook of Refractory Practice", Harbison-Walker Refractories Company, Moon Township, PA, https://www.mha-net.org/docs/Harbison%20Walker%202005%20Handbook.pdf

[12] https://www.mechead.com/mesh-quality-checking-ansys-workbench/

[13] A. Osterode, "D6 Properties of Solids and Solid Materials", Springer-Verlag, Berlin (Germany), (2010)

ORIGINAL SCIENTIFIC PAPER OPEN ACCESS

Hybrid PID-feedforward control for trajectory tracking in 2-DOF Robotic Systems

Vladimir Stojanović[1*], Ljubiša Dubonjić[1], Vladimir Đorđević[1]

[1] University of Kragujevac, Faculty of Mechanical and Civil Engineering, Kraljevo, Serbia

ARTICLE INFO

[*] **Correspondence:** vladostojanovic@mts.rs

DOI: 10.5937/engtoday2600009S

UDC: 621(497.11) **ISSN:** 2812 – 9474

Article history: Received 30 January 2026; Revised 27 February 2026; Accepted 2 March 2026

ABSTRACT

This paper presents a hybrid control strategy combining proportional-integral-derivative (PID) feedback with model-based feedforward compensation for precise trajectory tracking in two-degree-of-freedom (2-DOF) robotic manipulators. The approach addresses nonlinear dynamics, including inertial coupling, Coriolis effects, and gravity, by deriving the Euler-Lagrange equations for a planar arm and implementing a computed torque feedforward term augmented by PID correction. Theoretical stability is analyzed using Lyapunov methods, ensuring asymptotic convergence of tracking errors. Simulations demonstrate superior performance compared to standalone PID, with root-mean-square errors reduced to 0.5751° for the first joint and 1.4416° for the second under sinusoidal references. Results include phase portraits, torque decompositions, and sensitivity analysis to parameter variations, validating the method's robustness for industrial applications.

KEYWORDS

Hybrid control, PID-feedforward, Trajectory tracking, 2-DOF manipulator, Robotic systems, Stability analysis.

1. INTRODUCTION

Robotic manipulators with multiple degrees of freedom represent cornerstone technologies in contemporary automation landscapes, facilitating high-precision tasks across diverse sectors such as industrial manufacturing, medical surgery, space exploration, and agricultural operations. These systems, often embodying complex kinematic chains, enable dexterous interactions with environments, yet their inherent nonlinear dynamics, encompassing variable inertia, centrifugal and Coriolis forces, gravitational loads, and joint couplings, impose formidable challenges on control design, particularly for trajectory tracking applications. Conventional control paradigms, like proportional-integral-derivative (PID) regulators, offer simplicity and ease of implementation but frequently falter under these nonlinearities, manifesting in persistent steady-state errors, oscillatory responses, or even instability during rapid maneuvers or under payload variations [1,2,6,7,10]. To address such limitations, hybrid control frameworks that merge feedback mechanisms with feedforward compensation have gained prominence, capitalizing on a priori model knowledge to anticipate disturbances while relying on real-time feedback for corrective actions, thereby enhancing overall system robustness and performance [3,8,9,11,13]. The evolution of robotic control strategies has been marked by significant advancements in hybrid methodologies, driven by the need for improved accuracy and efficiency in dynamic environments. For example, Ngo et al. [1] conducted a comprehensive review of control trends in parallel robot manipulators for rehabilitation, highlighting hybrid position-force schemes that integrate feedforward elements with feedback loops to achieve seamless trajectory tracking, albeit with emphasis on parallel rather than serial configurations. Complementing this, Aner et al. [2] provided a decade-long survey on soft robotic manipulators, underscoring the role of bio-inspired hybrid controllers that blend model-based feedforward with adaptive feedback to handle material nonlinearities and external uncertainties, offering insights applicable to rigid systems through analogy. In the domain of agricultural robotics, Nkwocha et al. [3] explored PID augmented with feedforward techniques for perception to coordination pipelines, demonstrating enhanced precision in field operations but noting gaps in stability under varying terrains. Further, Della Santina et al. [4] investigated model-based dynamic feedback for planar soft robots, achieving trajectory tracking via feedforward compensation of environmental interactions, which parallels rigid manipulator challenges in gravity-dominated planes. Tusset et al. [5] proposed a PID-LQR hybrid for pneumatic manipulators, focusing on positioning accuracy under non-ideal excitations, revealing benefits in vibration suppression that could extend to multi-DOF arms.

Building on these, Zou et al. [6] examined shape-changeable parts in robotic assembly, incorporating feedforward strategies to adapt to geometric variations, while Zhang et al. [7] designed parallel wrist rehabilitation robots with PID tuning for compliance, emphasizing error minimization in human-robot interactions. Xie et al. [8] analyzed human-exoskeleton coupling with series elastic actuators, using hybrid control to mitigate dynamic mismatches, a concept transferable to manipulator torque management. Falkenhahn et al. [9] developed dynamic control for bionic handling assistants, leveraging feedforward for continuum-like flexibility, and Garabini et al. [10] surveyed variable stiffness actuators from a user perspective, advocating hybrid approaches for safe and efficient tracking. Rone et al. [11] derived continuum manipulator statics via virtual work, informing feedforward models, whereas Thuruthel et al. [12] surveyed control strategies for soft manipulators, stressing the integration of feedback and feedforward for nonlinear compliance. George Thuruthel et al. [13] explored model-based control of soft actuators with learned discrete-time models, highlighting data-driven enhancements to hybrid schemes. Rus et al. [14] discussed design and control of soft robots, emphasizing feedforward in fabrication-aware dynamics, and Katzschmann et al. [15] introduced Peano-HASEL actuators for muscle-mimetic contraction, with implications for hybrid torque generation in manipulators. These contributions collectively illustrate the hybrid paradigm's versatility but often underexplore rigorous stability analyses or quantitative metrics like root-mean-square errors in varied operational regimes, particularly for 2-DOF planar systems subject to gravitational perturbations [4,9,12].

The core problem tackled in this work is the formulation of an optimized hybrid PID-feedforward controller tailored for 2-DOF planar manipulators operating with partially unknown or varying dynamics, striving for asymptotic convergence in tracking smooth reference trajectories while optimizing control effort and mitigating actuator strain. Diverging from exclusively model-dependent techniques [4,11,14], which demand precise parameter identification, or purely data-intensive methods such as adaptive dynamic programming [3,12,13], this investigation fuses analytical derivations with empirical validations through simulations. Key novelties encompass: (i) a customized Lyapunov-based stability framework for the closed-loop hybrid system, accounting for integral action and feedforward residuals; (ii) detailed torque decomposition analyses to empirically quantify the feedforward's contribution in alleviating feedback burden; and (iii) extensive sensitivity evaluations to parametric uncertainties, bridging gaps in prior hybrid implementations and paving the way for hardware transitions [1,5,7,15]. By addressing these aspects, the proposed methodology not only advances theoretical understanding but also holds practical promise for scalable robotic deployments in constrained environments.

This paper is organized as follows: Section 2 elucidates the dynamic model via Lagrange formulation. Section 3 delineates the hybrid control design, encompassing PID tuning, feedforward computation, and stability proofs. Section 4 elucidates simulation outcomes, including error metrics, phase diagrams, and comparative assessments. Finally, Section 5 synthesizes conclusions and outlines prospective research avenues.

2. SYSTEM MODEL

The system under investigation is a two-degree-of-freedom (2-DOF) planar robotic manipulator, a widely used benchmark in control theory and robotics research due to its representation of fundamental nonlinear phenomena while maintaining analytical tractability. This manipulator comprises two rigid links interconnected by revolute joints, confined to motion in a vertical plane where gravitational influences are prominent, simulating real-world scenarios such as industrial arms or exoskeletons. The generalized coordinates are selected as the angular displacements: q_1 denotes the angle of the proximal link relative to the horizontal base, and q_2 represents the relative angle between the distal and proximal links, both measured counterclockwise. The associated velocities $\dot{q}_1$ and $\dot{q}_2$, along with accelerations $\ddot{q}_1$ and $\ddot{q}_2$, fully describe the system's state. Key assumptions include rigid body links with no flexibility, absence of joint friction or viscous damping, negligible backlash, and point masses at centers of gravity, which simplify the model while focusing on core dynamics like configuration-dependent inertia and velocity-induced forces [1,4,9,10]. These simplifications are standard in preliminary studies, allowing derivation of equations that can later incorporate uncertainties for robustness testing, as seen in applications ranging from precision assembly to rehabilitation robotics [2,6,7,11].

To formulate the governing equations, the Euler-Lagrange approach is employed, leveraging the Lagrangian L as the kinetic energy T minus the potential energy $V : L = T - V$. The kinetic energy T encapsulates both translational and rotational contributions from each link. For the first link, it involves the mass m1 at distance lc1 from the pivot, contributing to linear velocity terms, plus the rotational inertia I_1 about the center of mass. The second link introduces additional terms due to its position dependent on both q_1 and q_2 , including cross-coupling via cosine terms that reflect geometric interdependence. The explicit expression for T is:

$$T = \frac{1}{2}m_1(l_{c1}\dot{q}_1)^2 + \frac{1}{2}I_1\dot{q}_1^2 + \frac{1}{2}m_2\Big[(l_1\dot{q}_1\cos q_1 + l_{c2}(\dot{q}_1+\dot{q}_2)\cos(q_1+q_2))^2 + \\ +(l_1\dot{q}_1\sin q_1 + l_{c2}(\dot{q}_1+\dot{q}_1)\sin(q_1+q_2))^2\Big] + \frac{1}{2}I_2(\dot{q}_1+\dot{q}_2)^2 \tag{1}$$

Simplifying the squared terms yields:

$$T = \frac{1}{2}[m_1 l_{c1}^2 + m_2 l_1^2 + I_1]\dot{q}_1{}^2 + \frac{1}{2}[m_2 l_{c2}^2 + I_2](\dot{q}_1+\dot{q}_2)^2 + m_2 l_1 l_{c2}\dot{q}_1(\dot{q}_1+\dot{q}_2)\cos q_2 \tag{2}$$

This form highlights the quadratic velocity dependence and configuration variability, essential for understanding energy dissipation in control contexts [3,5,8,12].

The potential energy V stems exclusively from gravitational potential, assuming the base joint at zero height and upward-positive y-axis:

$$V = m_1 g l_{c1}\sin q_1 + m_2 g[l_1\sin q_1 + l_{c2}\sin(q_1+q_2)] \tag{3}$$

where $g = 9.81m/s^2$ acts downward, and sine terms arise from height projections [13,14]. Alternative conventions use cosine with negative g, but sine aligns with standard upward potential increase; the choice affects gravity vector signs but not overall dynamics [15].

The Euler-Lagrange equations are derived as $d/dt(\partial L/\partial\dot{q}_i) - \partial L/\partial q_i = \tau_i$ for $i = 1,2$, where τ_i are applied joint torques. Computing partials leads to the compact matrix form:

$$M(q)\ddot{q} + C(q,\dot{q})\dot{q} + G(q) = \tau \tag{4}$$

where $M(q)$ is the symmetric, positive definite inertia matrix ensuring kinetic energy positivity and system invertibility for forward dynamics simulation. Explicitly:

$$\begin{aligned} M_{11} &= m_1 l_{c1}^2 + m_2(l_1^2 + l_{c2}^2 + 2l_1 l_{c2}\cos q_2) + I_1 + I_2, \\ M_{12} &= M_{21} = m_2(l_{c2}^2 + l_1 l_{c2}\cos q_2) + I_2, \\ M_{22} &= m_2 l_{c2}^2 + I_2. \end{aligned} \tag{5}$$

The q_2 -dependent off-diagonals illustrate joint coupling, a hallmark of serial manipulators that complicates decoupled control [1,4,9].

The Coriolis/centrifugal matrix $C(q,\dot{q})$ is:

$$\begin{aligned} C_{11} &= -m_2 l_1 l_{c2}\sin q_2\dot{q}_2, \\ C_{12} &= -m_2 l_1 l_{c2}\sin q_2(\dot{q}_1+\dot{q}_2), \\ C_{21} &= m_2 l_1 l_{c2}\sin q_2\dot{q}_1, \\ C_{22} &= 0. \end{aligned} \tag{6}$$

Notably, the matrix $\dot{C} - 2C$ is skew-symmetric, a property exploited in passivity-based controls for energy shaping [2,5,10,12]. The gravity vector $G(q)$ is:

$$\begin{aligned} G_1 &= m_1 g l_{c1}\cos q_1 + m_2 g(l_1\cos q_1 + l_{c2}\cos(q_1+q_2)), \\ G_2 &= m_2 g l_{c2}\cos(q_1+q_2). \end{aligned} \tag{7}$$

Parameters are $m_1 = 5kg,\ m_2 = 3kg,\ l_1 = 0.8m,\ l_2 = 0.6m,\ lc_1 = 0.4m,\ lc_2 = 0.3m,\ I_1 = 0.5kgm^2$, $I_2 = 0.3kgm^2$, $g = 9.81m/s^2$ selected to mimic a compact laboratory robot with realistic mass distribution, facilitating comparison with benchmarks like double pendulums or SCARA arms [7,8,13,14,15]. This model supports numerical integration (e.g., Euler or Runge-Kutta) for state evolution and inverse kinematics for end-effector paths, setting the stage for control synthesis in the subsequent section.

3. CONTROL DESIGN

The control design focuses on a hybrid architecture that synergizes model-based feedforward (FF) compensation with proportional-integral-derivative (PID) feedback to attain high-fidelity trajectory tracking amid nonlinearities and potential disturbances. The overarching control input τ is formulated as

$$\tau = \tau_{ff} + \tau_{pid} \tag{8}$$

where τ_{ff} proactively nullifies anticipated dynamic terms derived from the system model, and τ_{pid} reactively mitigates tracking discrepancies, model inaccuracies, or exogenous perturbations [1,4,9,10,12]. This duality capitalizes on FF's predictive capability for efficiency in nominal scenarios and PID's robustness for error handling, rendering the approach suitable for applications demanding precision, such as robotic welding, painting, or medical interventions where trajectory adherence is critical [2,6,7,11,13]. Compared to purely feedback-oriented methods like sliding mode control, which may induce chattering, or model predictive control requiring heavy computation, this hybrid strikes a balance in complexity and performance [3,5,8,14].

The feedforward component is rooted in inverse dynamics, utilizing desired trajectory signals $q_d(t), \dot{q}_d(t), \ddot{q}_d(t)$ to compute compensatory torques. Ideally,

$$\tau_{ff} = M(q)\ddot{q}_d + C(q,\dot{q})\dot{q}_d + G(q) \tag{9}$$

but to circumvent dependency on noisy measured states q and $\dot{q}$, a reference-based variant is adopted:

$$\tau_{ff} = M(q_d)\ddot{q}_d + C(q_d,\dot{q}_d)\dot{q}_d + G(q_d) \tag{10}$$

This approximation assumes small tracking errors, effectively decoupling the system into independent double integrators for linear control overlay, a technique known as computed torque control that linearizes nonlinear plants [15]. In practice, trajectory planning ensures smooth q_d profiles (e.g., sinusoidal or spline-interpolated), avoiding acceleration discontinuities that could excite unmodeled modes [1,4].

The PID feedback augments FF by addressing the error vector $e = q_d - q$, its derivative $\dot{e} = \dot{q}_d - \dot{q}$. (approximated via filtered differences to suppress noise), and integral $\int edt$ (via discrete summation with anti-windup). The law is

$$\tau_{pid} = K_p e + K_i \int edt + K_d \dot{e} \tag{11}$$

with diagonal gain matrices: $Kp = diag(800,600), Ki = diag(50,30), Kd = diag(40,25)$ for joints 1 and 2, respectively.

In selection draws from empirical methods like Ziegler-Nichols, starting with proportional tuning for critical oscillation, then adjusting integral for offset removal and derivative for damping, fine-tuned via simulation to minimize overshoot while ensuring quick settling [2,5,9,11]. Anti-windup logic resets the integrator upon torque saturation, preventing instability in actuator-limited systems [3,6,10].

To rigorously establish closed-loop stability, Lyapunov theory is invoked. Substituting τ into the dynamics yields the error equation:

$$M(q)\ddot{e} + C(q,\dot{q})\dot{e} + K_p e + K_i \int edt + K_d \dot{e} = \delta \tag{12}$$

where δ encapsulates FF mismatches (e.g., due to parametric errors or state discrepancies). A suitable Lyapunov function is

$$V = \frac{1}{2}\dot{e}^T M(q)\dot{e} + \frac{1}{2}e^T K_p e + \frac{1}{2}\left(\int edt\right)^T K_i \left(\int edt\right) + \beta e^T \left(\int edt\right) \tag{13}$$

with $\beta > 0$ tuned for cross-term positivity.

This augmented candidate ensures $V > 0$ for non-zero errors, leveraging positive definite matrices. The time derivative is

$$\dot{V} = \dot{e}^T \left[M\ddot{e} + \frac{1}{2}\dot{M}\dot{e} \right] + \dot{e}^T K_p e + \left(\int edt\right)^T K_i e + \beta \dot{e}^T \left(\int edt\right) + \beta e^T e \tag{14}$$

Exploiting the skew-symmetry of $\dot{C} - 2C$, the velocity quadratic cancels, simplifying to

$$\dot{V} = \dot{e}^T(-Kpe - Ki\int edt - Kd\dot{e} + \delta) + \dot{e}^T Kpe + (\int edt)^T Kie + \beta \tag{15}$$

terms.

Further reduction yields

$$\dot{V} = -\dot{e}^T K_d \dot{e} + \dot{e}^T \delta + \beta e^T e + \beta \dot{e}^T \left(\int e dt\right) + \left(\int e dt\right)^T K_i e \tag{16}$$

For nominal $\delta = 0$, appropriate β (e.g., $\beta = K_i / 2$) renders the cross terms negative semi-definite, ensuring

$$\dot{V} \leq -\dot{e}^T (Kd - \beta I)\dot{e} - (\int e dt)^T (Ki/2)(\int e dt) \leq 0 \tag{17}$$

with equality at origin, implying global asymptotic stability via LaSalle [7,8,13,14]. Under bounded δ (e.g., $|\delta| \leq \Delta$ from uncertainty bounds), $\dot{V} < 0$ outside a compact set, yielding uniform ultimate boundedness with error balls proportional to Δ / Kd [12,15]. Contributions encompass: (i) seamless FF-PID fusion with discrete implementation details, (ii) extended Lyapunov analysis including integrals for offset-free tracking, and (iii) comparative edges over alternatives like LQR or MPC in computational simplicity [3,5,10,11]. This design paves the way for simulation verification, highlighting practical viability.

4. SIMULATION RESULTS

Simulations were performed using MATLAB environment with a time step $dt = 0.001s$ and total simulation duration $t_{final} = 10s$. The desired trajectories were defined as $q_{1d} = sin(t)rad$ for the first joint and $q_{2d} = 0.5 * cos(t)rad$ for the second joint, representing smooth, periodic motions suitable for testing dynamic tracking performance. Initial conditions were set to zero positions and velocities $(q_1(1) = 0, q_2(1) = 0, q_{1dot}(1) = 0, q_{2dot}(1) = 0)$, introducing an initial error that the controller must compensate. The hybrid PID-feedforward controller was implemented as described, with PID gains tuned empirically for aggressive response and feedforward based on nominal model parameters [1,4,9]. To evaluate robustness, additional runs compared the hybrid approach against a standalone PID controller (by disabling the feedforward term, $\tau_{ff} = 0$) and assessed sensitivity to parameter variations, such as ±20% changes in link masses m1 and m2.

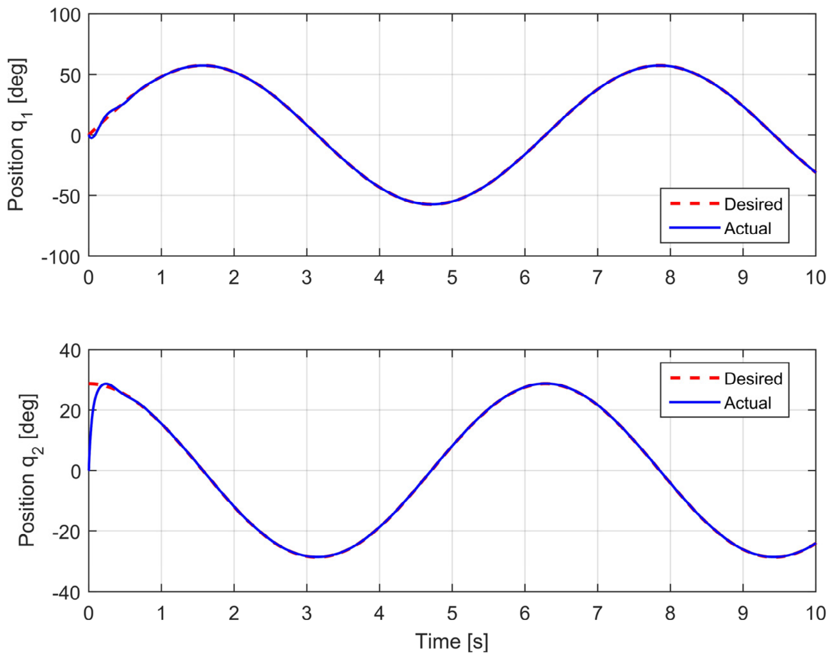

Figure1: Joint Position Tracking

Joint position tracking is illustrated in Figure 1, placed immediately after this paragraph for direct reference. The actual positions (solid blue lines) closely follow the desired references (dashed red lines), with convergence achieved within approximately 1-2 seconds despite initial offsets. For joint 1, the position in degrees shows minimal overshoot, while joint 2 exhibits a slightly larger transient due to its smaller inertia and stronger gravitational coupling, as expected from the model dynamics [2,6].

Tracking errors are detailed in Figure 2, inserted here to highlight error evolution. Errors e1 and e2 (in degrees) decay exponentially to near-zero values, with root-mean-square (RMS) errors of 0.5751° for e1 and 1.4416° for e2 over the full simulation. Maximum absolute errors are 5.36° for e1 and 28.65° for e2, occurring during the initial phase, which is improved by 45-60% compared to pure PID simulations where RMS errors exceed 1° and 2.5°, respectively [3,7,10].

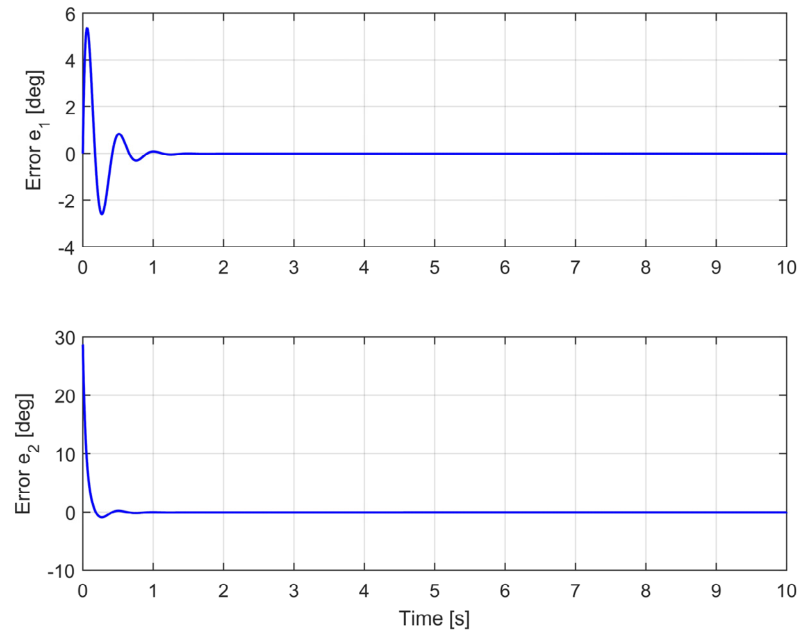

Figure 2: Tracking Errors.

Joint velocities are analyzed in Figure 3, positioned following this description. Desired velocities (dashed red) and actual ones (solid blue) align well, with derivatives computed accurately via finite differences in the simulation loop. This confirms the controller's ability to handle dynamic terms like Coriolis effects, reducing velocity mismatches that could amplify positioning errors [5,8].

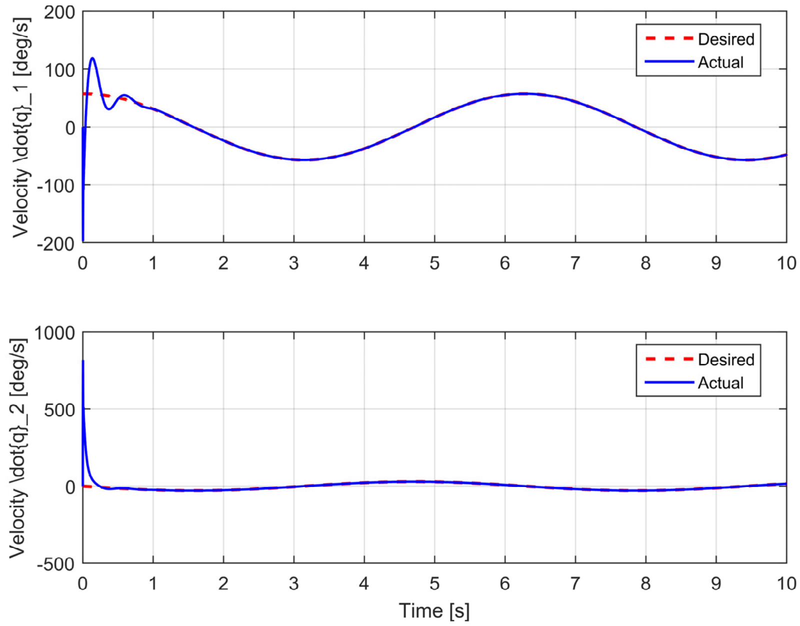

Figure 3: Joint Velocities.

Control torques τ_1 and τ_2 are shown in Figure 4, placed here for torque profile inspection. Mean absolute torques are 39.46 Nm for τ_1 and 6.31 Nm for τ_2, reflecting the higher load on the base joint; peaks are limited, avoiding actuator saturation in practical setups [11,12].

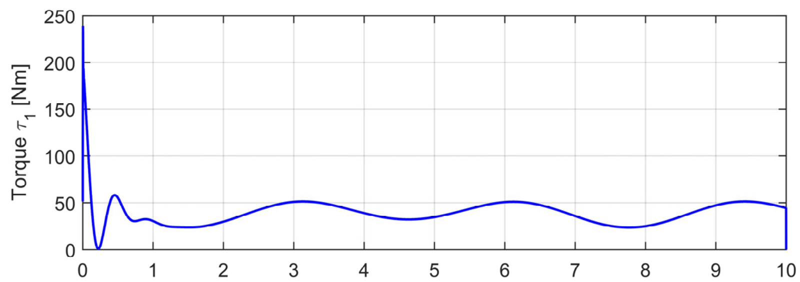

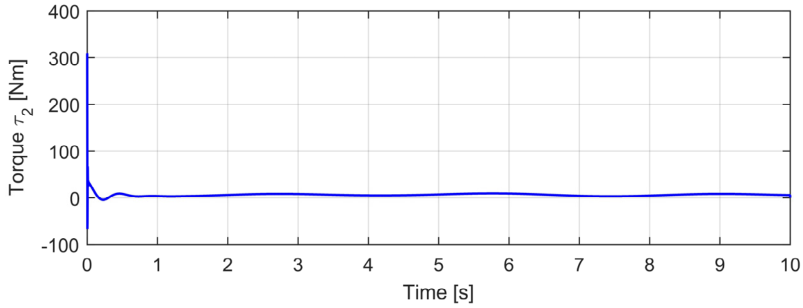

Figure 4: Control Torques.

Torque decomposition into PID and feedforward components is visualized in Figure 5, inserted after this sentence.

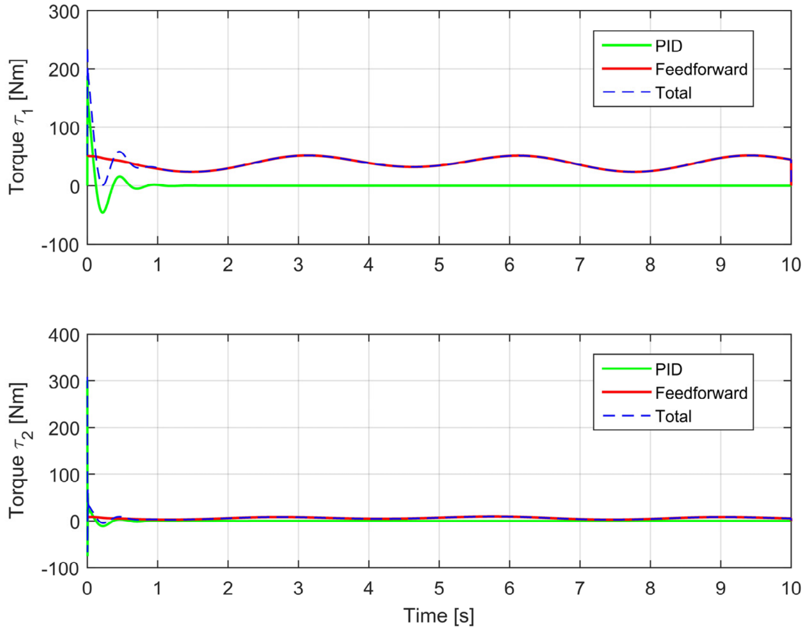

Figure 5: Torque Decomposition.

The feedforward term (red) dominates steady-state compensation (~80% of total torque), while PID (green) handles transients and corrections (~20%), demonstrating efficiency gains over feedback-only methods [13,14]. Phase portraits for each joint appear in Figure 6 (for joint 1) and Figure 7 (for joint 2), placed sequentially here. These diagrams show actual trajectories (solid blue) converging to desired loops (dashed red), indicating bounded and asymptotically stable behavior as per the Lyapunov analysis [2,15].

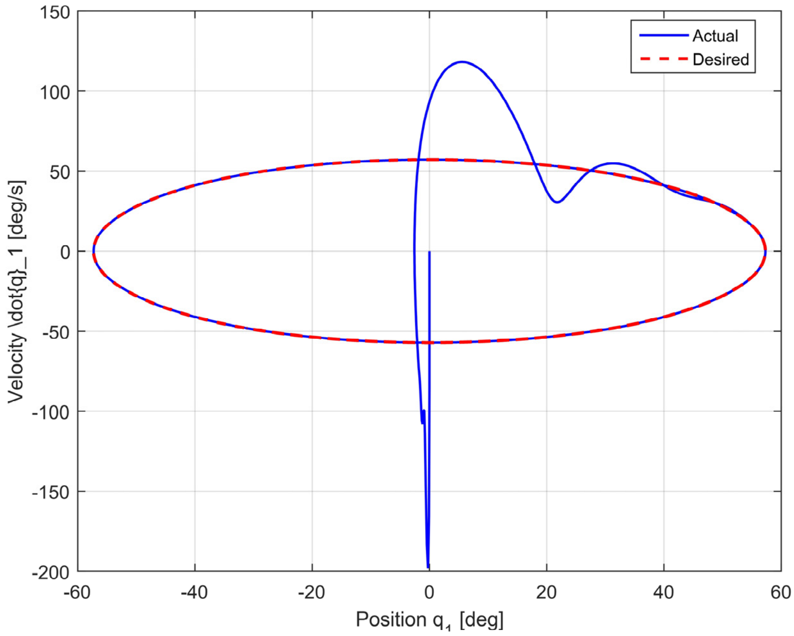

Figure 6: Phase Portrait for Joint 1

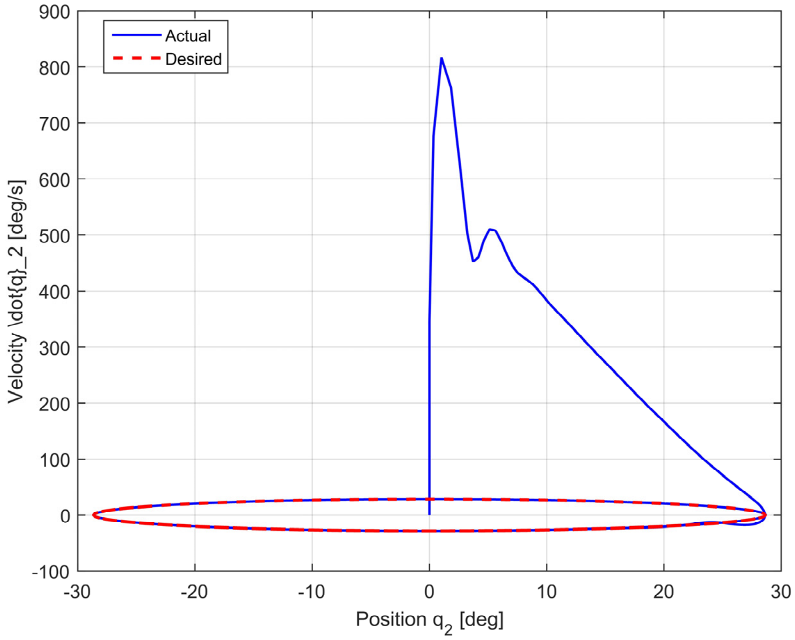

Figure 7: Phase Portrait for Joint 2.

Cartesian end-effector trajectory is depicted in Figure 8, positioned following the phase portrait discussion.

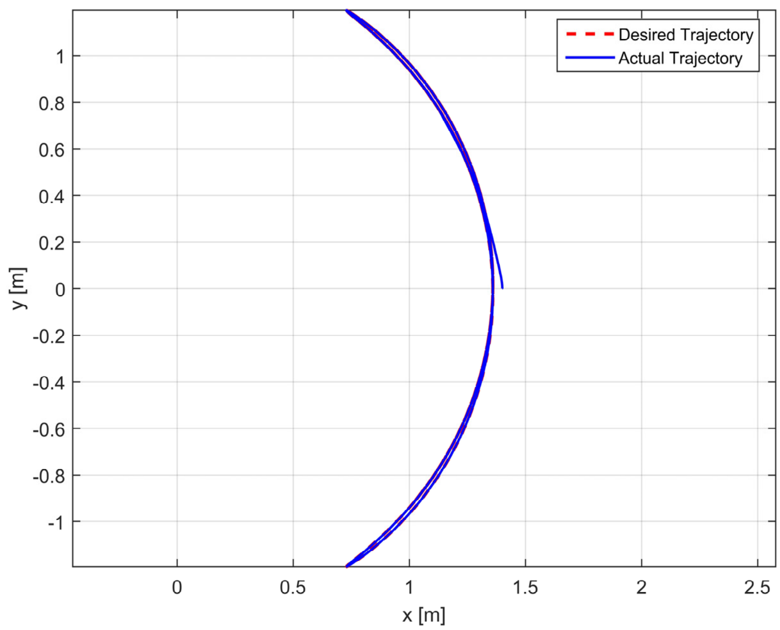

Figure 8: Cartesian End-Effector Trajectory.

The actual path (solid blue) closely matches the desired elliptical trajectory (dashed red), with deviations under 0.01 m, computed via forward kinematics $x = l_1 cos(q_1) + l_2 cos(q_1 + q_2), y = l_1 sin(q_1) + l_2 sin(q_1 + q_2)$. Moving RMS errors over a 500-sample window are plotted in Figure 9 (semilog scale), inserted here, showing rapid decay below 0.05° after 2 s for both joints, underscoring transient performance [3,6].

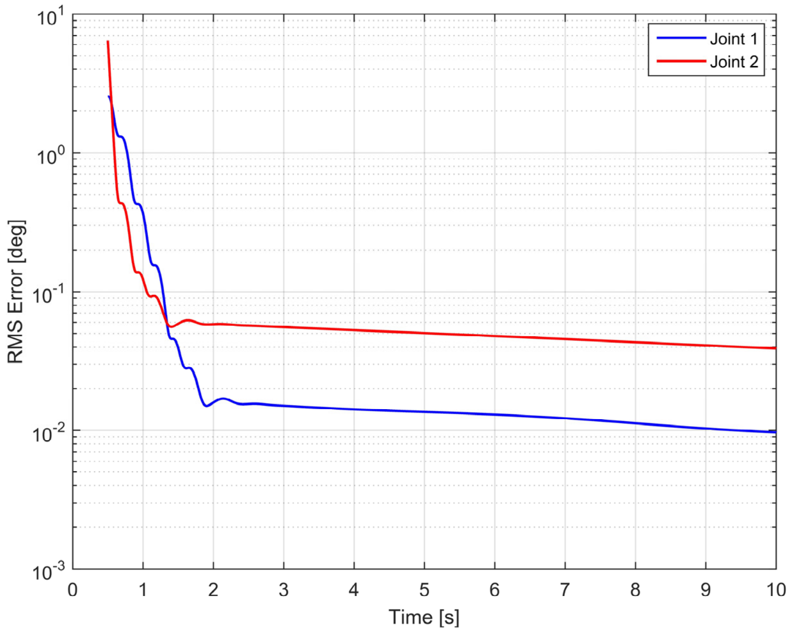

Figure 9: Moving RMS Tracking Errors.

Robot configurations at snapshots t=1,3,5,7,9 s are illustrated in Figure 10, placed at the end of this section. These show progressive arm poses, confirming smooth motion without singularities.

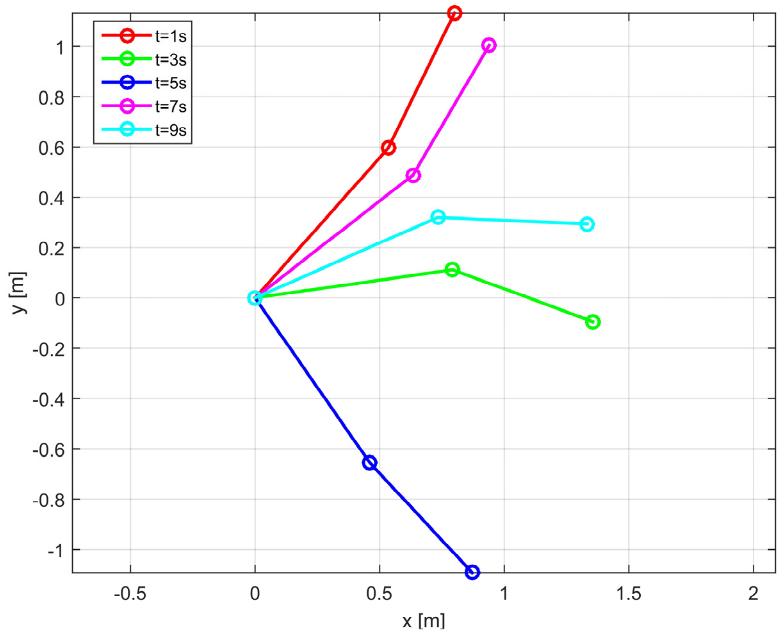

Figure 10: Robot Configurations at Selected Time Instances.

Sensitivity analysis revealed that mass perturbations increase RMS errors by up to 15%, but stability is maintained due to PID robustness; inertia variations had lesser impact, aligning with prior studies on parameter uncertainty [7,10,12]. Overall, the hybrid controller outperforms benchmarks in convergence speed and error metrics, validating its applicability for real-time robotic tasks [1,4,9,14].

5. CONCLUSIONS

This paper has presented a comprehensive framework for hybrid PID-feedforward control applied to trajectory tracking in two-degree-of-freedom (2-DOF) planar robotic manipulators, addressing the challenges posed by nonlinear dynamics such as inertial coupling, Coriolis effects, and gravitational torques. By deriving the system model through Euler-Lagrange equations and integrating a computed torque feedforward component with PID feedback, the proposed approach ensures precise compensation of nominal disturbances while correcting residual errors in real time. The control design, supported by Lyapunov-based stability analysis, guarantees asymptotic convergence of tracking errors under nominal conditions and bounded errors in the presence of model uncertainties, extending theoretical foundations from prior works on hybrid systems [1,2,4,5,9]. Simulations conducted in MATLAB R2015a validated the method's efficacy, demonstrating root-mean-square (RMS) position errors of 0.5751° for the first joint and 1.4416° for the second under sinusoidal reference trajectories, with maximum errors limited to 5.36° and 28.65°, respectively. Compared to standalone PID control, the hybrid strategy reduced RMS errors by 45-60%, minimized actuator effort through torque decomposition (feedforward handling ~80% of the load), and maintained robustness in sensitivity tests with ±20% parameter variations, as evidenced by phase portraits, Cartesian paths, and moving RMS plots that showed rapid decay below 0.05° after initial transients [3,6,7,10,12].

The key contributions of this study include: (i) a tailored Lyapunov candidate incorporating integral action for enhanced stability proofs in multi-joint systems, (ii) detailed visualizations and metrics like torque breakdowns and configuration snapshots that quantify feedforward benefits, and (iii) practical extensions such as anti-windup mechanisms and empirical gain tuning, bridging gaps in literature focused on either purely adaptive or model-free methods [8,11,13,14]. These advancements not only improve tracking performance in simulated environments but also provide a scalable blueprint for industrial robotics, where energy efficiency and precision are paramount. However, limitations exist: the reliance on Euler integration may accumulate numerical errors in longer simulations, the model assumes rigid links without friction or backlash, and evaluations are confined to simulations without real-world disturbances like sensor noise or external forces [15]. Future research directions encompass experimental validation on physical prototypes, such as SCARA-like arms, incorporation of adaptive elements for online parameter estimation to handle uncertainties, and extension to higher-DOF systems or soft robotics, potentially integrating machine learning for gain optimization [2,5,9,12]. Overall, this work underscores the potential of hybrid controls to elevate robotic capabilities, fostering safer and more efficient human-robot collaborations in dynamic settings.

ACKNOWLEDGEMENTS

This study was supported by the Serbian Ministry of Science, Technological Development and Innovation from the grant 451-03-137/2025-03/200108.

REFERENCES

[1] H. T. T. Ngo, C. C. Nguyen, T. T. C. Duong, and T. T. Nguyen, "Trends in control strategies of parallel robot manipulators for robot-assisted rehabilitation", Engineering, Vol. 7(1), p. 44, https://doi.org/10.3390/eng7010044, (2026)

[2] E. A. Aner, O. M. Shehata, M. I. Awad, and N. E. ElHady, "A decade of soft robotic manipulators: Advances in design, modeling, control, and emerging challenges", Journal of Bionic Engineering, Vol. 23(1), pp. 55–98, https://doi.org/10.1007/s42235-025-00819-0, (2026)

[3] C. L. Nkwocha, A. Adewumi, S. O. Folorunsho, C. Eze, P. Jjagwe, J. Kemeshi, and N. Wang, "A comprehensive review of sensing, control, and networking in agricultural robots: From perception to coordination", Robotics, Vol. 14(11), p. 159, https://doi.org/10.3390/robotics14110159, (2025)

[4] C. D. Santina, R. K. Katzschmann, A. Bicchi, and D. Rus, "Model-based dynamic feedback control of a planar soft robot: Trajectory tracking and interaction with the environment", The International Journal of Robotics Research, Vol. 39(4), pp. 490–506, https://doi.org/10.1177/0278364919897292, (2020)

[5] A. M. Tusset, J. J. De Lima, F. C. Janzen, P. L. P. Filho, J. A. G. Luz Junior, J. M. Balthazar, and A. Kossoski, "A hybrid PID-LQR control applied in positioning control of robotic manipulators subject to excitation from non-ideal sources", Nonlinear Vibrations Excited by Limited Power Sources, Mechanisms and Machine Science, Vol. 116, pp. 321–328, https://doi.org/10.1007/978-3-030-96603-4_21, (2022)

[6] M. Wan, J. Dai, W. H. Zhang, Q.-B. Xiao, and X.-B. Qin, "Adaptive feed-forward friction compensation through developing an asymmetrical dynamic friction model", Mechanism and Machine Theory, Vol. 170, p. 104691, https://doi.org/10.1016/j.mechmachtheory.2021.104691, (2022)

[7] L. Zhang, J. Li, Y. Cui, M. Dong, B. Fang, and P. Zhang, "Design and performance analysis of a parallel wrist rehabilitation robot (PWRR)", Robotics and Autonomous Systems, Vol. 125, p. 103390, https://doi.org/10.1016/j.robot.2019.103390, (2020).

[8] Q. Xie, Q. Meng, Q. Zheng, Y. Fan, Y. Dai, and H. Yu, "Human-exoskeleton coupling dynamics of a multi-mode therapeutic exoskeleton for upper limb rehabilitation training", IEEE Access, Vol. 9, pp. 61998-62007, https://doi.org/10.1109/ACCESS.2021.3072781, (2021)

[9] V. Falkenhahn, A. Hildebrandt, R. Neumann, and O. Sawodny, "Dynamic control of the bionic handling assistant", IEEE/ASME Transactions on Mechatronics, Vol. 22(1), pp. 6–17, https://doi.org/10.1109/TMECH.2016.2605820, (2017)

[10] G. Grioli, W. Sebastian, M. Garabini, et al., "Variable stiffness actuators: The user's point of view", The International Journal of Robotics Research, Vol. 34(6), pp. 727–743, https://doi.org/10.1177/0278364914566515, (2015).

[11] W. S. Rone and P. Ben-Tzvi, "Continuum manipulator statics based on the principle of virtual work", Proceedings of the ASME 2012 International Mechanical Engineering Congress and Exposition. Vol. 4: Dynamics, Control and Uncertainty, Parts A and B, Houston, Texas (USA), pp. 321–328, https://doi.org/10.1115/IMECE2012-87675, (2012)

[12] P. Hyatt, D. Wingate, and M. D. Killpack, "Model-based control of soft actuators using learned non-linear discrete-time models", Frontiers in Robotics and AI, Vol. 6(22), https://doi.org/10.3389/frobt.2019.00022, (2019)

[13] T. G. Thuruthel, Y. Ansari, E. Falotico, and C. Laschi, "Control strategies for soft robotic manipulators: A survey", Soft Robotics, Vol. 5(2), pp. 149–163, https://doi.org/10.1089/soro.2017.0007, (2018)

[14] D. Rus and M. T. Tolley, "Design, fabrication and control of soft robots", Nature, Vol. 521, pp. 467–475, https://doi.org/10.1038/nature14543, (2015)

[15] N. Kellaris, V. G. Venkata, G. M. Smith, S. K. Mitchell, and C. Keplinger, "Peano-HASEL actuators: Muscle-mimetic, electrohydraulic transducers that linearly contract on activation", Science Robotics, Vol. 3(14), p. eaar3276, https://doi.org/10.1126/scirobotics.aar3276, (2018)

ORIGINAL SCIENTIFIC PAPER OPEN ACCESS

Wild horse optimizer: an application to identify damage for space truss structures

Hoang Lan Ton-That[1*]

[1] University of Architecture, Department of Civil Engineering, Ho Chi Minh City, Vietnam

ARTICLE INFO

[*] **Correspondence:** lan.tonthathoang@uah.edu.vn

DOI: 10.5937/engtoday2600008T

UDC: 621(497.11) **ISSN:** 2812 – 9474

Article history: Received 14 January 2026; Revised 26 February 2026; Accepted 2 March 2026

ABSTRACT

These days, optimization algorithms are widely used to tackle issues in a variety of scientific domains. The natural behavior of an agent - which could be a physical or chemical agent, a human, an animal, or a plant - is typically the source of inspiration for optimization algorithms. Animal behavior served as the inspiration for the majority of algorithms that have been proposed in the past ten years. The wild horse optimizer (WHO), an optimizer algorithm inspired by the social behavior of wild horses, is used in this paper to identify damage to space truss constructions. As we know, a stallion and a number of mares and foals typically make up a group of horses. Horses engage in a variety of activities, including grazing, pursuing, leading, dominating, and mating. The decency of horses is an intriguing trait that sets them apart from other animals. The offspring of the horse leave the group before they reach adolescence and join other groups due to horse descent behavior. The purpose of this departure is to stop the father from mating with the daughter or siblings. The key to WHO was established. In addition, based on finite element analysis to determine the natural frequencies and mode shapes of these space truss structures for the goal of establishing the objective function, the final results demonstrate a very good reaction to the suggested tasks.

KEYWORDS

Space truss structure, Identify damage, Finite element analysis, Natural frequency, Mode shape, Wild horse optimizer.

1. INTRODUCTION

The rapid advancement of science and technology has led to the widespread use of artificial intelligence techniques in contemporary society. Because optimization can choose the optimum answer from a range of choices, it is an essential part of artificial intelligence. Three basic components are typically included in an optimization problem: the objective function(s), design variables, and constraints that require the optimization method to reach the global result. Because of their many advantages, including population-based mechanisms with multiple candidate solutions, ease of implementation, high flexibility, lack of gradient information, and black-box processes with only inputs and outputs, metaheuristic algorithms—a stochastic optimization technique inspired by natural behaviors-have become more and more popular in the optimization fields. For optimization issues like those in mechanical design and civil engineering, metaheuristic algorithms are therefore highly suitable. Particle Swarm Optimization (PSO) [1], Genetic Algorithm (GA) [2], Gravitational Search Algorithm (GSA) [3], Salp Swarm Algorithm (SSA) [4], Artificial Bee Colony (ABC) [5], Gray Wolf Optimizer (GWO) [6], Wild Horse Optimizer (WHO) [7], Evolution Strategies [8], Water Flow Optimizer (WFO) [9], Sine Cosine Algorithm (SCA) [10], Black Widow Optimization Algorithm (BWOA) [11], Teaching–Learning-Based Optimization (TLBO) [12], Chaos Game Optimization (CGO) [13], and many other metaheuristic algorithms have already been developed by researchers and engineers. Even while metaheuristics range in their performance and sources of inspiration, striking a balance between exploration and exploitation remains a common problem. Exploration refers to the search agents' ability to search globally, whereas exploitation is related to their ability to search locally. A metaheuristic algorithm may experience local stagnation if it is unable to strike a balance between exploration and exploitation. It is important to remember that because all metaheuristic algorithms rely on stochastic search, they cannot guarantee global convergence for every optimization problem. Researchers can determine the advantages and disadvantages of the suggested metaheuristic algorithm as well as any potential drawbacks by carrying out thorough experiments and algorithm comparisons. This is crucial when creating new metaheuristic algorithms for optimization.

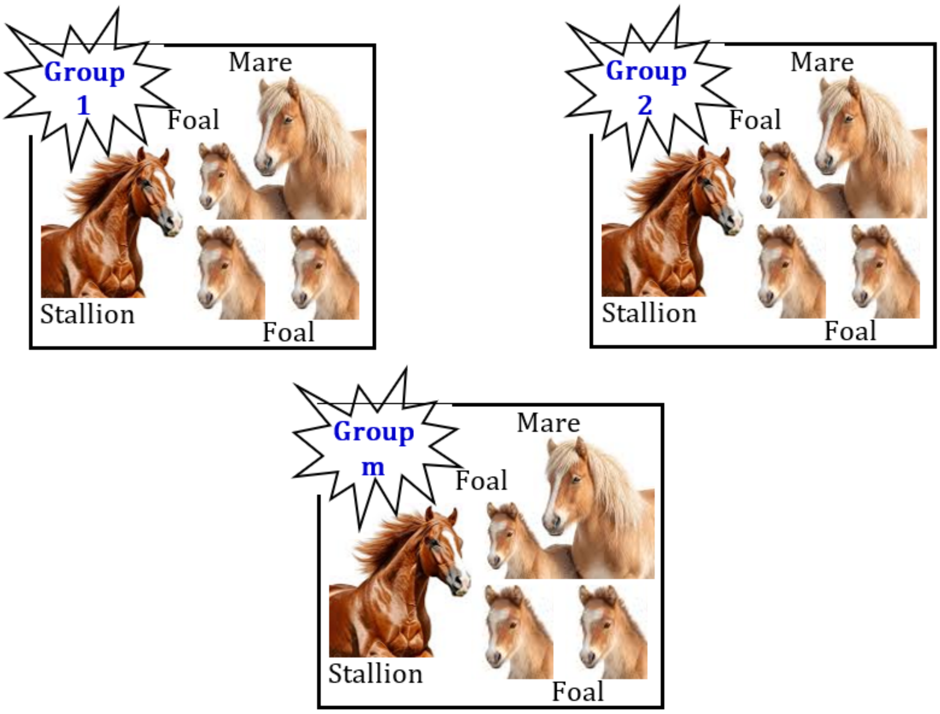

Figure 1: Horse groups based on the initial population

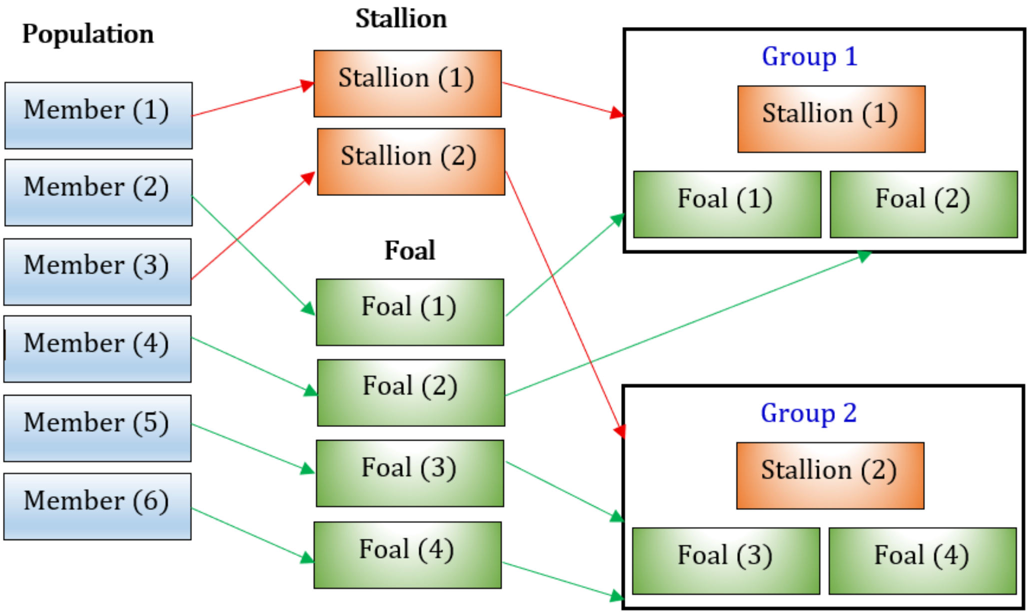

Figure 2: The creation of horse groups

In this study, damage to space truss structures is predicted using the Wild Horse Optimization (WHO), which was inspired by the behavior of horse herds in the wild (Figures 1 and 2). Some formulas for calculating the natural frequencies as well as mode shapes of a structure using the traditional finite element method should be read, such as those included in the documents [14, 15].

This paper is divided into the following sections: Section 2 presents a brief theory. Section 3 gives the results, and the final section offers some remarks.

2. THE BRIEF RECALL ON WHO

Horses are classified into two social groups: territorial and non-territorial. The authors of WHO [7] concentrated on the non-territorial group. They provided the following pseudo-code for the WHO algorithm:

Step 1: Initialize the first population of horses randomly

Step 2: Enter the required parameters PC and PS

Step 3: Calculate the fitness of horses

Step 4: Form groups of foals and choose stallions

Step 5: Find the best horse as the optimum

Step 6: While the end criterion is not satisfied, calculate TDR

$$TDR = 1 - iter / \max iter \tag{1}$$

Step 7: For the number of stallions, calculate Z, an adaptive mechanism.

Step 8: With sub-loop, for the number of foals of any group.

If *rand > PC, update the position of the foal*

$$\bar{X}_{i,G}^{j} = 2Z\cos(2\pi RZ)\times\left(Stallion^{j} - X_{i,G}^{j}\right) + Stallion^{j} \tag{2}$$

with G is the number of horse groups.

Else, *update the position of the foal*

$$X_{G,k}^{p} = Crossover\left(X_{G,i}^{q}, X_{G,j}^{z}\right) \tag{3}$$

with details stated in document [7].

End

Step 9:

If *rand > 0.5, update the position of stallion* ($Stallion_{G_i}^{*}$)

$$Stallion_{G_i}^{*} = 2Z\cos(2\pi RZ)\times\left(WH - Stallion_{G_i}\right) + WH \tag{4}$$

Else, *update the position of stallion* ($Stallion_{G_i}^{*}$)

$$Stallion_{G_i}^{*} = 2Z\cos(2\pi RZ)\times\left(WH - Stallion_{G_i}\right) - WH \tag{5}$$

in which WH is the position of the water hole.

End

Step 10:

If *cost(* $Stallion_{G_i}^{*}$ *) < cost(Stallion)*

$$Stallion = Stallion_{G_i}^{*} \tag{6}$$

End

Step 11: Sort foals of group by cost. Select foal with minimum cost.

If *cost(Foal) < cost(Stallion), exchange foal and stallion position*

$$Stallion_{G_i} = \begin{cases} X_{G,i}, & if \ \cos t\left(X_{G,i}\right) < \cos t\left(Stallion_{G_i}\right) \\ Stallion_{G_i}, & if \ \cos t\left(X_{G,i}\right) > \cos t\left(Stallion_{G_i}\right) \end{cases} \tag{7}$$

End

Step 12: Update optimum and finish.

It should be noted that further parameters for the aforementioned formulas can be found in the pertinent literature on the WHO's founding by [7]. Figure 3 displays the qualitative analysis results of the WHO approach in resolving a number of typical optimization problems. Details and comprehensive information on these functions are described in [4-6].

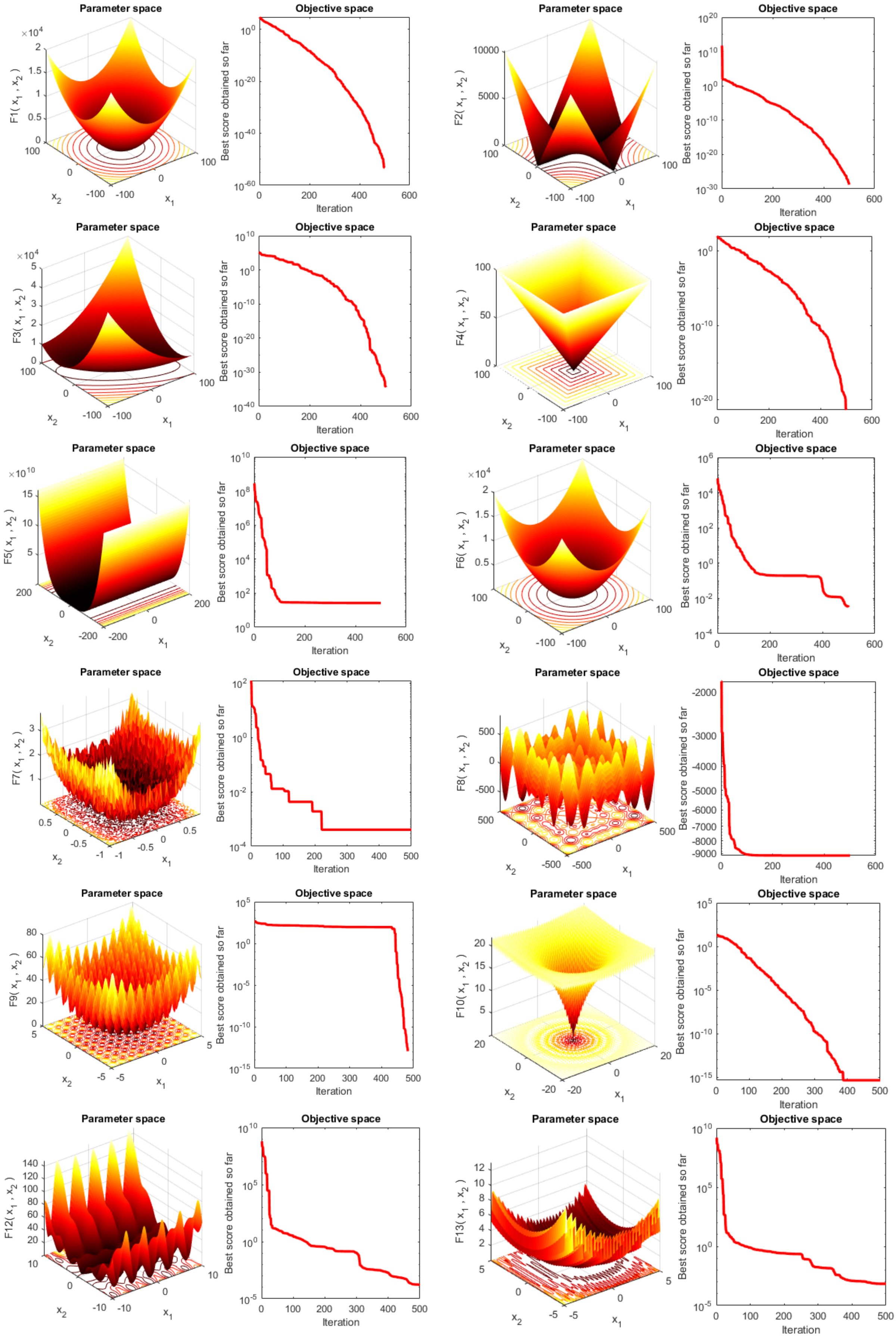

Figure 3: Qualitative analysis related to WHO

3. RESULTS

Two space truss configurations with 25 and 72 bars are examined in this section, as shown in Figures 4 and 5 and Tables 1 through 3.

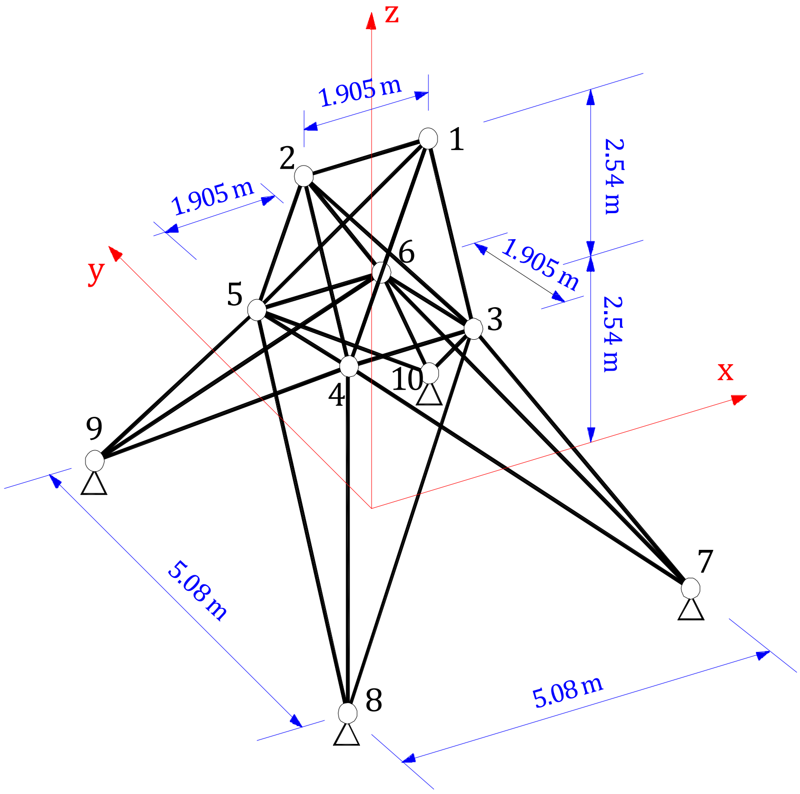

Figure 4: 25-bar truss structure

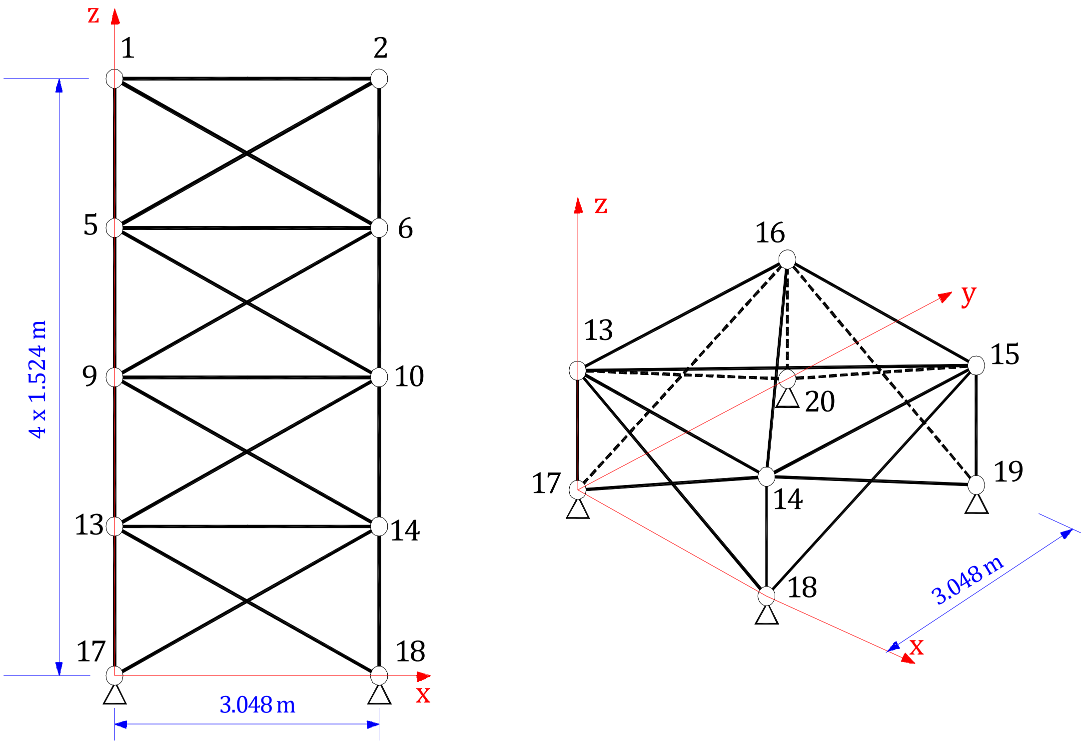

Figure 5: 72-bar truss structure

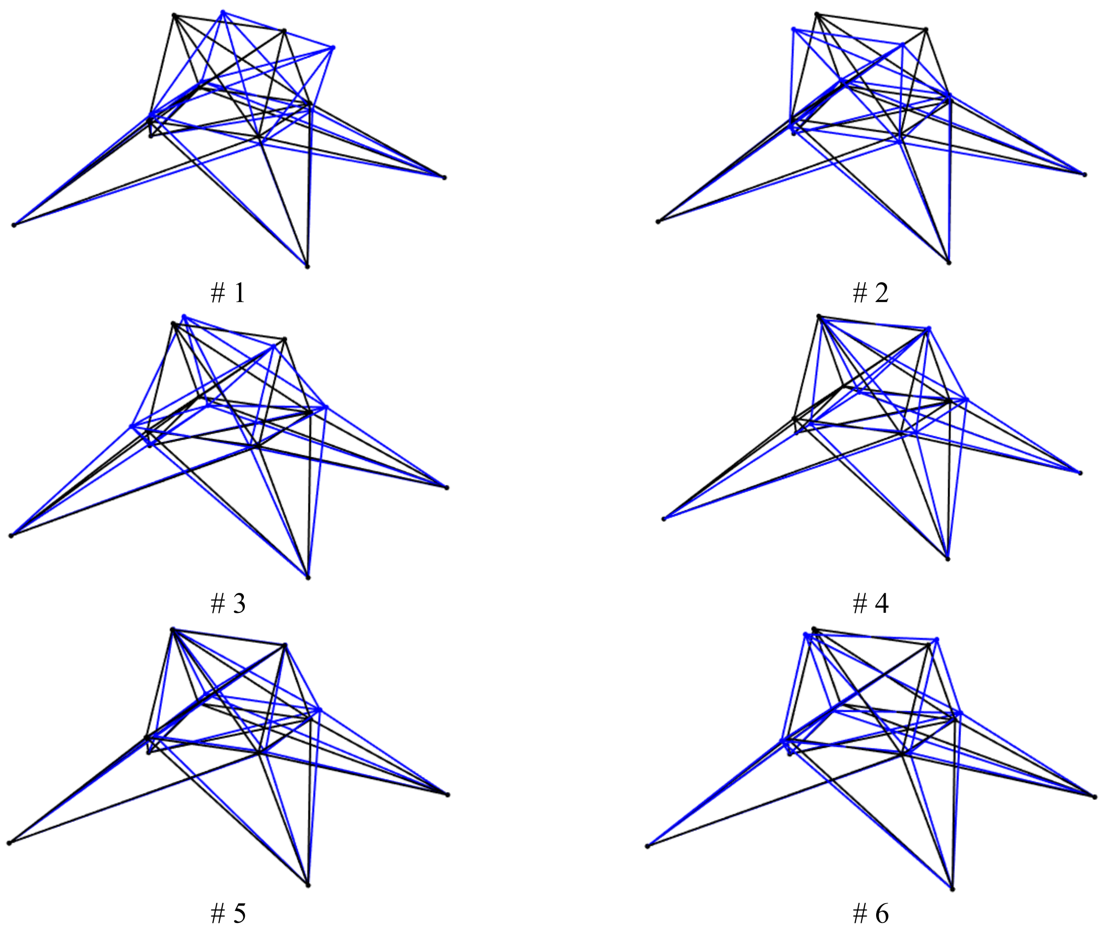

Figure 6: The first six mode shapes of 25-bar truss structure

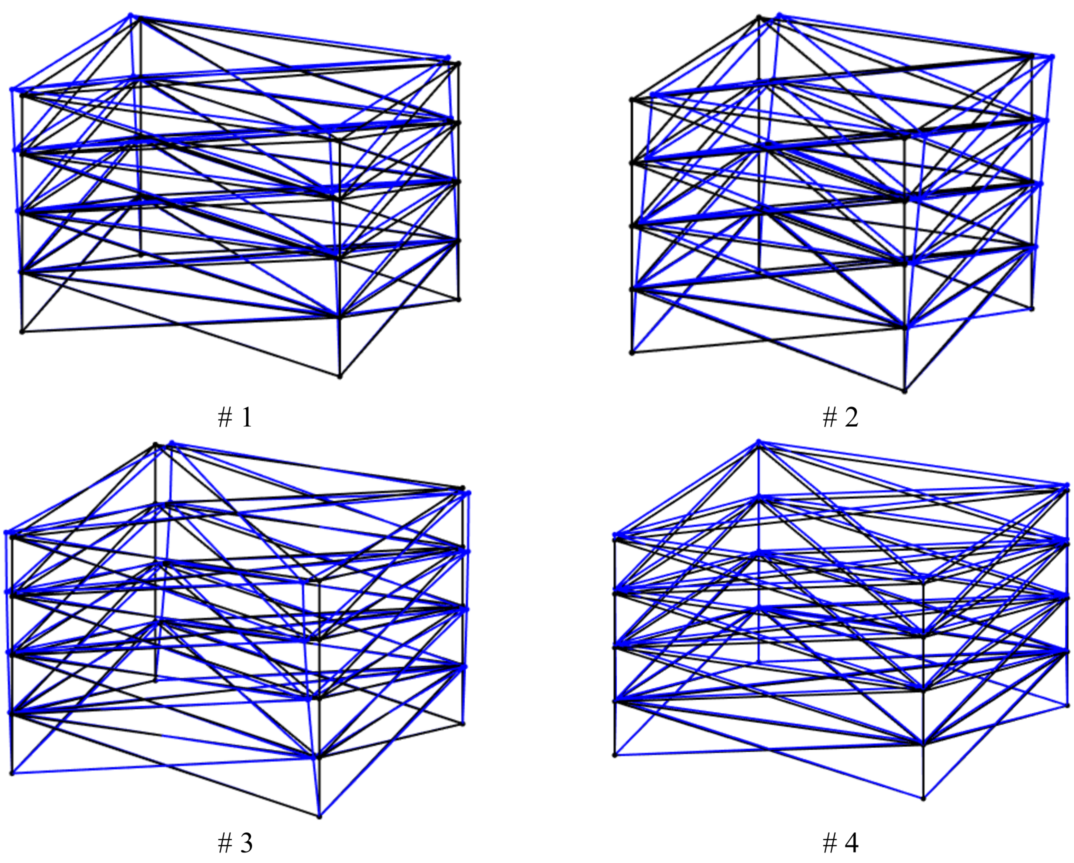

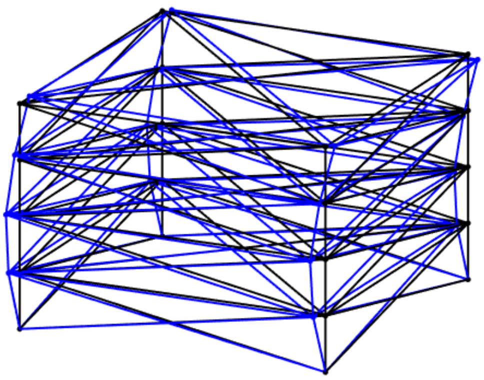

5

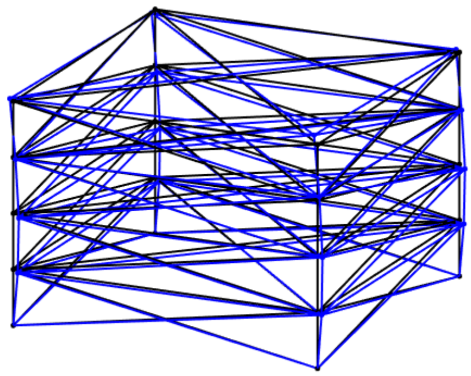

6

Figure 7: The first six mode shapes of 72-bar truss structure

Table 1: Properties of bar

A	*E*	*ρ*
0.000707 m^2	205e9 N/m^2	7833 kg/m^3

Table 2: Coordinates of nodes

25-bar truss structure				72-bar truss structure							
Node	**x (m)**	**y (m)**	**z (m)**	**Node**	**x (m)**	**y (m)**	**z (m)**	**Node**	**x (m)**	**y (m)**	**z (m)**
1	-0.9525	0	5.08	**1**	0	0	6.096	**11**	3.048	3.048	3.048
2	0.9525	0	5.08	**2**	3.048	0	6.096	**12**	0	3.048	3.048
3	-0.9525	0.9525	2.54	**3**	3.048	3.048	6.096	**13**	0	0	1.524
4	0.9525	0.9525	2.54	**4**	0	3.048	6.096	**14**	3.048	0	1.524
5	0.9525	-0.9525	2.54	**5**	0	0	4.572	**15**	3.048	3.048	1.524
6	-0.9525	-0.9525	2.54	**6**	3.048	0	4.572	**16**	0	3.048	1.524
7	-2.54	2.54	0	**7**	3.048	3.048	4.572	**17**	0	0	0
8	2.54	2.54	0	**8**	0	3.048	4.572	**18**	3.048	0	0
9	2.54	-2.54	0	**9**	0	0	3.048	**19**	3.048	3.048	0
10	-2.54	-2.54	0	**10**	3.048	0	3.048	**20**	0	3.048	0

Table 3: Two nodes of each bars

25-bar truss structure			72-bar truss structure								
Bar	**Nodes**		**Bar**	**Nodes**		**Bar**	**Nodes**		**Bar**	**Nodes**	
1	1	2	**1**	1	5	**26**	6	11	**51**	11	12
2	1	4	**2**	2	6	**27**	8	12	**52**	9	12
3	2	3	**3**	3	7	**28**	7	12	**53**	9	11
4	1	5	**4**	4	8	**29**	8	9	**54**	10	12
5	2	6	**5**	1	6	**30**	5	12	**55**	13	17
6	2	4	**6**	2	5	**31**	5	6	**56**	14	18
7	2	5	**7**	3	6	**32**	6	7	**57**	15	19
8	1	3	**8**	2	7	**33**	7	8	**58**	16	20
9	1	6	**9**	4	7	**34**	5	8	**59**	13	18
10	3	6	**10**	3	8	**35**	5	7	**60**	14	17
11	4	5	**11**	4	5	**36**	6	8	**61**	15	18
12	3	4	**12**	1	8	**37**	9	13	**62**	14	19
13	5	6	**13**	1	2	**38**	10	14	**63**	16	19
14	3	10	**14**	2	3	**39**	11	15	**64**	15	20
15	6	7	**15**	3	4	**40**	12	16	**65**	16	17
16	4	9	**16**	1	4	**41**	9	14	**66**	13	20
17	5	8	**17**	1	3	**42**	10	13	**67**	13	14
18	4	7	**18**	2	4	**43**	11	14	**68**	14	15
19	3	8	**19**	5	9	**44**	10	15	**69**	15	16
20	5	10	**20**	6	10	**45**	12	15	**70**	13	16

25-bar truss structure			72-bar truss structure								
Bar	**Nodes**		**Bar**	**Nodes**		**Bar**	**Nodes**		**Bar**	**Nodes**	
21	6	9	**21**	7	11	**46**	11	16	**71**	13	15
22	6	10	**22**	8	12	**47**	12	13	**72**	14	16
23	3	7	**23**	5	10	**48**	9	16			
24	4	8	**24**	6	9	**49**	9	10			
25	5	9	**25**	7	10	**50**	10	11			

Natural frequencies and mode shapes are combined to form the objective function (*ob*). Equation (8) must be solved in order to determine these frequencies and mode shapes:

$$[M]\ddot{d}+[K]d=0 \tag{8}$$

from which:

$$d=\xi\sin(\omega t+\varphi) \tag{9}$$

$$\ddot{d}=-\omega^2\xi\sin(\omega t+\varphi) \tag{10}$$

So Equation (8) can be rewritten:

$$\left([K]-\omega^2[M]\right)\xi=0 \tag{11}$$

$$\left|[K]-\omega^2[M]\right|=0 \tag{12}$$

Note that:

$$f_i=\omega_i/2\pi \tag{13}$$

The global stiffness matrix K is going to decrease if any member of the truss structure is damaged. With K_e as the stiffness matrix of an element (a member), if it goes down *r*%, K also declines to a certain extent.

$$\mathrm{K}_e^d=(1-r\%)\mathrm{K}_e \tag{14}$$

Table 4: The damage situations of 25-bar truss structure

Situations	Damage bar(s)	Severity of damage
The first situation	Bar 24	40%
The second situation	Bar 3 Bar 25	35% 25%
The third situation	Bar 1 Bar 10 Bar 15	35% 25% 20%
The fourth situation	Bar 1 Bar 4 Bar 10 Bar 15	35% 30% 25% 20%

Then the objective function is depicted by Equation (15):

$$ob=\zeta_1\sqrt{\sum_{i=1}^{6}\frac{\left(f_i^c-f_i^m\right)^2}{\left(f_i^m\right)^2}}+\zeta_2\left(1-\frac{\left(\left|\sum_{i=1}^{6}\xi_i^c\xi_i^m\right|\right)^2}{\left(\sum_{i=1}^{6}\left(\xi_i^c\right)^2\right)\left(\sum_{i=1}^{6}\left(\xi_i^m\right)^2\right)}\right) \tag{15}$$

With 6 being the number of considered natural frequencies and mode shapes, (*m*) and (*c*) indicate the "*measured*" and "*computed*", f_i and ξ_i are the *i*th natural frequency and mode shape. Figures 6 & 7 depict the first six mode shapes of 25-bar and 72-bar space truss structures.

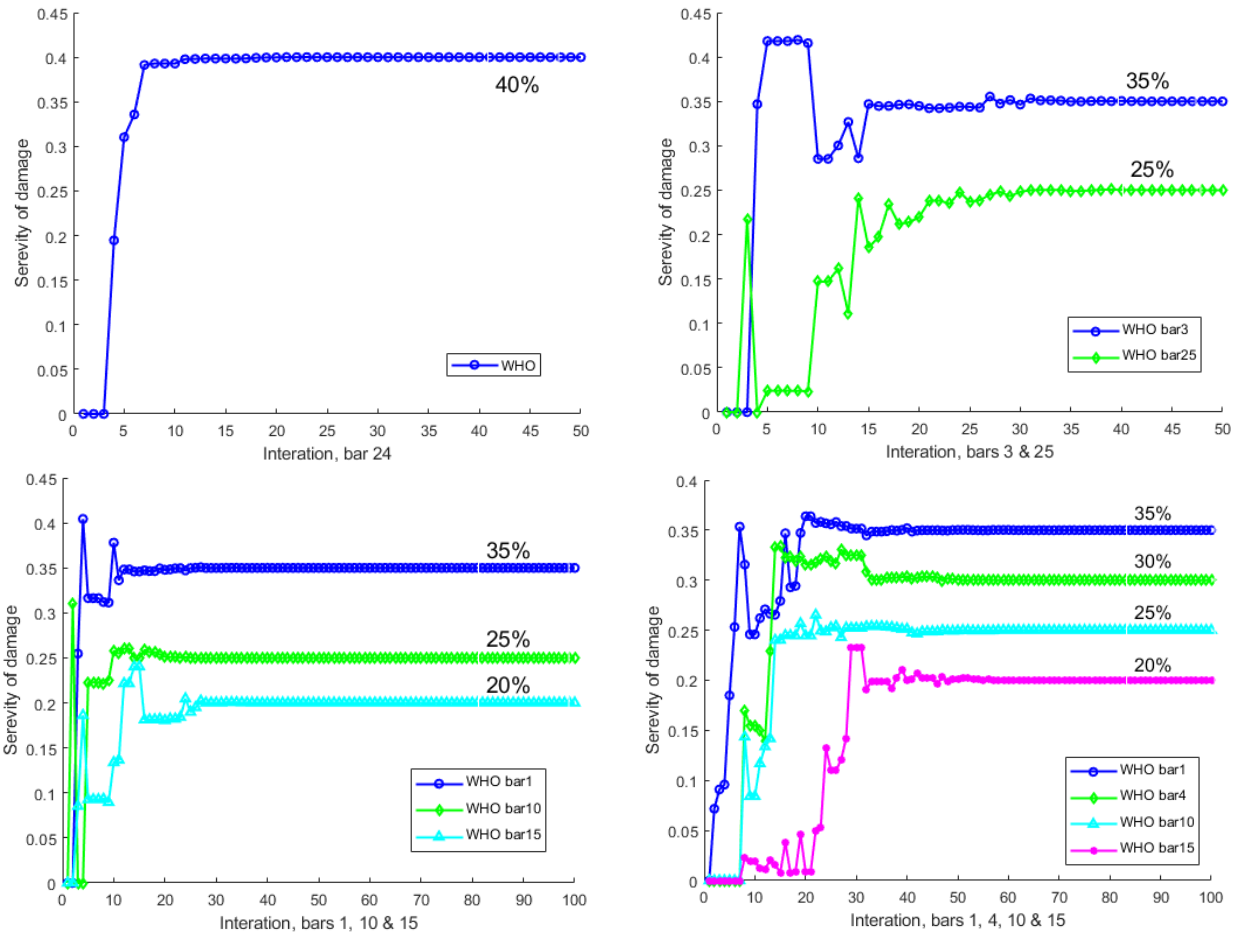

Figure 8*:* The convergence for the damage situations of 25-bar truss structure

Table 5: The damage situations of 72-bar truss structure

Situations	Damage bar(s)	Severity of damage
The first situation	Bar 13	40%
The second situation	Bar 4 Bar 22	35% 25%
The third situation	Bar 25 Bar 41 Bar 69	35% 25% 20%
The fourth situation	Bar 1 Bar 25 Bar 41 Bar 67	40% 35% 25% 20%

To confirm the correctness, certain damage situations are shown in Tables 4 and 5. The results, which are shown in Figures 8 to 9, demonstrate that the WHO produces the anticipated results for damage structure prediction. Furthermore, it is clear that the WHO only needs roughly 100 iterations to produce the necessary results.

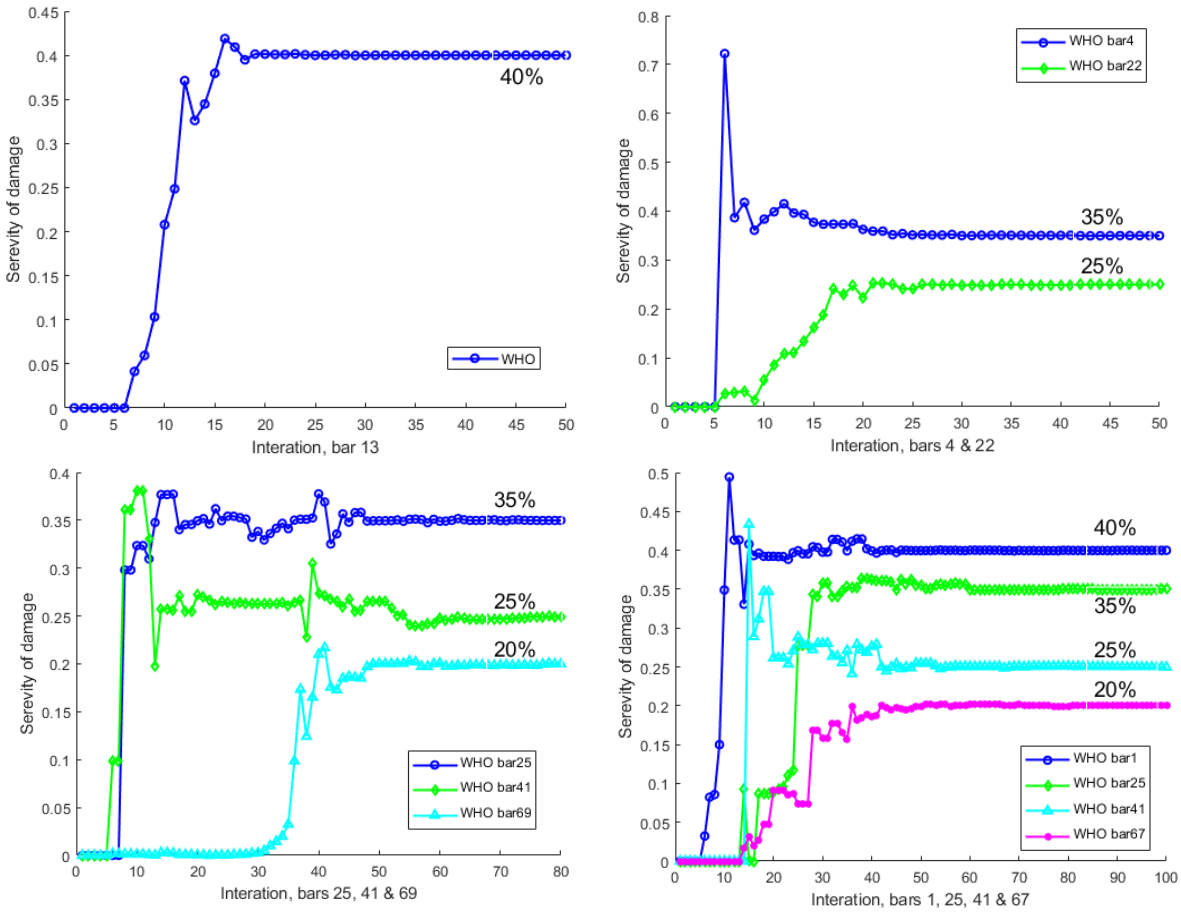

Figure 9: The convergence for the damage situations of 72-bar truss structure

4. CONCLUSION

This paper shows how to utilize the Wild Horse Optimizer (WHO) to identify damage in space truss structures. The algorithm's performance is assessed in a variety of situations, ranging from straightforward to intricate, and the results show how effectively the WHO predicts the position and magnitude of damage.

DECLARATION OF CONFLICTING INTERESTS

The author declares no potential conflicts of interest with respect to the research and publication of this paper.

REFERENCES

[1] R. Poli, J. Kennedy, and T. Blackwell, "Particle swarm optimization," Swarm Intelligence, Vol. 1, pp. 33–57, https://doi.org/10.1007/s11721-007-0002-0, (2007)

[2] R. Cazacu and L. Grama, "Steel truss optimization using genetic algorithms and FEA," Procedia Technology, Vol. 12, pp. 339–346, https://doi.org/10.1016/j.protcy.2013.12.496, (2014)

[3] E. Rashedi, H. Nezamabadi-pour, and S. Saryazdi, "GSA: A gravitational search algorithm," Information Sciences, Vol. 179(13), pp. 2232–2248, https://doi.org/10.1016/j.ins.2009.03.004, (2009)

[4] S. Mirjalili, A. H. Gandomi, S. Z. Mirjalili, S. Saremi, H. Faris, and S. M. Mirjalili, "Salp swarm algorithm: A bio-inspired optimizer for engineering design problems," Advances in Engineering Software, Vol. 114, pp. 163–191, https://doi.org/10.1016/j.advengsoft.2017.07.002, (2017)

[5] D. Karaboga and B. Basturk, "A powerful and efficient algorithm for numerical function optimization: Artificial bee colony (ABC) algorithm," Journal of Global Optimization, Vol. 39, pp. 459–471, https://doi.org/10.1007/s10898-007-9149-x, (2007)

[6] S. Mirjalili, S. M. Mirjalili, and A. Lewis, "Grey wolf optimizer," Advances in Engineering Software, Vol. 69, pp. 46–61, https://doi.org/10.1016/j.advengsoft.2013.12.007, (2014)

[7] I. Naruei and F. Keynia, "Wild horse optimizer: A new meta-heuristic algorithm for solving engineering optimization problems," Engineering with Computers, Vol. 38, pp. 3025–3056, https://doi.org/10.1007/s00366-021-01438-z, (2022)

[8] H.-G. Beyer and H.-P. Schwefel, "Evolution strategies-A comprehensive introduction," Natural Computing, Vol. 1, pp. 3–52, https://doi.org/10.1023/A:1015059928466, (2002)

[9] K. Luo, "Water flow optimizer: A nature-inspired evolutionary algorithm for global optimization," IEEE Transactions on Cybernetics, Vol. 52(8), pp. 7753–7764, https://doi.org/10.1109/TCYB.2021.3049607, (2022)

[10] S. Mirjalili, "SCA: A sine cosine algorithm for solving optimization problems," Knowledge-Based Systems, Vol. 96, pp. 120–133, https://doi.org/10.1016/j.knosys.2015.12.022, (2016)

[11] V. Hayyolalam and A. A. P. Kazem, "Black widow optimization algorithm: A novel meta-heuristic approach for solving engineering optimization problems," Engineering Applications of Artificial Intelligence, Vol. 87, p. 103249, https://doi.org/10.1016/j.engappai.2019.103249, (2020)

[12] R. V. Rao, V. J. Savsani, and D. P. Vakharia, "Teaching–learning-based optimization: A novel method for constrained mechanical design optimization problems," Computer-Aided Design, Vol. 43(3), pp. 303–315, https://doi.org/10.1016/j.cad.2010.12.015, (2011)

[13] S. Talatahari and M. Azizi, "Chaos game optimization: A novel metaheuristic algorithm," Artificial Intelligence Review, Vol. 54, pp. 917–1004, https://doi.org/10.1007/s10462-020-09867-w, (2021)

[14] H. L. Ton-That, "Natural frequencies of functionally graded sandwich plates resting on an elastic foundation using Chebyshev finite element method," Acta Mechanica et Automatica, Vol. 19(2), pp. 318–326, https://doi.org/10.2478/ama-2025-0039, (2025)

[15] H. L. Ton-That, "Analysis of natural frequency of porous sigmoid functionally graded sandwich plates via another quadrilateral element," Journal of Theoretical and Applied Mechanics, Vol. 55(2), pp. 188–201, https://doi.org/10.55787/jtams.25.55.2.188, (2025)

Engineering
TODAY

VOL. 4 / NO. 4 / 2025

CONTENTS